Charles University, Faculty of Science
Univerzita Karlova, Přírodovědecká fakulta

Ph.D. study program: Parasitology
Doktorský studijní program: Parazitologie

Nadine Zimmann MSc.

Analysis of lysosomes of *Trichomonas vaginalis*
Analýza lysosomů *Trichomonas vaginalis*

Ph.D. Thesis
Thesis supervisor: Prof. RNDr. Jan Tachezy, Ph.D.

Prague, 2021

Declaration of the author

I declare that I prepared this Ph.D. thesis independently and that all literary sources were properly cited. Neither this work nor a substantial part of it was used to reach the same or any other academic degree.

Nadine Zimmann MSc.

Declaration of the thesis supervisor

The data presented in this thesis resulted from a team collaboration at the Laboratory of Molecular and Biochemical Protistology and from the cooperation with our collaborators. I declare that the involvement of Nadine Zimmann in this work was substantial and that she contributed significantly to obtain the results.

Prof. RNDr. Jan Tachezy, Ph.D.

Acknowledgements

First and foremost, I would like to thank my supervisor Jan Tachezy for the unwavering support and the opportunity to pursue my Ph.D. and work on this project in his laboratory. Furthermore, I am grateful to my colleagues who encouraged me and provided a pleasant working atmosphere. I would like to give a special thanks to my office mates for the many jovial jokes and wonderful laughter they provided me during this journey. I am also thankful to the BIOCEV core facilities for their help, the Grant Agency of the Charles University (GAUK), and the Operational Program Research, Development and Education (OP RDE) which funded this work and enabled me to attend international conferences. I would also like to express my sincere thanks to my husband whose support can be barely put into words.

TABLE OF CONTENTS

ABSTRACT

Lysosomes represent the central degradative compartment of eukaryote cells. Harboring a variety of acid hydrolases at acidic pH, this organelle is designed for the degradation and recycling of material for cellular homeostasis and sustenance.

Studies on mammalian lysosomes have been extensive and revealed a long list of lysosomal proteins. While the function of most of these remains elusive, it is not surprising that a large subset have been found to be hydrolases. However, little is known about the biogenesis and function of this organelle in parasitic protists, and even less about its role in secretion. This work aimed to shed light on the (phago-)lysosomal proteome of the human parasite *Trichomonas vaginalis*, its protein targeting, and involvement in hydrolase secretion. Our studies revealed a lysosomal proteome of 462 proteins in 21 functional classes. Hydrolases represented the largest functional class and included proteases, lipases, phosphatases, and glycosidases. The identification of a large set of proteins involved in vesicular trafficking and cytoskeleton rearrangement indicates a dynamic phagolysosomal compartment. Our research, as well as the research of others, have identified several hydrolases also in the secretome, including the cysteine protease TvCP2. However, previously the mode of their secretion has been unclear. This work revealed that TvCP2 secretion occurs through lysosomes rather than the classical secretory pathway.

Unexpectedly, we showed that the lysosome-resident cysteine protease CLCP is targeted to lysosomes in a glycosylation-dependent manner. Similarly, the introduction of glycosylation sites to a secreted β-amylase redirected this protein to lysosomes. However, even though divergent homologues of the mannose-6-phosphate (M6P) receptor, TvMPR, were identified in the phagolysosomal proteome, *T. vaginalis* lacks enzymes for M6P formation and thus the character of the lysosomal signal recognition remains unclear.

Taken together, this work suggests a deep evolutionary origin of lysosomes across eukaryotes as they share a large set of common components, but also important differences that might be relevant for the parasite virulence. Whether TvMPR or other possible receptors are involved in lysosomal targeting and the precise structure of the lysosomal recognition marker need to be clarified in future studies.

ABSTRAKT (CZECH)

Lysozomy představují centrální degradační kompartment eukaryotních buněk. Tyto organely s kyselým pH a řadou kyselých hydroláz jsou určeny k degradaci a recyklaci materiálu pro buněčnou homeostázu a výživu.

Rozsáhlé studie savčích lysozomů odhalily dlouhý seznam lysozomálních proteinů. Jak lze očekávat, největší podskupinu tvoří hydrolázy, avšak funkce většiny z nich zůstává nejasná. O biogenezi a funkci lysozomů parazitických protistů je známo jen málo a ještě méně o jejich roli v sekreci. Cílem této studie bylo objasnit složení (fago-)lysozomálního proteomu lidského parazita *Trichomonas vaginalis* a jeho zapojení do sekrece hydroláz. Naše studie odhalili, že lysozomální proteom zahrnuje 462 proteinů ve 21 funkčních třídách. Hydrolázy představovaly největší funkční třídu a zahrnovaly proteázy, lipázy, fosfatázy a glykosidázy. Identifikace velkého souboru proteinů zapojených do vezikulárního transportu a přestavbě cytoskeletu ukazuje, že fagolysozomální kompartment je velmi dynamickou strukturou. Několik hydroláz jsme také identifikovali v sekretomu *T. vaginalis*, včetně cysteinové proteázy TvCP2, avšak způsob jejich sekrece byl nejasný. Studium lysosomů odhalilo, že k sekreci TvCP2 dochází spíše prostřednictvím lysozomů než klasickou sekreční cestou.

Dále jsme ukázali, že cysteinová proteáza CLCP, která je rezidentní v lysozomech je specificky rozpoznána a importována do lysozomů v závislosti na glykosylaci. Zavedení glykosylačních míst do sekvence β-amylázy, která je sekretována klasickou sekreční drahou přesměrovalo tento protein do lysozomů, což potvrdilo klíčovou úlohy glycosylace pro transport do lysoszomů K rozpoznání glykosylačního lysosomálního markeru jako je manóso-6-fosfát (M6P) by mohl sloužit M6P-receptor, TvMPR, který jsme našli v lysozomálním proteomu. Avšak *T. vaginalis* postrádá enzymy pro tvorbu M6P a tak způsob rozpoznání lysozomálního signálu zůstává nejasný.

Celkově tato studie ukazuje na společný evoluční původ lysozomů protistů jako je *T. vaginalis* a mnohobuněčných organismů, vzhledem k tomu, že sdílejí velký soubor společných lysozomálních komponentů. Jsou však také patrné důležité rozdíly, které by mohly být relevantní pro virulence parazitů. V budoucích studiích je třeba objasnit, zda se TvMPR nebo jiné možné receptory podílejí na rozpoznání a importu proteinů do lysozomů a přesnou strukturu lysozomálního rozpoznávacího markeru.

1. INTRODUCTION

1.1 Lysosomal research history

Lysosomes were first described in the nineteen fifties as cytoplasmic granules marked by the presence of acid phosphatase [1]. More detailed surveys on this organelle were conducted shortly after by de Duve and Novikoff [2–4] yielding a limited proteome of a handful of hydrolytic enzymes that have an acidic pH optimum [4]. However, lysosomes are not uniform but greatly vary in size and shape between cell types and within cells [4], depending on the last “meal” and time elapsed since ingestion [5]. Initially called “suicide bag” [6] and considered a death warrant for any particle ending up in this vesicle, over the past 70 years the lysosome has been recognized as a metabolic hub for cell homeostasis with over 400 proteins assigned to this organelle across different cell lines [7]. Presently, lysosomes are seen as key players in a plethora of intracellular mechanisms and lysosomal dysfunction has been connected to a number of conditions including neurodegenerative diseases, inflammatory and autoimmune disorders, cancer, and metabolic disorders [8]. Besides its involvement in programmed cell death, it has been shown that the lysosome participates in the degradation of intra- and extracellular material, plasma membrane repair, pathogenic defense, secretion, and antigen presentation [9–11].

1.2 Characteristics of lysosomes and lysosome-related organelles

Eukaryotic cells possess two major routes for the degradation of material: the proteasome and the lysosome [reviewed in 9,12]. While the proteasome degrades individual cytosolic proteins in a highly targeted fashion, lysosomes break down any intra- or extracellular material that reaches the organelle [9,13]. Therefore, lysosomes represent the major catabolic compartment in eukaryotic cells [14], with the end products being reused [15]. Lysosomes typically have an acidic pH and possess

around 60 acid hydrolases to fulfill the degradative function [5,16–18]. In electron microscopy, lysosomes appear as dense bodies in the cytosol with a spherical to tubular shape and often show a perinuclear distribution [19]. Lysosomes are surrounded by a single phospholipid-bilayer membrane of 7-10 nm thickness [20] and organellar size ranges from 100 nm to several microns depending on cell type and availability of nutrients [9,17,19].

Specialized compartments that present lysosomal properties are generally referred to as “lysosome-related organelles” and include melanosomes in melanocytes, lytic granules in lymphocytes, dense granules in platelets, pigment granules in *Drosophila*, MHC class II compartments in antigen-presenting cells [9,21,22], fungi and yeast vacuoles [23,24], and the lytic vacuole of plants [25].

1.3 Endo-lysosomal pathways

1.3.1 Endocytosis

Endocytosis is a receptor-mediated process of plasma membrane invagination by which surface proteins and small external particles are taken up into clathrin-coated pits (Fig. 1A) [26]. Thus, endocytosis plays two important roles for the cell: (1) it is involved in signaling by removing receptors from the cell surface, and (2) is inevitable for nutrient acquisition [26,27]. Internalized material is first packed into vesicles, the early endosomes, also called sorting endosomes. From there, cargo is either recycled back to the plasma membrane or further targeted for degradation through the endosomal-lysosomal pathway [28]. In the latter case, early endosomes mature into late endosomes that contain distinct intraluminal vesicles. Therefore, late endosomes are also called multivesicular bodies (MVBs) [29]. MVBs fuse and thereby grow in size [30]. The maturation process from early to late endosome is accompanied by a luminal pH decrease from ~6.2 in early to ~5.5 in late endosomes [28,31]. Maturation is

regulated by the largest subfamily of the Ras superfamily, the Rab GTPases [30,32,33]. Members of the Ras superfamily regulate a broad range of processes such as trafficking, cytoskeletal remodeling, and sensory perception and signaling [33]. In endosomal maturation, Rab5 and Rab7 possess key functions: The exchange of Rab5 for Rab7 on the endosomal surface marks the transition from early to late endosome and primes the organelle for fusion with a lysosome, which also harbors Rab7 on its surface [30,34]. Tethering and fusion then depend on soluble N-ethylmaleimide-sensitive factor-attachment receptors (SNAREs) that become enriched on both membranes surrounding the future fusion site. Once late endosome and lysosome are in close proximity, SNARE proteins form a “zipper”-complex that triggers Rab7-coordinated membrane fusion [30].

1.3.2 Phagocytosis

Phagocytosis represents the receptor-mediated uptake of particles larger than 0.5 µm in size, for example bacteria, by plasma membrane protrusions (Fig. 1B) [35–37]. It is an evolutionarily highly conserved process that is best studied in professional phagocytes of the human immune system; however, it is also evident in unicellular eukaryotes [35,36,38], out of which it is best studied in the protist *Entamoeba histolytica* [36]. Upon close cell-cell contact, the actin cytoskeleton undergoes rearrangements that are coordinated by various actin-binding proteins (ABPs) [39]. ABPs are a diverse group that includes formins, profilins, cofilins, twinfilins, gelsolins, coronins, and calponins [39]. Interestingly, the *T. vaginalis* genome has been reported to express 23 isoforms of actin [40], whereas only six isoforms were found in higher mammals [41] and four isoforms in *E. histolytica* [39,42]. The actin cytoskeleton polymerizes to form membrane protrusions that close around the particle to build a phagocytic cup [39,43]. Then, the membranes of the phagocytic cup fuse and the early phagosome is formed [35,37]. The initiation of the phagocytic cup and its maturation to

the phagosome is regulated by cytosolic calcium. *Entamoeba histolytica* expresses over 27 Ca^{2+}-binding proteins (CaBPs) that regulate different steps in the maturation process, some of which have been reviewed by Babuta et al. [44]. For example, the protein kinase EhC2PK has been shown to participate in initiating phagocytosis [45,46], whereas the calmodulin-like EhCaBP3 interacts with myosin and is involved in the formation of the early phagosome by separating it from the plasma membrane [47]. Fusion events of an early phagosome with an early endosome are frequent as both vesicles are marked by Rab5 on their surface [35,36]. The switch of Rab5 to Rab7 on the phagosomal surface marks the vesicle transition from an early to a late phagosome. The late phagosome either fuses directly with a lysosome to generate a phagolysosome or with a late endosome prior to the fusion with a lysosome [35,36].

1.3.3 Pinocytosis

Pinocytosis refers to the non-specific engulfment of extracellular fluid [48,49]. It is also called bulk-phase endocytosis and, in contrast to receptor-mediated endocytosis, does not show saturation [48]. Pinocytosis has been described in animals and several branches of Amoebozoa, which indicates an early evolutionary origin [49]. However, while a non-specific, non-saturable uptake has been observed in *Tritrichomonas foetus* [50], it is not certain whether *T. vaginalis* is capable of pinocytosis [51]. In pinocytosis, the external fluid is engulfed into a pinosome, whose size can range from a few nanometers (micropinocytosis) up to 5 µm (macropinocytosis) (Fig. 1C) [48]. The pinosome is progressively acidified as it matures, which is accompanied by fusions with the endosomes. Once Rab5 is exchanged for Rab7 on the pinosome surface, it fuses with a lysosome for content degradation [48,49,52].

1.3.4 Autophagy

In contrast to the endocytic pathways discussed before, which take up material from the cell environment, autophagy is a recycling process in which intracellular components such as harmful protein aggregates and aged or damaged organelles are degraded [30,53,54]. Selective autophagy is thus an important way of organellar quality control [53]. However, nutrient deficiency and other stress conditions can induce non-selective autophagy that leads to the consumption of a portion of the cell's cytoplasm for self-sustenance [30,54]. The autophagic pathway starts with the engulfment of material by an endoplasmic reticulum (ER)-derived isolating membrane, also called phagophore (Fig. 1D) [30,53,54]. The phagophore is sealed with the help of the proteins produced from autophagy-related genes (Atg), forming a closed double-membrane early autophagosome [30,53]. Atg8 is thought to be the key player in the sealing and maturation process as a loss of this protein from the outer autophagosomal membrane leads to the disassembly of the autophagy-initiating machinery from the newly built autophagosome in yeast [30,32,53,54]. Early autophagosomes mature to late autophagosomes, which are very dynamic organelles that fuse with single-membrane early and late endosomes, forming a hybrid organelle called amphisome [30,53]. The fusion events lead to a stepwise acquisition of lysosomal membrane proteins, hydrolases and luminal acidification [53]. Eventually, Rab7 is recruited to the late autophagosome/amphisome and the fusion with a lysosome is initiated [54].

The first evidence of autophagy in trichomonads dates back to the late nineteen nineties. Benchimol [55] observed a rough ER-derived membrane enclosing hydrogenosomes in *T. foetus* under both normal and stress conditions. However, the molecular mechanisms governing these events were not investigated. Huang et al. [56] later found a reduced autophagic machinery in *T. vaginalis* that requires only Atg8 for autophagosome formation, and that both inhibition of the proteasome and glucose-restriction induce autophagy. Thus, autophagy represents an inevitable proteolytic mechanism in *T. vaginalis* [56].

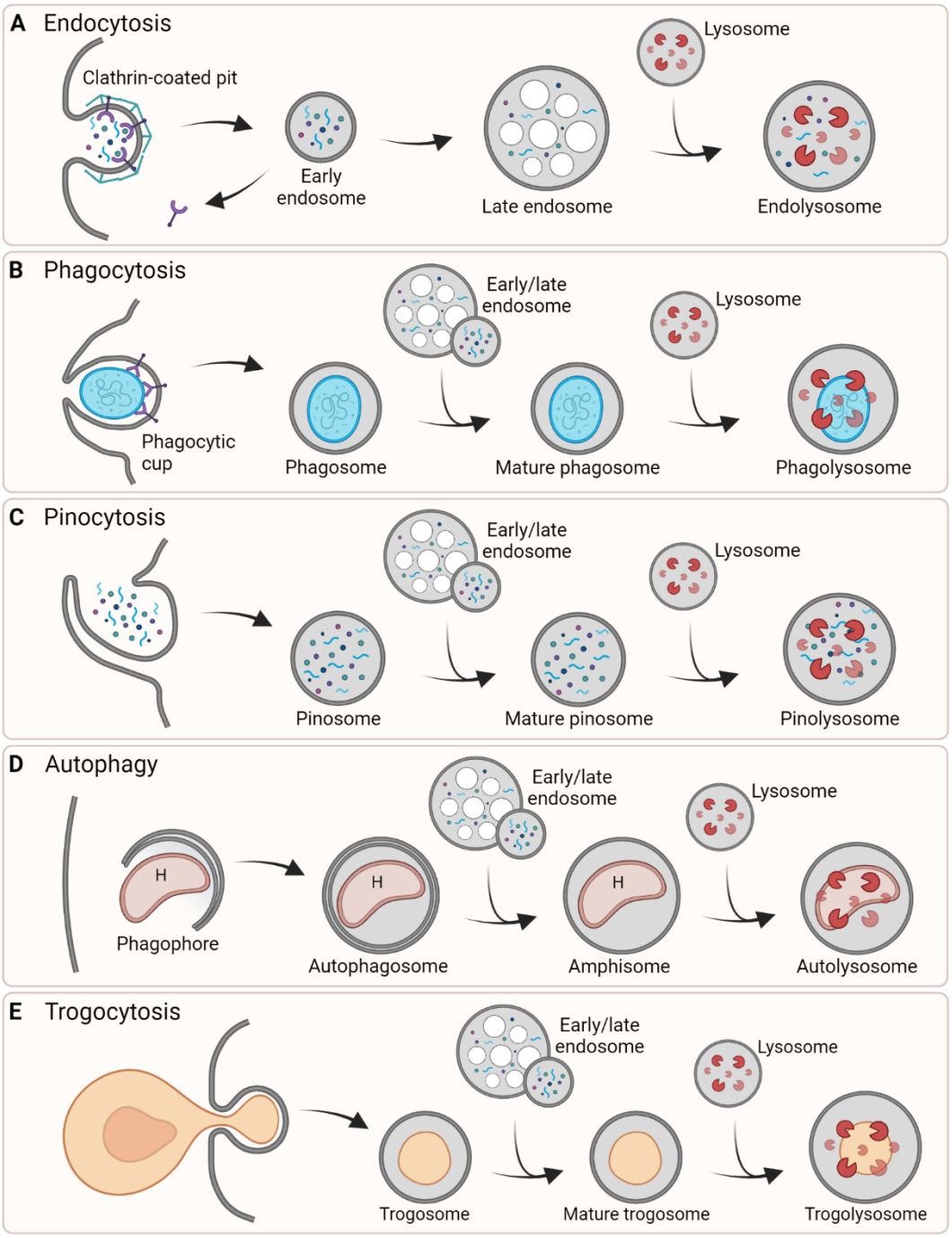

Figure 1. Endo-lysosomal pathways. (A) Endocytosis. Receptor-mediated endocytosis leads to the uptake of smaller particles into clathrin-coated pits. Engulfed material is sorted in early endosomes and either recycled back to the cell surface or sent through the endo-lysosomal pathway. An early endosome matures into a late endosome by a decrease in pH and fusion events between the organelles. A late endosome eventually fuses with a lysosome to an endolysosome. (B) Phagocytosis. A cell is engulfed in a receptor-mediated fashion. The forming phagosome undergoes a maturation process in which it fuses with early and late endosomes. The mature phagosome eventually fuses with a lysosome. (C) Pinocytosis. Extracellular fluid-phase particles are taken up non-specifically. The size of the resulting pinosome can range depending on the engulfed volume. The pinosome is progressively acidified as it matures and fuses with endosomes. It eventually fuses with a lysosome. (D) Autophagy. Autophagy is a recycling process to break down intracellular components either for quality control or in case of nutritional deficiencies. A double-membrane phagophore forms around the compartment to be degraded, here a hydrogenosome (H). Once the phagophore is sealed, the autophagosome is formed. The autophagosome fuses with endocytic vesicles, thereby forming a single-membrane amphisome. The amphisome and autophagosome eventually fuse with a lysosome. (E) Togocytosis. A trogocytosing cell bites off pieces of another cell that are taken up into a trogosome. The trogosome matures, fuses with endosomes, and eventually with a lysosome.

1.3.5 Trogocytosis

Trogocytosis is a process of “nibbling” on cells and biting off pieces (Fig. 1E). It differs from phagocytosis which engulfs cells and other large particles in their entirety. In metazoans, trogocytosis plays an important role in the immune system, nervous system, and during embryonic development [57]; for example, trogocytosis is used by microglia to remodel neuronal synapses. While trogocytosis between immune cells has a benign nature and is used for cell-cell communication [57], it may serve for killing certain target cells. For example, neutrophils kill parasites such as *T. vaginalis*, and macrophages were shown to trogocytose antibody-opsonized breast cancer cells [58–60]. Vice versa, trogocytosis was adapted by multiple pathogenic amoeba species including *E. histolytica*, *Naegleria fowleri*, *Acanthamoeba*, and *Hartmannella* to kill host cells [61–64]. Similar to phagocytosis, the trogocytic pathway is regulated by cytosolic calcium and follows the EhC2PK-mediated pathway [61]. However, initiation of trogocytosis depends on the AGC family kinase 1 [65]. Interestingly, *E. histolytica* was shown to differentiate between live and dead host cells, with the former being trogocytosed and the latter phagocytosed [61]. Trogocytosis does not lead to immediate death of the nibbled cell but is lethal when too much damage has been done [61,64]. As of today, trogocytosis has been described only in metazoans and amoebae [66]. It has not been observed in *T. vaginalis* and is believed to be absent in this parasite.

1.4 Secretory pathways

Secretion is a major anabolic process that is highly conserved in eukaryotes and displays an important way for the cell to respond to a changing environment. Changing factors include nutrients, growth factors, but also heat and oxidative stress [67]. The majority of secretory proteins possesses an amino-terminal signal peptide (SP) that

primes the protein for the conventional secretory pathway, a route employing the ER and Golgi body (Golgi) [68,69]. However, multiple studies have shown that a substantial number of proteins are secreted despite the absence of an SP, a process termed unconventional secretion [reviewed in 68]. The next two chapters will elaborate on conventional and unconventional secretion in more detail.

1.4.1 Conventional protein secretion

Conventional protein secretion (CPS) involves the ER, Golgi, secretory vesicles, and the plasma membrane [70], and is considered the default pathway for eukaryote protein secretion (Fig. 2) [71]. The majority of secretory proteins possesses an amino-terminal SP that, once recognized by the signal recognition particle (SRP), leads to a translation pause and protein transport to the ER surface. Then, the translation of the protein is resumed into the ER lumen through a Sec protein channel complex. After translocation, the SP is cleaved off by signal peptidases [71–73]. Early glycosylations take place in the ER during translation. For N-glycosylation, the pre-assembled oligosaccharide $Glc_3Man_9GlcNAc_2$ is transferred to the asparagine in the sequence Asn-X-[Ser/Thr] by the oligosaccharyltransferase [reviewed in 74]. In O-glycosylation, on the other hand, mannoses are transferred to serine or threonine by protein O-mannosyl transferase [71]. However, *T. vaginalis* has been shown to possess a limited set of glycosyltransferases that are available for glycan synthesis. This leads to a simplified glycan structure in *T. vaginalis* consisting of only five mannoses and two N-acetyl glucosamines [75,76]. N-glycans have been shown to be an important factor in the quality control of protein folding [77]. If misfolding is detected, the protein is subjected to the ER-associated degradation pathway (ERAD) for proteasomal degradation [71]. Well-folded glycoproteins are directed to the ER-exit sites (ERES) by the N-glycan binding lectin ERGIC-53 [71,78] and then transported to the Golgi via COPII vesicles. Transported proteins undergo cisternal migration from the cis-Golgi

(CGN), which is facing the ER, to the trans-Golgi (TGN), which is directed toward the cytosol [71,73,79]. This migration is often accompanied by glycan modifications [71,73,80]. Simultaneously, a constant retrograde transport by COPI vesicles retrieves proteins to earlier compartments: ER-resident proteins are retrieved from the CGN and CGN-resident proteins from the TGN, both to ensure that ER- and Golgi-resident proteins are not secreted [71,73]. ER-resident proteins possess the C-terminal ER-retention signal XDEL [71,81], which is KQEL in *T. vaginalis* [75,82].

Secretory proteins that arrive at the TGN are packed either into transport vesicles that directly move to the cell surface or into secretory vesicles whose fusion with the plasma membrane is tightly regulated [73]. The vesicles are transported to the plasma membrane along the actin cytoskeleton [71]. Cytosolic calcium is considered the master regulator of exocytosis and leads the secretory vesicles to migrate to and fuse with the plasma membrane [73,83]. The transmembrane protein synaptotagmin, located in the vesicular membrane and part of the SNARE protein complex, is the major calcium sensor on the vesicular surface [83]. Besides intracellular factors, secretion is also stimulated by external factors such as nutrients [84].

1.4.2 Unconventional protein secretion

The term unconventional protein secretion (UPS) does not describe a single mechanism but a collection of pathways that lead to the secretion of proteins lacking an SP either vesicle-dependently or vesicle-independently [85]. Proteins secreted by UPS often fulfill important extracellular functions [86]. Even though UPS has been known for almost four decades [87], the mechanistic understanding behind it is still lacking, while the number of leaderless proteins found in the secretomes and surface proteomes keeps rising [88]. Initially, four types of UPS were described by Rabouille et al. [68]

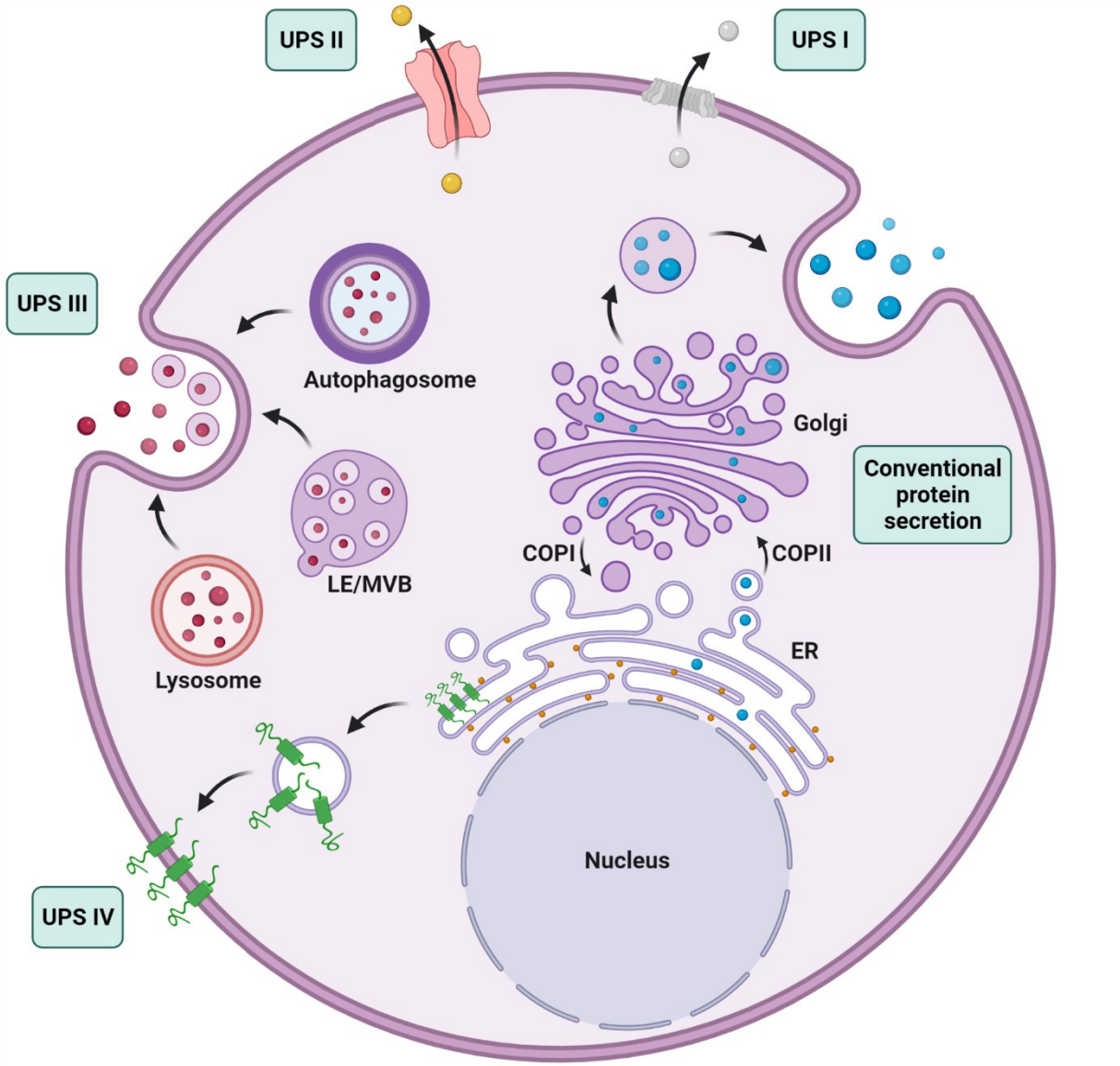

Figure 2. Secretory pathways. In conventional protein secretion, the secretory protein is translated into the ER and transported to the Golgi. It migrates through the Golgi and is packed into a secretory vesicle that fuses with the plasma membrane. Four types of unconventional protein secretion (UPS) have been described. In UPS I, the protein forms its own plasma membrane pore by oligomerization through which it is released. UPS II makes use of ABC-transporters. UPS III describes secretion through vesicles of endo-lysosomal and autophagic origin such as lysosomes, late endosomes (LE), multivesicular bodies (MVB), autophagosomes, autosomes, exosomes, and microvesicles. In UPS IV, transmembrane proteins synthesized in the ER bypass the Golgi and are transported to the plasma membrane by ER-derived vesicles.

(Fig. 2): (1) Self-sustained protein secretion by oligomerization and pore-creation into the plasma membrane (UPS Type I); (2) Secretion through ABC transporters (UPS Type II); (3) Secretion by autophagosome-like vesicles (UPS Type III); (4) Golgi bypass of SP-harboring transmembrane proteins through ER-derived vesicles (UPS Type IV) [88]. However, additional studies showed that vesicles of the endo-lysosomal pathway

other than autophagosomes can also serve for secretion as well, such as the endosomes, lysosomes, amphisomes, microvesicles, and exosomes [86,89,90]. Metazoan lysosomes and endo-lysosomes have been shown to fuse with the plasma membrane in a calcium-dependent manner, thereby secreting vesicle content [24,91]. However, it is not fully understood how a leaderless protein reaches the endo-lysosomal compartment prior to secretion. The cytoplasmic fatty acid-binding protein 4 has been suggested to be imported into lysosomes by a receptor, but the particular receptor has not yet been elucidated [91]. Other leaderless proteins have been shown to be secreted through lysosomes including heat shock protein 70, aldo-keto reductase family 1 member B8 (AKR1B8), and AKR1B10. Their import into lysosomes is facilitated by ABC transporters [91]. Furthermore, the same protein might be secreted through different routes depending on the cellular status [88]. This became particularly evident through the cytokine interleukin 1β, which is secreted via lysosomes under starvation but through pores in the plasma membrane upon inflammation [89,92–94]. Whereas UPS is often stress-induced in mammalian cells, it is a common mechanism in parasitic protists to release virulence factors such as glycolytic enzymes during normal growth conditions [88]. These glycolytic proteins often have moonlighting functions upon secretion that are essential for invasion and persistence [88]. Secretome and surface proteome studies on protists have led to the understanding of the importance of UPS for these organisms [88].

1.5 Targeting of lysosomal constituents

Lysosomal proteins possess an amino-terminal SP and are thus imported cotranslationally into the ER [95]. As the default pathway of ER-synthesized proteins is secretion, lysosomal proteins need targeting signals that segregate them from the secretory pathway and direct them to the endo-lysosomal compartment. Thus, sorting of most mammalian lysosomal hydrolases depends on the mannose-6-phosphate

(M6P) pathway that relies on M6P on the lysosomal glycoprotein and an M6P receptor (MPR) that delivers the protein to the endo-lysosomal compartment (Fig. 3) [96,97]. The formation of M6P depends on the consecutive action of two proteins in the Golgi. First, N-acetylglucosamine-1-phosphotransferase (GlcNAc-PT) transfers GlcNAc-1-phosphate from UDP-GlcNAc onto mannoses within the $Glc_3Man_9GlcNAc_2$ oligosaccharide [95,97]. Then, N-acetylglucosamine-1-phosphodiester-α-N-acetyl-glucosaminidase ("uncovering enzyme", UCE) trims the oligosaccharide, which results in the exposure of M6P. The M6P of the lysosomal glycoprotein is then bound by MPR in the TGN [95,97]. Two MPRs have been found, a cation-dependent (CD-MPR) and a cation-independent (CI-MPR) [18,95–99]. Both are type I transmembrane glycoproteins that differ in mass: while CI-MPR has 300 kDa (MPR300), CD-MPR has only 46 kDa (MPR46) [95,97]. MPR300 consists of fifteen M6P receptor homology (MRH) domains of around 147 amino acids each in length, with three M6P binding sites in domains 3, 5, and 9. MPR46 possesses only a single repeat and M6P binding site, however, MPR46 exists mainly in dimers and thus can bind M6P in a similar manner as MPR300 [95–97]. MPRs localize mainly to the TGN and endosomes, but a small proportion can be found on the plasma membrane for the endocytosis of ligands [95,97]. However, it has been shown that up to 20% of luminal proteins escape MPR binding and are secreted instead [95]. Trafficking of cargo-loaded receptors and transmembrane proteins is directed via two routes, the canonical and the alternative route, and depends on targeting signals in their cytosolic tails, which are, most frequently, dileucine-based ([DE]xxxL[LI], DxxLL) or tyrosine-based (YxxØ) motifs [96,100,101]. Lysosomal targeting sequences of transmembrane proteins (t-LTS) not only mediate lysosomal delivery but also rapid internalization from the plasma membrane [95,101]. In the canonical pathway, t-LTSs are bound by cytosolic Golgi-localized, γ-ear-containing ADP ribosylation factor-binding proteins (GGAs) and the adaptor proteins AP1 and AP4 that mediate sorting at the TGN [95,96,99,102–104]. The receptor-cargo complex leaves the TGN via clathrin-coated vesicles that fuse with the endosomes.

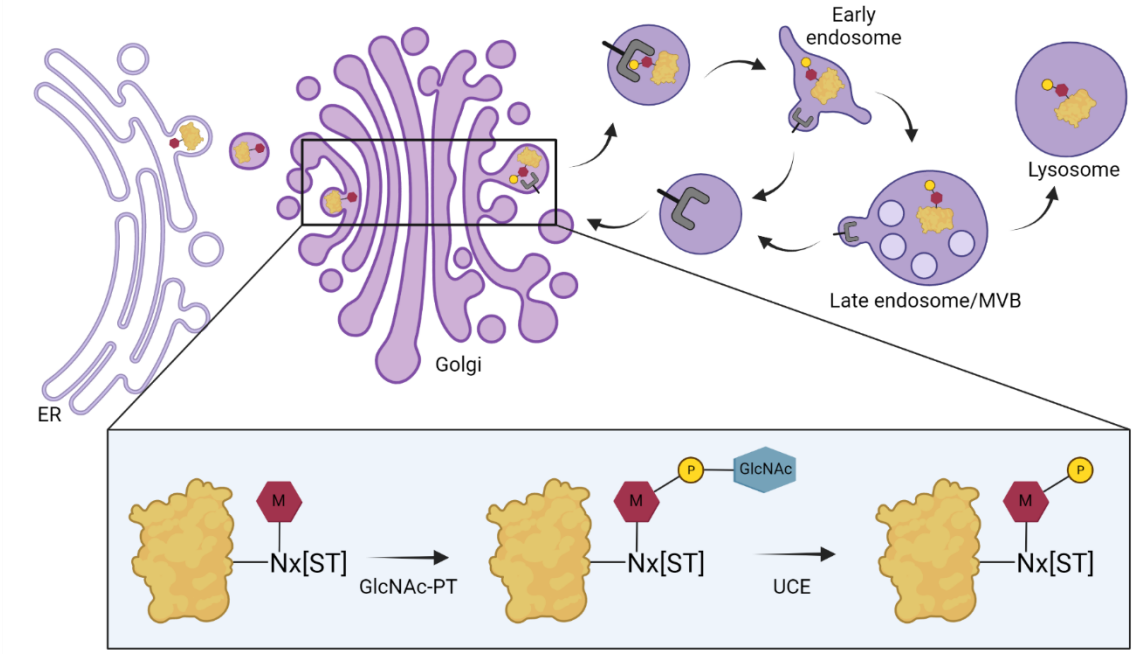

Figure 3. Mannose-6-phosphate pathway. In the endoplasmic reticulum (ER), soluble lysosomal proteins are glycosylated on asparagine residues within the sequence Nx[S/T]. In the Golgi body, N-acetylglucosamine-1-phosphotransferase (GlcNAc-PT) transfers GlcNAc-1-phosphate from UDP-GlcNAc onto mannose within the oligosaccharide. Next, the uncovering enzyme (UCE) trims the oligosaccharide and mannose-6-phosphate (M6P) is exposed. The M6P is then bound by M6P-receptor (MPR) in the trans-Golgi network (TGN). The complex of MPR and lysosomal protein is then targeted through the endolysosomal pathway. MPR dissociates from the lysosomal protein in the acidified pH of early and late endosomes and is recycled back to the TGN.

The cargo is released in early and late endosomes due to the decreasing pH and migrates intraluminally to lysosomes. MPRs are retrieved to the TGN from early endosomes by the retromer protein complex and from late endosomes by Rab9 and its effector TIP47 [95,97–99,101,105]. In the alternative pathway, lysosomal membrane proteins and receptors travel to the plasma membrane first and are then internalized through signals on the cytosolic tail [95–97]. Internalization of the MPRs is mediated through the YxxØ signal, which is recognized and bound by the adaptor proteins AP2 and AP3 that initiate endocytosis into clathrin-coated vesicles [95,96,106,107].

M6P-independent lysosomal sorting receptors have been described including lysosomal integral membrane protein (LIMP) 2 (mammals), vacuolar sorting receptors (VSRs; plants, algae, alveolates), and sortilin/Vps10 that were studied in mammals and yeast. However, sortilin homologues have been found in members of all eukaryotic

groups [96,98]. Interestingly, in *E. histolytica*, a novel class of receptors for the lysosomal delivery of cysteine peptidases (cysteine peptidase-binding protein family, CPBF) was identified [108]. Most receptors that are involved in lysosomal targeting bind their cargo in the late Golgi. However, LIMP-2 and CPBF1 have been shown to bind substrate in the ER [96,108].

1.6 The lysosomal degradome

Lysosomes possess three major components: (1) luminal proteins that are either acid hydrolases or their activators; (2) transmembrane proteins; and (3) cytosolic lysosome-associated proteins [17,109,110]. The number of proteins identified in lysosomal isolations differs tremendously between studies and depends on the methods used and interpretation of the data [110]. For example, Zhang et al. [111] identified 90 proteins in lysosomal isolations from murine liver cells, whereas Schröder et al. [112] found 1,565 lysosomal proteins in human placental cells. Akter et al. [113] analyzed four human and two murine cell lines and found 2,173 lysosomal proteins as a common set. However, only around 450 proteins can be reproducibly detected in lysosomal isolations from eukaryotic cells [7]. This includes around 60 hydrolases and more than 100 transmembrane proteins that were assigned to this organelle [17,110,114]. Whereas soluble hydrolases are directly involved in the proteolytic processing or degradation of incoming material, the functions of membrane proteins are more diverse. Some membrane proteins serve for the structural stability of the organelle, while others regulate the lysosomal pH or the exchange of metabolites with the cytosol that were derived from the digested material [110,115]. The most frequent lysosomal membrane proteins are the lysosome-associated membrane protein 1 (LAMP-1), LAMP-2, LIMP-1, and LIMP-2 that account for more than 50% of the lysosomal membrane protein content. As they are heavily glycosylated on their luminal parts, they are believed to protect the organelle from self-digestion by creating a dense sugar-lining along the

lysosomal membrane [17,110,115–118]. However, LAMPs have also been shown to regulate the intracellular positioning of the mitochondria [119]. Other membrane-resident proteins are displayed by over 50 channels and transporters that are important for ion homeostasis and nutrient exchange [17,32]. Vacuolar-type ATPases (v-ATPases) import protons from the cytosol to establish and maintain the acidic pH that not only hydrolases need for their degradative function, but also many catabolite exporters depend on [17,120,121]. Nicastrin is a component of the secretase-complex that has a proteolytic function within its hydrophobic domain [122]. Ca^{2+} transporters regulate the calcium efflux from endosomes and lysosomes, a signal necessary for membrane fusion. Other exporters found in the lysosomal membrane include amino acid, sugar, and lipid exporters [17]. To date, more than 30 solute transporters have been described [123]. Thus, lysosomal membrane constituents play essential roles in lysosomal homeostasis [17].

Luminal hydrolases include phosphatases, nucleases, lipases, glycosidases, sulfatases, and proteases [110,124,125]. Mutations have been implicated in lysosomal storage disorders through which undigested cargo accumulates within the lysosome [109]. More than 15 groups of matrix proteases are involved in cargo turnover, primarily cathepsins [116]. Cathepsins were first described in the gastric fluid in 1929 and the term literally means “to digest” [125,126]. These proteases are grouped based on their structure and catalytic type into cysteine, aspartic, and serine cathepsins [127], some of which have also been shown to be secreted [128,129]. While initially thought to be responsible for the non-specific bulk proteolysis of incoming cargo [130], it became evident that cathepsins are important for the proteolytic processing and regulation of lysosomal cargo and for controlling normal and pathological processes including macroautophagy [116,125,130]. Other soluble proteins assigned to lysosomes include β-hexosaminidase and acid phosphatase, both of which are used as lysosomal markers [110,122]. Acid phosphatase plays an important role in M6P removal from newly synthesized lysosomal hydrolases [131,132] and its presence was the main

feature that led to the description of the lysosomal organelle [1]. β-hexosaminidase has later been found important for the hydrolysis of glycoproteins, glycosaminoglycans, and glycolipids [133]. Whereas lipases are crucial for energy metabolism and signaling, nucleases degrade RNA and DNA in a process known as RNautophagy and DNautophagy [125].

Besides *bona fide* lysosomal proteins, some cytosolic proteins and protein complexes are, either transiently or constitutively, associated with the lysosomal surface and regulate vesicular interaction and fusion [110]. They include the fusion-machinery of Rab GTPases, SNAREs, and adaptor proteins described earlier and also cytoskeletal proteins [134–136]. Interaction of lysosomes with the cytoskeleton enables the organelle to migrate within the cell, an ability that is necessary for the lysosome to meet its diverse functions in a spatially regulated manner [137].

1.7 *Trichomonas vaginalis*, its lysosomes and secretome

Trichomonas vaginalis is a unicellular, microaerophilic, flagellated, parasitic protist that causes the most common non-viral sexually transmitted disease in humans and is responsible for more than 150 million infections worldwide each year [138–141]. Its primary localization is the urogenital tract of women and the urethra and prostate of men; however, the majority of infections is asymptomatic [140,141]. Upon infection, *T. vaginalis* undergoes morphological changes from a pyriform to amoeboid shape and establishes close contact with the squamous epithelium [141,142]. Carbohydrates are its main energy source, however, *T. vaginalis* also phagocytoses vaginal epithelial cells, erythrocytes, immune cells such as lymphocytes and monocytes, and components of the vaginal microbiota including yeast and bacteria [141–143]. *Trichomonas vaginalis* phagocytic activity changes the vaginal microbiome in a way that is favorable to parasite survival [144]. As Lactobacilli form a natural protective

barrier on the vaginal epithelium to prevent pathogen adhesion [145], it is not surprising that the *T. vaginalis* infection has been associated with a decrease in the Lactobacilli population [146,147]. Nutrients are taken up by *T. vaginalis* through receptor-mediated endocytosis, which is also important for the neutralization of host defense proteins [142]. Even though little is known about host-parasite interactions, *T. vaginalis* is suggested to secrete perforin-like pore-forming proteins [148]. Furthermore, secreted proteases have repeatedly been implicated in parasite virulence [149–153], and the importance of this class of proteins for *T. vaginalis* becomes apparent from its genome: it encodes an enormous set of over 440 peptidases, half of which account for cysteine peptidases [40]. The legumain-like cysteine peptidase TvLEGU-1 is one of the few that has been analyzed regarding its cellular localization and has been assigned to the lysosomes, Golgi, and cell surface [154]. Only a few secreted proteins that are implicated in pathogenicity and virulence toward the host have been described, including TvCP2, TvCP3, TvCP4, and TvCPT, all of which are cysteine peptidases [149,155]. However, their cellular localization is mostly unknown [155].

Besides the crucial role of cysteine peptidases in virulence, a few more proteins have been found secreted although initially assigned to other organelles and are believed to have secondary functions. These include enolase, glyceraldehyde-3-phosphate dehydrogenase, and triosephosphate isomerase [88]. These proteins were also shown to be secreted through UPS [88]. However, little is known about the parasite's vesicular trafficking machinery. *Trichomonas vaginalis* likely encodes the most complex machinery associated with vesicular trafficking, which is due to massive gene duplication events in its genome [142]. As an example, unicellular eukaryotes usually encode between 5 and 20 Rab GTPases, whereas metazoans possess a repertoire of between 25 and 60 [156]. Humans encode around 60 Rab GTPases, *Saccharomyces cerevisiae* and *Plasmodium falciparum* 11, and *Giardia lamblia* only 8 [157–159]. In contrast, *T. vaginalis* has been found to encode 292 Rab GTPases [40], however, their functions remain to be elucidated.

The massively expanded trafficking system together with the huge expansion of genes that encode (cysteine) peptidases emphasize the importance of the lysosomal and secretory system for this parasite and highlights the necessity of studies on the endo-lysosomal and secretory compartment. This work's purpose is to help fill this knowledge gap.

2. AIMS AND OBJECTIVES

1. To develop and optimize a protocol for the isolation of lysosomes from *T. vaginalis*

2. To analyse the lysosomal proteome of *T. vaginalis*

3. To elucidate the role of N-linked glycosylation in lysosomal protein targeting

4. To investigate the role of lysosomes in hydrolase secretion

5. To analyse the secretome regarding lysosome-derived virulence factors

3. RESULTS AND CONCLUSIONS

3.1 Lysosomal proteome

Most studies on the lysosomal proteome have been conducted on human and other mammalian cell lines as the implications of lysosomal dysfunction became clear through a variety of diseases. However, the interest in lysosomes of parasitic protists is quite different. First, lysosomes can be a useful drug target to treat a parasite infection. For example, chloroquine (CLQ) targets the *Plasmodium* vacuole and increases its pH, and thus impairing its function [160]. Second, as lysosomes are involved in protein secretion, knowledge of lysosomal protein content may help understand pathogenicity and reveal potential virulence factors. However, there is surprisingly limited information on parasite lysosomes. Thus, this work focused on the analysis of the lysosomal proteome, lysosomal biogenesis, and the role of lysosomes in unconventional protein secretion in *T. vaginalis*.

3.1.1 TvRab7a as a lysosomal marker

Bioinformatic analysis revealed three Rab7 paralogues in the *T. vaginalis* genome, of which TvRab7a was selected. Its lysosomal localization was verified by fluorescence microscopy using LysoTracker Deep Red and fluorescein isothiocyanate (FITC)-coupled lactoferrin, which is engulfed by receptor-mediated endocytosis, as lysosomal markers. Co-localization of FITC-lactoferrin and LysoTracker Deep Red with Rab7 was observed in larger vesicles of approximately 1 µm in size, corresponding to late endosomes and lysosomes. Thus, we validated Rab7a as a late endosomal/lysosomal marker in *T. vaginalis*.

3.1.2 Proof of principle of lysosomal isolation methods

Three methods were used for the isolation of (phago-)lysosomes: (1) 45% Percoll gradient centrifugation as previously described [161]; (2) OptiPrep gradient centrifugation; and (3) isolation by phagocytosed lactoferrin-covered magnetic beads. Isolated fractions were analyzed by Western Blot regarding the presence of marker proteins. Rab7a was used as a lysosomal marker [156], OsmC as a hydrogenosomal marker [162], and soluble protein disulfide-isomerase (sPDI) as an ER marker. Lysosomal fractions isolated by Percoll and Optiprep were positive for Rab7 but contaminated with ER-derived vesicles, as shown by a weak sPDI signal. This was, however, not surprising, as lysosomes often co-purify with other organelles such as ER and Golgi or contain proteins of other organellar origins due to autophagy [55,110,163]. Thus, phagocytosed magnetic beads were used to isolate phagolysosomes. This approach resulted in the purest isolations that showed a strong signal for Rab7 and no OsmC or sPDI signal.

3.1.3 Proteomic analysis

The combination of the three isolation methods and manual curation of the data resulted in a set of 462 proteins, which is comparable to the lysosomal proteome reported from mouse embryonic fibroblasts [7]. The 462 phagolysosomal proteins were sorted manually into 21 functional classes, out of which acid hydrolases represented the largest set. These included typical lysosomal proteins such as phosphatases, lipases, proteases, and glycosidases. Out of the proteases, the majority belonged to the cysteine proteases, some of which (TvCP2, TvCP3, TvCP4, TvCPT) had previously been shown to be secreted [153]. Proteases are key players in *T. vaginalis* virulence [149,150], which is not surprising given the large set of 440 peptidases encoded in the parasite's genome [40]. Seventeen proteins identified are involved in carbohydrate

metabolism, including glucanotransferases and a glycogen debranching enzyme. Furthermore, our proteomic analysis identified six acidifying v-ATPases and three ABC transporters that couple ATP hydrolysis with the transfer of cargo across membranes and have been observed to be involved in UPS [88]. The second-largest class that we identified is involved in vesicle formation and vesicular trafficking, which includes Rab proteins (including Rab7a), Vps proteins, SNARE complex proteins, clathrin, and adaptor proteins [164–166]. Furthermore, we identified 29 proteins that are connected to the cytoskeleton, which is in line with the established model of lysosomal movement along the cytoskeleton [134–136].

When the lysosomal proteome is compared to previous proteomic studies on hydrogenosomes [167], exosomes [168], and the cell surface [169], only a small overlap can be observed, which supports a correct organellar separation. However, as some lysosomal proteins reach their organellar destination through the indirect route employing the cell surface, and since lysosomes can serve as membrane reservoir for plasma membrane repairs, a certain overlap of the lysosomal proteome with the surface proteome is expected. A total of 55 proteins of our phagolysosomal proteome was also identified in the surface proteome [169]. These proteins include adhesins of the BspA family [170], the tetraspanin protein 1 (TSP1), which is associated with MVBs [168], β-hexosaminidase, the surface adhesin TvAD1 [171], a v-ATPase [169], and five *Trichomonas* beta-sandwich repeat (TBSR) proteins.

3.2 Lysosomal targeting

In metazoans, soluble lysosomal proteins are typically targeted via the M6P-dependent pathway, whereas in other eukaryotes, sorting of lysosomal hydrolases is independent of oligosaccharides. Alternative receptors such as sortilins/Vps10 and plant VSRs have been shown to directly recognize sequence motifs of the cargo protein [96], while the

recognition particle for the *Drosophila* lysosomal enzyme receptor protein LERP is still unknown [172]. Whereas Vps10 is conserved in most eukaryote lineages [105,173,174], no orthologue was found in the *T. vaginalis* genome [105]. Thus, we aimed to elucidate how lysosomal hydrolases are targeted in *T. vaginalis* in order to separate them from the secretory pathway.

3.2.1 Mannose-6-phosphate-like receptors

Interestingly, we identified six transmembrane proteins that are homologues to the mammalian MPR300 in the *T. vaginalis* genome, TvMPR-1 to TvMPR-6. Of these, TvMPR-1 to TvMPR-4 were also found in the phagolysosomal proteome. However, TvMPRs contain only five out of fifteen characteristic MRH domains and lack the M6P binding sites, which makes them more alike to *Drosophila* LERP. All TvMPRs contain either the Yxx*Ø* or DxxL[LI] sorting motif for the recognition by adaptor proteins, however, only TvMPR-1, -4, and -5 appeared to be type I membrane proteins similar to human MPR300 (hMPR300) and LERP. The other three TvMPRs possess two transmembrane domains that result in their C-terminal sorting motif to be in the lysosomal lumen and thus unrecognizable for cytosolic adaptor proteins. The homology to hMPR300 and the presence of sorting signals at the C-termini support TvMPRs role as receptors. However, as the M6P binding sites are missing, TvMPRs likely do not recognize cargo through M6P. Moreover, the searches for GlcNAc-PT and UCE in the *T. vaginalis* database using the human α/β GlcNAc-PT (Q3T906) and UCE (Q9UK23) amino acid sequences as queries did not reveal any homologues. The absence of GlcNAc-PT and UCE together with the lack of M6P recognition sites makes it unlikely that TvMPRs recognize lysosomal hydrolases through M6P modifications. Thus, we hypothesize that TvMPRs bind lysosomal cargo through features or modifications other than M6P.

3.2.2 Glycosylation dependent targeting to lysosomes

As we identified MPR-like proteins in *T. vaginalis*, we were interested in whether glycans are involved in the lysosomal targeting of hydrolases. First, we chose the lysosome resident Cathepsin L-like cysteine peptidase CLCP, which possesses two putative N-glycosylation sites Nx[ST]. Upon mutation of single amino acids of this motif, the localization of CLCP changed from lysosome-resident to being secreted. Then, we introduced both glycosylation sites of CLCP into the non-lysosomal, non-glycosylated β-amylase 2 (BA2). This introduction partially changed the protein location to the lysosomal compartment. Thus, glycosylations are involved in lysosomal targeting. However, as other proteins such as BA1 are also glycosylated but not targeted to lysosomes, we concluded that structural features such as a specific conformation are necessary to provide the lysosomal signal. Furthermore, whether TvMPRs or other receptors are involved in the sorting and recognition of glycosylated proteins needs to be elucidated in future studies.

3.3 Secretome

As secretion is the major pathway for virulence factors to reach host cells, and secreted proteins modulate host-parasite relationships, we were interested in elucidating the secretome of *T. vaginalis*. Secretome analysis of *T. vaginalis* revealed 89 proteins that are actively secreted in a time-dependent manner and are thus considered *bona fide* secreted proteins. The proteins were sorted manually into 13 functional groups. More than 1/3 of the secretome was represented by hydrolases. Identified proteins which might be involved in parasite virulence included DNaseII, pore-forming proteins, phospholipases, β-hexosaminidase, a single α-amylase, and β-amylases, some of which we also identified in the lysosomal proteome. Secreted phospholipases have been observed to kill bacteria [175] and possess antiviral activity [176], whereas β-

hexosaminidase is suggested to degrade host mucin [177]. This supports the fact that secreted proteins are key players in host-parasite relationships and *T. vaginalis* virulence. Interestingly, almost half of the secreted proteins (40) were previously found in the surface proteome [169], including TBSR proteins. This overlap of proteins is consistent with the finding that the surface rhomboid protease TvROM1 cleaves membrane-bound proteins [178] that are then released and thus identified in the secretome. Hence, the relatively large overlap of the secretome with the surface proteome highlights the dynamics in the localization of cell-associated and secreted proteins. The β-amylases that we identified in the secretome are a particularly interesting group of secreted proteins. We found four paralogues in the *T. vaginalis* genome (BA1-BA4). However, we showed that only BA1 and BA2 were secreted to the cell environment, whereas BA3 and BA4 were not. Experiments with brefeldin A (BFA), which leads to a retrograde transport from the Golgi to the ER, and FLI-06, which blocks TGN exit sites, further indicated that BA1 and BA2 are secreted through the classical secretory pathway. In contrast, BA3 and BA4 localized to lysosomes in fluorescence microscopy. These proteins hydrolyze α-1,4-linkages of glycogen [179,180] and thus represent important enzymes for the nutrient acquisition of *T. vaginalis* in the vaginal mucosa. By feeding on free glycogen, *T. vaginalis* competes with the vaginal microbiota including Lactobacilli that lack β-amylases [181].

3.4 Lysosomes in secretion

Lysosomes are known to be involved in protein secretion, and by fusing with the plasma membrane, this organelle can also repair membrane damage. Parasitic protists, however, depend on secreted factors for nutrient acquisition and fighting host cells, for which lysosomal hydrolases might represent powerful tools. Thus, we investigated whether *T. vaginalis* employs lysosomes for the secretion of lysosomal hydrolases.

3.4.1 Unconventional secretion of cysteine peptidases

To answer the question of whether *T. vaginalis* lysosomes are involved in unconventional protein secretion, we selected the two proteins TvCP2 and acid phosphatase that were identified in our phagolysosomal proteome as well as in the secretome. Upon incubation with CLQ, which blocks the endo-lysosomal pathway by increasing the lysosomal pH [160], and BFA, which increases a retrograde transport from the Golgi to the ER [182,183], we observed a decreased secretion of TvCP2 in both cases. We concluded that TvCP2 is indeed secreted via lysosomes. Surprisingly, acid phosphatase secretion was reduced only upon BFA treatment but was unaffected by CLQ. This indicates secretion along the classical secretory pathway like BA1 and BA2. Indeed, acid phosphatases have been described to travel to the plasma membrane, and in a second step, become internalized to reach the lysosomes [184,185].

The experiments with CLQ and BFA led us to the conclusion that *T. vaginalis* employs an unconventional secretory pathway through lysosomes to secrete hydrolases.

3.4.2 Overlap of lysosomal proteome and secretome

The phagolysosomal proteome (462 proteins) and the secretome (89 proteins) of *T. vaginalis* overlap by 26 proteins. The overlap includes hydrolases such as β-hexosaminidase, acid phosphatase, serine and cysteine peptidases, phospholipases, and glucosaminidase. This result indicates that not only TvCP2 is secreted through lysosomes, as we have shown experimentally, but a broad range of hydrolases might be unconventionally secreted by *T. vaginalis*. The parasite virulence has repeatedly been shown to rely on a massive set of proteases that its genome encodes [40,149,150]. An interesting investigation in future studies might be whether (and how)

the secretome of *T. vaginalis* changes upon contact with the host cells or bacteria and whether such a contact stimulates lysosomal secretion.

4. LIST OF PUBLICATIONS AND CONTRIBUTIONS

4.1 **Zimmann N**, Rada P, Žárský V, Smutná T, Záhonová K, Dacks J, Harant K, Hrdý I,Tachezy J (2021) Proteomic analysis of Trichomonas vaginalis phagolysosome, lysosomal targeting, and unconventional secretion of cysteine peptidases. *Molecular and Cellular Proteomics:* https://doi.org/10.1016/j.mcpro.2021.100174. IF 5.911

Contribution: Design and performance of the experiments, data analysis, manuscript preparation (75%)

4.2 Štáfková J, Rada P, Meloni D, Žárský V, Smutná T, **Zimmann N**, Harant K, Pompach P, Hrdý I, Tachezy J (2018) Dynamic secretome of Trichomonas vaginalis: Case study of β-amylases. *Molecular and Cellular Proteomics* 17(2): 304–320. IF 5.911

Contribution: Lactoferrin assay, immunofluorescence microscopy (15%)

5. ABBREVIATIONS

ABP	Actin-binding protein
AKR	Aldo-keto reductase family
AP	Adaptor protein
Atg	Autophagy-related gene
BA	β-amylase
BFA	Brefeldin A
CaBP	Calcium-binding protein
CD-MPR	Cation-dependent MPR
CGN	Cis-Golgi body
CI-MPR	Cation-independent MPR
CLCP	Cathepsin L-like cysteine peptidase
CLQ	Chloroquine
CPBF	Cysteine peptidase-binding protein family
CPS	Conventional protein secretion
ER	Endoplasmic reticulum
ERAD	ER-associated degradation pathway
ERES	ER-exit site
FITC	Fluorescein isothiocyanate
GGA	Golgi-localized, γ-ear-containing, ADP ribosylation factor-binding protein

GlcNAc-PT	N-acetylglucosamine-1-phosphotransferase
Golgi	Golgi body
hMPR300	Human MPR300
LAMP	Lysosome-associated membrane protein
LERP	Lysosomal enzyme receptor protein
LIMP	Lysosomal integral membrane protein
M6P	Mannose-6-phosphate
MPR	M6P-receptor
MPR46	46 kDa MPR
MPR300	300 kDa MPR
MRH	M6P receptor homology
MVB	Multivesicular body
SNARE	Soluble N-ethylmaleimide-sensitive factor-attachment receptor
sPDI	Soluble protein disulfide isomerase
SP	Signal peptide
SRP	Signal recognition particle
t-LTS	Lysosomal targeting sequence of a transmembrane protein
TBSR	*Trichomonas* beta-sandwich repeat
TGN	Trans-Golgi body
TSP1	Tetraspanin protein 1

TvMPR	*Trichomonas vaginalis* MPR
UCE	Uncovering enzyme
UPS	Unconventional protein secretion
v-ATPase	Vacuolar-type ATPase
VSR	Vacuolar sorting receptor

6. REFERENCES

1. Appelmans, F., Wattiaux, R., de Duve, C. (1955) Tissue fractionation studies. 5. The association of acid phosphatase with a special class of cytoplasmic granules in rat liver. Biochem. J. 59, 438-445

2. de Duve, C. (1959) Lysosomes, a new group of cytoplasmic particles. In: Hayashi, T. (Ed.) Subcellular Particles, pp. 128–159, Ronald Press

3. Novikoff, A. B. (1961) Lysosomes and related particles. In: Bracket, J., Mirsky, A. E. (Eds.) The Cell, pp. 423–488, Academic Press

4. de Duve, C. (1963) Structure and functions of lysosomes. In: Funktionelle und Morphologische Organisation der Zelle, pp. 209–218, Springer

5. Bainton, D.F. (1981) The discovery of lysosomes. J. Cell Biol. 91, 66–76

6. de Duve, C. (2005) The lysosome turns fifty. Nat. Cell Biol. 7, 847–849

7. Mosen, P., Sanner, A., Singh, J., Winter, D. (2021) Targeted quantification of the lysosomal proteome in complex samples. Proteomes 9, 1–17

8. Bonam, S. R., Wang, F., Muller, S. (2019) Lysosomes as a therapeutic target. Nat. Rev. Drug Discov. 18, 923–948

9. Appelqvist, H., Wäster, P., Kågedal, K., Öllinger, K. (2013) The lysosome: From waste bag to potential therapeutic target. J. Mol. Cell Biol. 5, 214–226

10. Soldati, T., Neyrolles, O. (2012) Mycobacteria and the intraphagosomal environment: Take it with a pinch of salt(s)! Traffic 13, 1042–1052

11. Watts, C. (2012) The endosome–lysosome pathway and information generation in the immune system. Biochim. Biophys. Acta. 1824, 14-21

12. Marrero, M. C., Barrio-Hernandez, I. (2021) Toward understanding the biochemical determinants of protein degradation rates. ACS Omega 6, 5091-5100

13. Wang, X., Robbins, J. (2014) Proteasomal and lysosomal protein degradation and heart disease. J. Mol. Cell. Cardiol. 71, 16-24

14. Saftig, P., Klumperman, J. (2009) Lysosome biogenesis and lysosomal membrane proteins: Trafficking meets function. Nat. Rev. Mol. Cell Biol. 10, 623–635

15. Lloyd, J. B. (1996) Metabolite efflux and influx across the lysosome membrane. Subcell. Biochem. 27, 361–386

16. Perera, R. M., Zoncu, R. (2016) The lysosome as a regulatory hub. Annu. Rev. Cell Dev. Biol. 32, 223–253

17. Xu, H., Ren, D. (2015) Lysosomal physiology. Annu. Rev. Physiol. 77, 57–80

18. Castonguay, A. C., Lasanajak, Y., Song, X., Olson, L. J., Cummings, R. D., Smith, D. F., Dahms, N. M. (2012) The glycan-binding properties of the cation-independent mannose 6-phosphate receptor are evolutionary conserved in vertebrates. Glycobiology 22, 983–996

19. Lüllmann-Rauch, R. (2005) History and morphology of the lysosome. Eurekah Bioscience 1, 251–258

20. Saftig, P., Schröder, B., Blanz, J. (2010) Lysosomal membrane proteins: Life between acid and neutral conditions. Biochem. Soc. Trans. 38, 1420–1423

21. Dell'Angelica, E. C., Mullins, C., Caplan, S., Bonifacino, J. S. (2000) Lysosome-related organelles. FASEB J. 14, 1265–1278

22. Huizing, M., Helip-Wooley, A., Westbroek, W., Gunay-Aygun, M., Gahl, W. A. (2008) Disorders of lysosome-related organelle biogenesis: Clinical and molecular genetics. Annu. Rev. Genomics Hum. Genet. 9, 359-386

23. Armstrong, J. (2010) Yeast vacuoles: More than a model lysosome. Trends Cell Biol. 20, 580–585

24. Li, S. C., Kane, P. M. (2009) The yeast lysosome-like vacuole: Endpoint and crossroads. Biochim. Biophys. Acta 1793, 650–663

25. Tan, X., Li, K., Wang, Z., Zhu, K., Tan, X., Cao, J. (2019) A review of plant vacuoles: Formation, located proteins, and functions. Plants 8, doi: 10.3390/plants8090327

26. Inpanathan, S., Botelho, R. J. (2019) The lysosome signaling platform: Adapting with the times. Front. Cell Dev. Biol. 7, doi: 10.3389/fcell.2019.00113

27. Doherty, G. J., McMahon, H. T. (2009) Mechanisms of endocytosis. Annu. Rev. Biochem. 78, 857-902

28. Naslavsky, N., Caplan, S. (2018) The enigmatic endosome – sorting the ins and outs of endocytic trafficking. J. Cell Sci. 131, doi: 10.1242/jcs.216499

29. Futter, C. E., Pearse, A., Hewlett, L. J., Hopkins, C. R. (1996) Multivesicular endosomes containing internalized EGF-EGF receptor complexes mature and then fuse directly with lysosomes. J. Cell Biol. 132, 1011–1023

30. Hyttinen, J. M. T., Niittykoski, M., Salminen, A., Kaarniranta, K. (2013) Maturation of autophagosomes and endosomes: A key role for Rab7. Biochim. Biophys. Acta 1833, 503–510

31. Scott, C. C., Vacca, F., Gruenberg, J. (2014) Endosome maturation, transport and functions. Semin. Cell Dev. Biol. 31, 2–10

32. Ganley, I. G. (2013) Autophagosome maturation and lysosomal fusion. Essays Biochem. 55, 65–78

33. Brighouse, A., Dacks, J. B., Field, M. C. (2010) Rab protein evolution and the history of the eukaryotic endomembrane system. Cell. Mol. Life Sci. 67, 3449-3465

34. Poteryaev, D., Datta, S., Ackema, K., Zerial, M., Spang, A. (2010) Identification of the switch in early-to-late endosome transition. Cell 141, 497–508

35. Uribe-Querol, E., Rosales, C. (2020) Phagocytosis: Our current understanding of a universal biological process. Front. Immunol. 11, doi: 10.3389/fimmu.2020.01066

36. Verma, K., Datta, S. (2017) The monomeric GTPase Rab35 regulates phagocytic cup formation and phagosomal maturation in *Entamoeba histolytica*. J. Biol. Chem. 292, 4960–4975

37. Lim, J. J., Grinstein, S., Roth, Z. (2017) Diversity and versatility of phagocytosis: Roles in innate immunity, tissue remodeling, and homeostasis. Front. Cell. Infect. Microbiol. 7, doi: 10.3389/fcimb.2017.00191

38. Okada, M., Nozaki, T. (2006) New insights into molecular mechanisms of phagocytosis in *Entamoeba histolytica* by proteomic analysis. Arch. Med. Res. 37, 244–252

39. Rath, P. P., Gourinath, S. (2020) The actin cytoskeleton orchestra in *Entamoeba histolytica*. Proteins 88, 1361–1375

40. Carlton, J. M., Hirt, R. P., Silva, J. C., Delcher, A. L., Schatz, M., Zhao, Q., Wortman, J. R., Bidwell, S. L., Alsmark, U. C. M., Besteiro, S., Sicheritz-Ponten, T., Noel, C. J., Dacks, J. B., Foster, P. G., Simillion, C., Van de Peer, Y., Miranda-Saavedra, D., Barton, G. J., Westrop, G. D., Müller, S., Dessi, D., Fiori,

P. L., Ren, Q., Paulsen, I., Zhang, H., Bastida-Corcuera, F. D., Simoes-Barbosa, A., Brown, M. T., Hayes, R. D., Mukherjee, M., Okumura, C. Y., Schneider, R., Smith, A. J., Vanacova, S., Villalvazo, M., Haas, B. J., Pertea, M., Feldblyum, T. V., Utterback, T. R., Shu, C. L., Osoegawa, K., de Jong, P. J., Hrdy, I., Horvathova, L., Zubacova, Z., Dolezal, P., Malik, S. B., Logsdon, J. M., Henze, K., Gupta, A., Wang, C. C., Dunne, R. L., Upcroft, J. A., Upcroft, P., White, O., Salzberg, S. L., Tang, P., Chiu, C. H., Lee, Y. S., Embley, T. M., Coombs, G. H., Mottram, J. C., Tachezy, J., Fraser-Liggett, C. M., Johnson, P. J. (2007) Draft genome sequence of the sexually transmitted pathogen *Trichomonas vaginalis*. Science 315, 207–212

41. Vandekerckhove, J., Weber, K. (1978) At least six different actins are expressed in a higher mammal: An analysis based on the amino acid sequence of the amino-terminal tryptic peptide. J. Mol. Biol. 126, 783–802

42. Hon, C. C., Nakada-Tsukui, K., Nozaki, T., Guillén, N. (2010) Dissecting the actin cytoskeleton of *Entamoeba histolytica* from a genomic perspective. In: Clark, C. G., Johnson, P. J., Adam, R. D. (Eds.) Anaerobic Parasitic Protozoa: Genomics and Molecular Biology, doi: 10.21775/9781912530076, Caister Academic Press

43. Bailey, G. B., Day, D. B., Gasque, J. W. (1985) Rapid polymerization of *Entamoeba histolytica* actin induced by interaction with target cells. J. Exp. Med. 162, 546-558

44. Babuta, M., Bhattacharya, S., Bhattacharya, A. (2020) *Entamoeba histolytica* and pathogenesis: A calcium connection. PLoS Pathog. 16, doi: 10.1371/journal.ppat.1008214

45. Somlata, N., Kamanna, S., Agrahari, M., Babuta, M., Bhattacharya, S., Bhattacharya, A. (2012) Autophosphorylation of Ser428 of EhC2PK plays a

critical role in regulating erythrophagocytosis in the parasite *Entamoeba histolytica*. J. Biol. Chem. 287, 10844–10852

46. Somlata, N., Bhattacharya, S., Bhattacharya, A. (2011) A C2 domain protein kinase initiates phagocytosis in the protozoan parasite *Entamoeba histolytica*. Nat. Commun. 2, doi: 10.1038/ncomms1199

47. Aslam, S., Bhattacharya, S., Bhattacharya, A. (2012) The calmodulin-like calcium binding protein EhCaBP3 of *Entamoeba histolytica* regulates phagocytosis and is involved in actin dynamics. PLOS Pathog. 8, e1003055

48. Kruth, H. S. (2011) Receptor-independent fluid-phase pinocytosis mechanisms for induction of foam cell formation with native low-density lipoprotein particles. Curr. Opin. Lipidol. 22, 386-393

49. King, J. S., Kay, R. R. (2019) The origins and evolution of macropinocytosis. Philos. Trans. R. Soc. Lond. B. Biol. Sci. 374, doi: 10.1098/rstb.2018.0158

50. Sutak, R., Chamot, C., Tachezy, J., Camadro, J. M., Lesuisse, E. (2004) Siderophore and haem iron use by *Tritrichomonas foetus*. Microbiology Reading 150, 3979–3987

51. Costamagna, S. R., Figueroa, M. P. (2001) On the ultrastructure of *Trichomonas vaginalis*: Cytoskeleton, endocytosis and hydrogenosomes. Parasitología al día 25, 100–108

52. Buckley, C. M., King, J. S. (2017) Drinking problems: Mechanisms of macropinosome formation and maturation. FEBS J. 284, 3778–3790

53. Zhao, Y. G., Zhang, H. (2019) Autophagosome maturation: An epic journey from the ER to lysosomes. J. Cell Biol. 218, 757–770

54. Reggiori, F., Ungermann, C. (2017) Autophagosome maturation and fusion. J. Mol. Biol. 429, 486–496

55. Benchimol, M. (1999) Hydrogenosome autophagy: An ultrastructural and cytochemical study. Biol. Cell 91, 165–174

56. Huang, K. Y., Chen, R. M., Lin, H. C., Cheng, W. H., Lin, H. A., Lin, W. N., Huang, P. J., Chiu, C. H., Tang, P. (2019) Potential role of autophagy in proteolysis in *Trichomonas vaginalis*. J. Microbiol. Immunol. Infect. 52, 336–344

57. Bettadapur, A., Miller, H. W., Ralston, K. S. (2020) Biting off what can be chewed: Trogocytosis in health, infection, and disease. Infect. Immun. 88, e00930-19

58. Weinhard, L., di Bartolomei, G., Bolasco, G., Machado, P., Schieber, N., Neniskyte, U., Exiga, M., Vadisiute, A., Raggioli, A., Schertel, A., Schwab, Y., Gross, C. T. (2018) Microglia remodel synapses by presynaptic trogocytosis and spine head filopodia induction. Nat. Commun. 9, doi: 10.1038/s41467-018-03566-5

59. Mercer, F., Ng, S. H., Brown, T. M., Boatman, G., Johnson, P. J. (2018) Neutrophils kill the parasite *Trichomonas vaginalis* using trogocytosis. PLoS Biol. 16, doi: 10.1371/journal.pbio.2003885

60. Velmurugan, R., Challa, D., Ram, S., Ober, R., Ward, E. (2016) Macrophage-mediated trogocytosis leads to death of antibody-opsonized tumor cells. Mol. Cancer Ther. 15, 1879–1889

61. Ralston, K. S., Solga, M. D., Mackey-Lawrence, N. M., Somlata, Bhattacharya, A., Petri, W. A. (2014) Trogocytosis by *Entamoeba histolytica* contributes to cell killing and tissue invasion. Nature 508, 526–530

62. Culbertson, C. G. (1971) The pathogenicity of soil amebas. Annu. Rev. Microbiol. 25, 231–254

63. Culbertson, C. G. (1970) Pathogenic *Naegleria* and *Hartmannella* (*Acanthamoeba*). Annals of the New York Academy of Sciences 174, 1018–1022

64. Brown, T. (1979) Observations by immunofluorescence microscopy and electron microscopy on the cytopathogenicity of *Naegleria fowleri* in mouse embryo-cell cultures. J. Med. Microbiol. 12, 363–371

65. Somlata, Nakada-Tsukui, K., Nozaki, T. (2017) AGC family kinase 1 participates in trogocytosis but not in phagocytosis in *Entamoeba histolytica*. Nat. Commun. 8, doi: 10.1038/s41467-017-00199-y

66. Dance, A. (2019) Core Concept: Cells nibble one another via the under-appreciated process of trogocytosis. Proc. Natl. Acad. Sci. U. S. A. 116, 17608–17610

67. Van Leeuwen, W., Van der Krift, F., Rabouille, C. (2018) Modulation of the secretory pathway by amino-acid starvation. J. Cell Biol. 217, 2261-2271

68. Rabouille, C., Malhotra, V., Nickel, W. (2012) Diversity in unconventional protein secretion. J. Cell Sci. 125, 5251–5255

69. Ponpuak, M., Mandell, M., Kimura, T., Chauhan, S., Cleyrat, C., Deretic, V. (2015) Secretory autophagy. Curr. Opin. Cell Biol. 35, 106-116

70. Viotti, C. (2016) ER to Golgi-dependent protein secretion: The conventional pathway. Methods Mol. Biol. 1459, 3–29

71. Delic, M., Valli, M., Graf, A., Pfeffer, M., Mattanovich, D., Gasser, B. (2013) The secretory pathway: Exploring yeast diversity. FEMS Microbiol. Rev. 37, 872–914

72. Park, S., Arrell, D. K., Reyes, S., Park, E. Y., Terzic, A. (2017) Conventional and unconventional secretory proteins expressed with silkworm bombyxin

signal peptide display functional fidelity. Sci. Rep. 7, doi: 10.1038/s41598-017-14833-8

73. Lodish, H., Berk, A., Zipursky, S. L., Matsudaira, P., Baltimore, D., Darnell, J. (2000) Overview of the secretory pathway. In: Lodish, H., Berk, A., Zipursky, S. L., Matsudaira, P., Baltimore, D., Darnell, J., Molecular Cell Biology, 4th edition, pp. Section 17.3, W. H. Freeman

74. Burda, P., Aebi, M. (1999) The dolichol pathway of N-linked glycosylation. Biochim. Biophys. Acta 1426, 239–257

75. Štáfková, J., Rada, P., Meloni, D., Žárský, V., Smutná, T., Zimmann, N., Harant, K., Pompach, P., Hrdý, I., Tachezy, J. (2018) Dynamic secretome of *Trichomonas vaginalis*: Case study of β-amylases. Mol. Cell. Proteomics 17, 304-320

76. Samuelson, J., Banerjee, S., Magnelli, P., Cui, J., Kelleher, D. J., Gilmore, R., Robbins, P. W. (2005) The diversity of dolichol-linked precursors to Asn-linked glycans likely results from secondary loss of sets glycosyltranferases. Proc. Natl. Acad. Sci. U. S. A. 102, 1548–1553

77. Roth, J., Zuber, C., Park, S., Jang, I., Lee, Y., Kysela, K. G., Fourn, V. L., Santimaria, R., Guhl, B., Cho, J. W. (2010) Protein N-glycosylation, protein folding, and protein quality control. Mol. Cells 30, 497–506

78. Schrag, J. D., Procopio, D. O., Cygler, M., Thomas, D. Y., Bergeron, J. J. M. (2003) Lectin control of protein folding and sorting in the secretory pathway. Trends Biochem. Sci. 28, 49–57

79. Farhan, H., Rabouille, C. (2011) Signalling to and from the secretory pathway. J. Cell Sci. 124, 171–180

80. Sreelatha, A., Kinch, L. N., Tagliabracci, V. S. (2015) The secretory pathway kinases. Biochim. Biophys. Acta 1854, 1687-1693

81. Pidoux, A. L., Armstrong, J. (1992) Analysis of the BiP gene and identification of an ER retention signal in *Schizosaccharomyces pombe*. EMBO J. 11, 1583-1591

82. Rada, P., Kellerová, P., Verner, Z., Tachezy, J. (2019) Investigation of the secretory pathway in *Trichomonas vaginalis* argues against a moonlighting function of hydrogenosomal enzymes. J. Eukaryot. Microbiol. 66, 899–910

83. Bennett, M. K., Scheller, R. H. (1993) The molecular machinery for secretion is conserved from yeast to neurons. Proc. Natl. Acad. Sci. U. S. A. 90, 2559-2563

84. Blagoveshchenskaya, A., Fei, Y. C., Rohde, H. M., Glover, G., Knödler, A., Nicolson, T., Boehmelt, G., Mayinger, P. (2008) Integration of Golgi trafficking and growth factor signaling by the lipid phosphatase SAC1. J. Cell Biol. 180, 803–812

85. Nickel, W. (2010) Pathways of unconventional protein secretion. Curr. Opin. Biotechnol. 21, 621–626

86. Cohen, M. J., Chirico, W. J., Lipke, P. N. (2020) Through the back door: Unconventional protein secretion. Cell Surf. 6, doi: 10.1016/j.tcsw.2020.100045

87. Auron, P. E., Webb, A. C., Rosenwasser, L. J., Mucci, S. F., Rich, A., Wolff, S. M., Dinarello, C. A. (1984) Nucleotide sequence of human monocyte interleukin 1 precursor cDNA. Proc. Natl. Acad. Sci. U. S. A. 81, 7907–7911

88. Balmer, E. A., Faso, C. (2021) The road less traveled? Unconventional protein secretion at parasite-host interfaces. Front. Cell Dev. Biol. 9, doi: 10.3389/fcell.2021.662711

89. Popa, S. J., Stewart, S. E., Moreau, K. (2018) Unconventional secretion of annexins and galectins. Semin. Cell Dev. Biol. 83, 42-50

90. Kim, J., Gee, H. Y., Lee, M. G. (2018) Unconventional protein secretion - new insights into the pathogenesis and therapeutic targets of human diseases. J. Cell Sci. 131, doi: 10.1242/jcs.213686

91. Villeneuve, J., Bassaganyas, L., Lepreux, S., Chiritoiu, M., Costet, P., Ripoche, J., Malhotra, V., Schekman, R. (2018) Unconventional secretion of FABP4 by endosomes and secretory lysosomes. J. Cell Biol. 217, 649–665

92. Martín-Sánchez, F., Diamond, C., Zeitler, M., Gomez, A., Baroja-Mazo, A., Bagnall, J., Spiller, D., White, M., Daniels, M. J. D., Mortellaro, A., Penalver, M., Paszek, P., Steringer, J. P., Nickel, W., Brough, D., Pelegrin, P. (2016) Inflammasome-dependent IL-1β release depends upon membrane permeabilisation. Cell Death Differ. 23, 1219–1231

93. Heilig, R., Dick, M., Sborgi, L., Meunier, E., Hiller, S., Broz, P. (2018) The gasdermin-D pore acts as a conduit for IL-1β secretion in mice. Eur. J. Immunol. 48, 584–592

94. Rubartelli, A., Cozzolino, F., Talio, M., Sitia, R. (1990) A novel secretory pathway for interleukin-1 beta, a protein lacking a signal sequence. EMBO J. 9, 1503-1510

95. Braulke, T., Bonifacino, J. S. (2009) Sorting of lysosomal proteins. Biochim. Biophys. Acta 1793, 605–614

96. Lousa, C. D. M., Denecke, J. (2016) Lysosomal and vacuolar sorting: Not so different after all! Biochem. Soc. Trans. 44, 891–897

97. Ni, X., Canuel, M., Morales, C. R. (2006) The sorting and trafficking of lysosomal proteins. Histol. Histopathol. 21, 899–913

98. Yuan, L., Carvelli, F. L., Morales, C. R. (2012) Dynamic microscopy: Reconstructing a novel lysosomal trafficking pathway. In: Mendez-Vilas, A. (Ed.) Current Microscopy Contributions to Advances in Science and Technology, pp. 445-457, Formatex

99. Coutinho, M. F., Prata, M. J., Alves, S. (2012) Mannose-6-phosphate pathway: A review on its role in lysosomal function and dysfunction. Mol. Genet. Metab. 105, 542–550

100. Bonifacino, J. S., Traub, L. M. (2003) Signals for sorting of transmembrane proteins to endosomes and lysosomes. Annu. Rev. Biochem. 72, 395–447

101. Rouillé, Y., Rohn, W., Hoflack, B. (2000) Targeting of lysosomal proteins. Semin. Cell Dev. Biol. 11, 165–171

102. Höning, S., Sandoval, I. V., von Figura, K. (1998) A di-leucine-based motif in the cytoplasmic tail of LIMP-II and tyrosinase mediates selective binding of AP-3. EMBO J. 17, 1304–1314

103. Kyttälä, A., Yliannala, K., Schu, P., Jalanko, A., Luzio, J. P. (2005) AP-1 and AP-3 facilitate lysosomal targeting of Batten disease protein CLN3 via its dileucine motif. J. Biol. Chem. 280, 10277–10283

104. Puertollano, R., Aguilar, R. C., Gorshkova, I., Crouch, R. J., Bonifacino, J. S. (2001) Sorting of mannose 6-phosphate receptors mediated by the GGAs. Science 292, 1712–1716

105. Koumandou, V. L., Klute, M. J., Herman, E. K., Nunez-Miguel, R., Dacks, J. B., Field, M. C. (2011) Evolutionary reconstruction of the retromer complex and its function in *Trypanosoma brucei*. J. Cell Sci. 124, 1496–1509

106. Peden, A. A., Oorschot, V., Hesser, B. A., Austin, C. D., Scheller, R. H., Klumperman, J. (2004) Localization of the AP-3 adaptor complex defines a

novel endosomal exit site for lysosomal membrane proteins. J. Cell Biol. 164, 1065–1076

107. Janvier, K., Bonifacino, J. S. (2005) Role of the endocytic machinery in the sorting of lysosome-associated membrane proteins. Mol. Biol. Cell 16, 4231–4242.

108. Nakada-Tsukui, K., Tsuboi, K., Furukawa, A., Yamada, Y., Nozaki, T. (2012) A novel class of cysteine protease receptors that mediate lysosomal transport. Cell. Microbiol. 14, 1299–1317

109. Rajkumar, V., Dumpa, V. (2021) Lysosomal storage disease. In: StatPearls, https://www.ncbi.nlm.nih.gov/books/NBK563270/

110. Schröder, B. A., Wrocklage, C., Hasilik, A., Saftig, P. (2010) The proteome of lysosomes. Proteomics 10, 4053–4076

111. Zhang, H., Fan, X., Bagshaw, R. D., Zhang, L., Mahuran, D. J., Callahan, J. W. (2007) Lysosomal membranes from beige mice contain higher than normal levels of endoplasmic reticulum proteins. J. Proteome Res. 6, 240–249

112. Schröder, B., Wrocklage, C., Pan, C., Jäger, R., Kösters, B., Schäfer, H., Elsässer, H. P., Mann, M., Hasilik, A. (2007) Integral and associated lysosomal membrane proteins. Traffic 8, 1676–1686

113. Akter, F., Ponnaiyan, S., Kögler-Mohrbacher, B., Bleibaum, F., Damme, M., Renard, B. Y., Winter, D. (2020) Multi cell line analysis of lysosomal proteomes reveals unique features and novel lysosomal proteins. bioRxiv, doi: https://doi.org/10.1101/2020.12.21.423747

114. Ballabio, A. (2016) The awesome lysosome. EMBO Mol. Med. 8, 73-76

115. Eskelinen, E. L. (2006) Roles of LAMP-1 and LAMP-2 in lysosome biogenesis and autophagy. Mol. Aspects Med. 27, 495–502

116. Schwake, M., Schröder, B., Saftig, P. (2013) Lysosomal membrane proteins and their central role in physiology. Traffic 14, 739–748

117. Fukuda, M. (1991) Lysosomal membrane glycoproteins. Structure, biosynthesis, and intracellular trafficking. J. Biol. Chem. 266, 21327–21330

118. Granger, B., Green, S., Gabel, C., Howe, C., Mellman, I., Helenius, A. (1990) Characterization and cloning of lgp110, a lysosomal membrane glycoprotein from mouse and rat cells. J. Biol. Chem. 265, 12036–12043

119. Rajapakshe, A. R., Podyma-Inoue, K. A., Terasawa, K., Hasegawa, K., Namba, T., Kumei, Y., Yanagishita, M., Hara-Yokoyama, M. (2015) Lysosome-associated membrane proteins (LAMPs) regulate intracellular positioning of mitochondria in MC3T3-E1 cells. Exp. Cell Res. 331, 211–222

120. Mindell, J. A. (2012) Lysosomal acidification mechanisms. Annu. Rev. Physiol. 74, 69–86

121. Ohkuma, S., Moriyama, Y., Takano, T. (1982) Identification and characterization of a proton pump on lysosomes by fluorescein-isothiocyanate-dextran fluorescence. Proc. Natl. Acad. Sci. U. S. A. 79, 2758–2762

122. Bagshaw, R. D., Mahuran, D. J., Callahan, J. W. (2005) A proteomic analysis of lysosomal integral membrane proteins reveals the diverse composition of the organelle. Mol. Cell. Proteomics 4, 133–143

123. Bissa, B., Beedle, A. M., Govindarajan, R. (2016) Lysosomal solute carrier transporters gain momentum in research. Clin. Pharmacol. Ther. 100, 431–436.

124. Lübke, T., Lobel, P., Sleat, D. (2009) Proteomics of the lysosome. Biochim. Biophys. Acta 1793, 625-635

125. Trivedi, P. C., Bartlett, J. J., Pulinilkunnil, T. (2020) Lysosomal biology and function: Modern view of cellular debris bin. Cells 9, doi: 10.3390/cells9051131

126. Willstätter, R., Bamann, E. (1929) Über die Proteasen der Magenschleimhaut. Erste Abhandlung über die Enzyme der Leukocyten. Biol. Chem. 180, 127–143

127. Müller, S., Dennemärker, J., Reinheckel, T. (2012) Specific functions of lysosomal proteases in endocytic and autophagic pathways. Biochim. Biophys. Acta 1824, 34-43

128. Gocheva, V., Joyce, J. A. (2007) Cysteine cathepsins and the cutting edge of cancer invasion. Cell Cycle 6, 60–64

129. Mort, J. S., Recklies, A. D, Poole, A. R. (1984) Extracellular presence of the lysosomal proteinase cathepsin B in rheumatoid synovium and its activity at neutral pH. Arthritis Rheum. 27, 509–515

130. Turk, V., Stoka, V., Vasiljeva, O., Renko, M., Sun, T., Turk, B., Turk, D. (2012) Cysteine cathepsins: From structure, function and regulation to new frontiers. Biochim. Biophys. Acta 1824, 68–88

131. Ashtari, N., Jiao, X., Rahimi-Balaei, M., Amiri, S., Mehr, S. E., Yeganeh, B., Marzban, H. (2016) Lysosomal acid phosphatase biosynthesis and dysfunction: A mini review focused on lysosomal enzyme dysfunction in brain. Curr. Mol. Med. 16, 439–446

132. Sun, P., Sleat, D. E., Lecocq, M., Hayman, A. R., Jadot, M., Lobel, P. (2008) Acid phosphatase 5 is responsible for removing the mannose 6-phosphate recognition marker from lysosomal proteins. Proc. Natl. Acad. Sci. U. S. A. 105, 16590–16595

133. Solovyeva, V. V., Shaimardanova, A. A., Chulpanova, D. S., Kitaeva, K. V., Chakrabarti, L., Rizvanov, A. A. (2018) New approaches to Tay-Sachs disease therapy. Front. Physiol. 9, doi: 10.3389/fphys.2018.01663

134. Caviston, J. P., Holzbaur, E. L. F. (2006) Microtubule motors at the intersection of trafficking and transport. Trends Cell Biol. 16, 530–537

135. Krendel, M., Mooseker, M. S. (2005) Myosins: Tails (and heads) of functional diversity. Physiology (Bethesda) 20, 239–251

136. Bálint, Š., Vilanova, I. V., Álvarez, Á. S., Lakadamyali, M. (2013) Correlative live-cell and superresolution microscopy reveals cargo transport dynamics at microtubule intersections. Proc. Natl. Acad. Sci. U. S. A. 110, 3375–3380

137. Pu, J., Guardia, C. M., Keren-Kaplan, T., Bonifacino, J. S. (2016) Mechanisms and functions of lysosome positioning. J. Cell Sci. 129, 4329-4339

138. Rowley, J., Hoorn, S. V., Korenromp, E., Low, N., Unemo, M., Abu-Raddad, L. J., Chico, R. M., Smolak, A., Newman, L., Gottlieb, S., Thwin, S. S., Broutet, N., Taylor, M. M. (2019) Chlamydia, gonorrhoea, trichomoniasis and syphilis: Global prevalence and incidence estimates, 2016. Bull. World Health Organ. 97, 548-562

139. Leitsch, D. (2021) Recent advances in the molecular biology of the protist parasite *Trichomonas vaginalis*. Fac. Rev. 10, doi: 10.12703/r/10-26

140. Van Gerwen, O. T., Muzny, C. A. (2019) Recent advances in the epidemiology, diagnosis, and management of *Trichomonas vaginalis* infection. F1000Res. 8, doi: 10.12688/f1000research.19972.1

141. Kissinger, P. (2015) *Trichomonas vaginalis*: A review of epidemiologic, clinical and treatment issues. BMC Infect. Dis. 15, doi: 10.1186/s12879-015-1055-0

142. Kusdian, G, Gould, S. B. (2014) The biology of *Trichomonas vaginalis* in the light of urogenital tract infection. Mole. Biochem. Parasitol. 198, 92–99

143. Rendón-Maldonado, J. G., Espinosa-Cantellano, M., González-Robles, A., Martínez-Palomo, A. (1998) *Trichomonas vaginalis*: In vitro phagocytosis of lactobacilli, vaginal epithelial cells, leukocytes, and erythrocytes. Exp. Parasitol. 89, 241–250

144. Martin, D. H., Zozaya, M., Lillis, R. A., Myers, L., Nsuami, M. J., Ferris, M. J. (2013) Unique vaginal microbiota that includes an unknown *Mycoplasma*-like organism is associated with *Trichomonas vaginalis* infection. J. Infect. Dis. 207, 1922-1931

145. Phukan, N., Parsamand, T., Brooks, A., Nguyen, T., Simoes-Barbosa, A. (2013) The adherence of *Trichomonas vaginalis* to host ectocervical cells is influenced by lactobacilli. Sex. Transm. Infect. 89, 455–459

146. Brotman, R. M., Bradford, L. L., Conrad, M., Gajer, P., Ault, K., Peralta, L., Forney, L. J., Carlton, J. M., Abdo, Z., Ravel, J. (2012) Association between *Trichomonas vaginalis* and vaginal bacterial community composition among reproductive-age women. Sex. Transm. Dis. 39, 807-812

147. Chiu, S. F., Huang, P. J., Cheng, W. H., Huang, C. Y., Chu, L. J., Lee, C. C., Lin, H. C., Chen, L. C., Lin, W. N., Tsao, C. H., Tang, P., Yeh, Y. M., Huang, K. Y. (2021) Vaginal microbiota of the sexually transmitted infections caused by *Chlamydia trachomatis* and *Trichomonas vaginalis* in women with vaginitis in Taiwan. Microorganisms 9, doi: https://doi.org/10.3390/microorganisms9091864

148. Fiori, P. L., Rappelli, P., Rocchigiani, A. M., Cappuccinelli, P. (1993) *Trichomonas vaginalis* haemolysis: Evidence of functional pores formation on red cell membranes. FEMS Microbiol. Letters. 109, 13–18

149. Arroyo, R., Cárdenas-Guerra, R. E., Figueroa-Angulo, E. E., Puente-Rivera, J., Zamudio-Prieto, O., Ortega-López, J. (2015) *Trichomonas vaginalis* cysteine proteinases: Iron response in gene expression and proteolytic activity. BioMed. Res. Int. 2015, doi: 10.1155/2015/946787

150. Hernández, H. M., Marcet, R., Sarracent, J. (2014) Biological roles of cysteine proteinases in the pathogenesis of *Trichomonas vaginalis*. Parasite. 21, doi: 10.1051/parasite/2014054

151. Piña-Vázquez, C., Reyes-López, M., Ortíz-Estrada, G., de La Garza, M., Serrano-Luna, J. (2012) Host-parasite interaction: Parasite-derived and -induced proteases that degrade human extracellular matrix. J. Parasitol. Res. 2012, doi:10.1155/2012/748206

152. Carvajal-Gamez, B. I., Quintas-Granados, L. I., Arroyo, R., Vázquez-Carrillo, L. I., Ramón-Luing, L. D. L. A., Carrillo-Tapia, E., Alvarez-Sanchez, M. E. (2014) Putrescine-dependent re-localization of TvCP39, a cysteine proteinase involved in *Trichomonas vaginalis* cytotoxicity. PLoS One. 9, doi: 10.1371/journal.pone.0107293

153. Sommer, U., Costello, C. E., Hayes, G. R., Beach, D. H., Gilbert, R. O., Lucas J. J., Singh, B. N. (2005) Identification of *Trichomonas vaginalis* cysteine proteases that induce apoptosis in human vaginal epithelial cells. J. Biol. Chem. 280, 23853–23860

154. Rendón-Gandarilla, F. J., Ramón-Luing, L. D. L. A., Ortega-López, J., De Andrade, I. R., Benchimol, M., Arroyo, R. (2013) The TvLEGU-1, a legumain-like cysteine proteinase, plays a key role in *Trichomonas vaginalis* cytoadherence. BioMed. Res. Int. 2013, doi: 10.1155/2013/561979

155. Rivera-Rivas, L. A., Lorenzo-Benito, S., Sánchez-Rodríguez, D. B., Miranda-Ozuna, J. F., Euceda-Padilla, E. A., Ortega-López, J., Chavez-Munguia, B.,

Lagunes-Guillen, A., Velazquez-Valassi, B., Jasso-Villazul, L., Arroyo, R. (2020) The effect of iron on *Trichomonas vaginalis* TvCP2: A cysteine proteinase found in vaginal secretions of trichomoniasis patients. Parasitology 147, 760–774

156. Lal, K., Field, M. C., Carlton, J. M., Warwicker, J., Hirt, R. P. (2005) Identification of a very large Rab GTPase family in the parasitic protozoan *Trichomonas vaginalis*. Mol. Biochem. Parasitol. 143, 226–235

157. Pereira-Leal, J. B., Seabra, M. C. (2001) Evolution of the Rab family of small GTP-binding proteins. J. Mol. Biol. 313, 889–901

158. Loftus, B., Anderson, I., Davies, R., Alsmark, U. C. M., Samuelson, J., Amedeo, P., Roncaglia, P., Berriman, M., Hirt, R. P., Mann, B. J., Nozaki, T., Suh, B., Pop, M., Duchene, M., Ackers, J., Tannich, E., Leippe, M., Hofer, M., Bruchhaus, I., Willhoeft, U., Bhattacharya, A., Chillingworth, T., Churcher, C., Hance, Z., Harris, B., Harris, D., Jagels, K., Moule, S., Mungall, K., Ormond, D., Squares, R., Whitehead, S., Quail, M. A., Rabbinowitsch, E., Norbertczak, H., Price, C., Wang, Z., Guillen, N., Gilchrist, C., Stroup, S. E., Bhattacharya, S., Lohia, A., Foster, P. G., Sicheritz-Ponten, T., Weber, C., Singh, U., Mukherjee, C., El-Sayed, N. M., Petri, W. A., Clark, C. G., Embley, T. M., Barrell, B., Fraser, C. M., Hall, N. (2005) The genome of the protist parasite *Entamoeba histolytica*. Nature 433, 865–868

159. Marti, M., Regös, A., Li, Y., Schraner, E., Wild, P., Müller, N., Knopf, L. G., Hehl, A. B. (2003) An ancestral secretory apparatus in the protozoan parasite *Giardia intestinalis*. J. Biol. Chem. 278, 24837–24848

160. Krogstad, D. J., Schlesinger, P. H. (1987) The basis of antimalarial action: Non-weak base effects of chloroquine on acid vesicle pH. Am. J. Trop. Med. Hyg. 36, 213–220

161. Bradley, P. J., Lahti, C. J., Plumper, E., Johnson, P. J. (1997) Targeting and translocation of proteins into the hydrogenosome of the protist *Trichomonas*: Similarities with mitochondrial protein import. EMBO J. 16, 3484–3493

162. Nývltová, E., Smutná, T., Tachezy, J., Hrdý, I. (2016) OsmC and incomplete glycine decarboxylase complex mediate reductive detoxification of peroxides in hydrogenosomes of *Trichomonas vaginalis*. Mol. Biochem. Parasitol. 206, 29–38

163. Gao, Y., Chen, Y., Zhan, S., Zhang, W., Xiong, F., Ge, W. (2017) Comprehensive proteome analysis of lysosomes reveals the diverse function of macrophages in immune responses. Oncotarget 8, 7420–7440

164. Guerra, F., Bucci, C. (2016) Multiple Roles of the small GTPase Rab7. Cells 5, doi: 10.3390/cells5030034

165. Hu, Z. Q., Rao, C. L., Tang, M. L., Zhang, Y., Lu, X. X., Chen, J. G., Mao, C., Deng, L., Li, Q., Mao, X. H. (2019) Rab32 GTPase, as a direct target of miR-30b/c, controls the intracellular survival of *Burkholderia pseudomallei* by regulating phagosome maturation. PLoS Pathog. 15, doi: 10.1371/journal.ppat.1007879

166. Gutierrez, M.G. (2013) Functional role(s) of phagosomal Rab GTPases. Small GTPases. 4, 148-158

167. Rada, P., Doležal, P., Jedelský, P. L., Bursac, D., Perry, A. J., Šedinová, M., Smíšková, K., Novotný, M., Beltrán, N. C., Hrdý, I., Lithgow, T., Tachezy, J. (2011) The core components of organelle biogenesis and membrane transport in the hydrogenosomes of *Trichomonas vaginalis*. PLoS One. 6, doi: 10.1371/journal.pone.0024428

168. Twu, O., de Miguel, N., Lustig, G., Stevens, G. C., Vashisht, A. A., Wohlschlegel, J. A., Johnson, P. J. (2013) *Trichomonas vaginalis* exosomes deliver cargo to host cells and mediate host:parasite interactions. PLoS Pathog. 9, doi: 10.1371/journal.ppat.1003482

169. de Miguel, N., Lustig, G., Twu, O., Chattopadhyay, A., Wohlschlegel, J. A., Johnson, P. J. (2010) Proteome analysis of the surface of *Trichomonas vaginalis* reveals novel proteins and strain-dependent differential expression. Mol. Cell. Proteomics. 9, 1554–1566

170. Noël, C. J., Diaz, N., Sicheritz-Ponten, T., Safarikova, L., Tachezy, J., Tang, P., Fiori, P. L., Hirt, R. P. (2010) *Trichomonas vaginalis* vast BspA-like gene family: Evidence for functional diversity from structural organisation and transcriptomics. BMC Genomics. 11, doi: 10.1186/1471-2164-11-99

171. Molgora, B. M., Rai, A. K., Sweredoski, M. J., Moradian, A., Hess, S., Johnson, P. J. (2021) A novel *Trichomonas vaginalis* surface protein modulates parasite attachment via protein:host cell proteoglycan interaction. mBio. 12, doi: https://doi.org/10.1128/mBio.03374-20

172. Dennes, A., Cromme, C., Suresh, K., Kumar, N. S., Eble, J. A., Hahnenkamp, A., Pohlmann, R. (2005) The novel *Drosophila* lysosomal enzyme receptor protein mediates lysosomal sorting in mammalian cells and binds mammalian and *Drosophila* GGA adaptors. J. Biol. Chem. 280, 12849–12857

173. Rivero, M. R., Miras, S. L., Feliziani, C., Zamponi, N., Quiroga, R., Hayes, S. F., Ropolo, A. S., Touz, M. C. (2012) Vacuolar protein sorting receptor in *Giardia lamblia*. PLoS One. 7, doi: 10.1371/journal.pone.0043712

174. Sloves, P. J., Delhaye, S., Mouveaux, T., Werkmeister, E., Slomianny, C., Hovasse, A., Alayi, T. D., Callebaut, I., Gaji, R. Y., Schaeffer-Reiss, C., Van Dorsselear, A., Carruthers, V. B., Tomavo, S. (2012) *Toxoplasma* sortilin-like

receptor regulates protein transport and is essential for apical secretory organelle biogenesis and host infection. Cell Host Microbe. 11, 515–527

175. Harwig, S. S. L., Tan, L., Qu, X. D., Cho, Y., Eisenhauer, P. B., Lehrer, R. I. (1995) Bactericidal properties of murine intestinal phospholipase A2. J. Clin. Invest. 95, 603–610

176. Fenard, D., Lambeau, G., Valentin, E., Lefebvre, J. C., Lazdunski, M., Doglio, A. (1999) Secreted phospholipases A2, a new class of HIV inhibitors that block virus entry into host cells. J. Clin. Invest. 104, 611–618

177. Sanon, A., Tournaire-Arellano, C., Younes El Hage S, Bories, C., Caujolle, R., Loiseau, P. M. (2005) N-acetyl-β-d-hexosaminidase from *Trichomonas vaginalis*: Substrate specificity and activity of inhibitors. Biomed. Pharmacother. 59, 245–248

178. Riestra, A. M., Gandhi, S., Sweredoski, M. J., Moradian, A., Hess, S., Urban, S., Johnson, P. J. (2015) A *Trichomonas vaginalis* rhomboid protease and its substrate modulate parasite attachment and cytolysis of host cells. PLoS Pathog. 11, doi: 10.1371/journal.ppat.1005294

179. Thalmann, M., Coiro, M., Meier, T., Wicker, T., Zeeman, S. C., Santelia, D. (2019) The evolution of functional complexity within the β-amylase gene family in land plants. BMC Evol. Biol. 19, doi: 10.1186/s12862-019-1395-2

180. Manners, D. J. (1963) Enzymic synthesis and degradation of starch and glycogen. Adv. Carbohydr. Chem. 17, 371–430

181. Mirmonsef, P., Hotton, A. L., Gilbert, D., Burgad, D., Landay, A., Weber, K. M., Cohen, M., Ravel, J., Spear, G. T. (2014) Free glycogen in vaginal fluids is associated with *Lactobacillus* colonization and low vaginal pH. PLoS One 9, doi: 10.1371/journal.pone.0102467

182. Sciaky, N., Presley, J., Smith, C., Zaal, K. J., Cole, N., Moreira, J. E., Terasaki, M., Siggia, E., Lippincott-Schwartz, J. (1997) Golgi tubule traffic and the effects of brefeldin A visualized in living cells. J. Cell Biol. 139, 1137–1155

183. Klausner, R. D., Donaldson, J. G., Lippincott-Schwartz, J. (1992) Brefeldin A: Insights into the control of membrane traffic and organelle structure. J. Cell Bio. 116, 1071–1080

184. Braun, M., Waheed, A., von Figura, K. (1989) Lysosomal acid phosphatase is transported to lysosomes via the cell surface. EMBO J. 8, 3633–3640

185. Hille, A., Klumperman, J., Geuze, H. J., Peters, C., Brodsky, F. M., von Figura, K. (1992) Lysosomal acid phosphatase is internalized via clathrin-coated pits. Eur. J. Cell Biol. 59, 106–115

Journal Pre-proof

Proteomic analysis of *Trichomonas vaginalis* phagolysosome, lysosomal targeting, and unconventional secretion of cysteine peptidases

Nadine Zimmann, Petr Rada, Vojtěch Žárský, Tamara Smutná, Kristína Záhonová, Joel Dacks, Karel Harant, Ivan Hrdý, Jan Tachezy

PII: S1535-9476(21)00146-8

DOI: https://doi.org/10.1016/j.mcpro.2021.100174

Reference: MCPRO 100174

To appear in: *Molecular & Cellular Proteomics*

Received Date: 5 August 2021

Revised Date: 25 October 2021

Accepted Date: 4 November 2021

Please cite this article as: Zimmann N, Rada P, Žárský V, Smutná T, Záhonová K, Dacks J, Harant K, Hrdý I, Tachezy J, Proteomic analysis of *Trichomonas vaginalis* phagolysosome, lysosomal targeting, and unconventional secretion of cysteine peptidases, *Molecular & Cellular Proteomics* (2021), doi: https://doi.org/10.1016/j.mcpro.2021.100174.

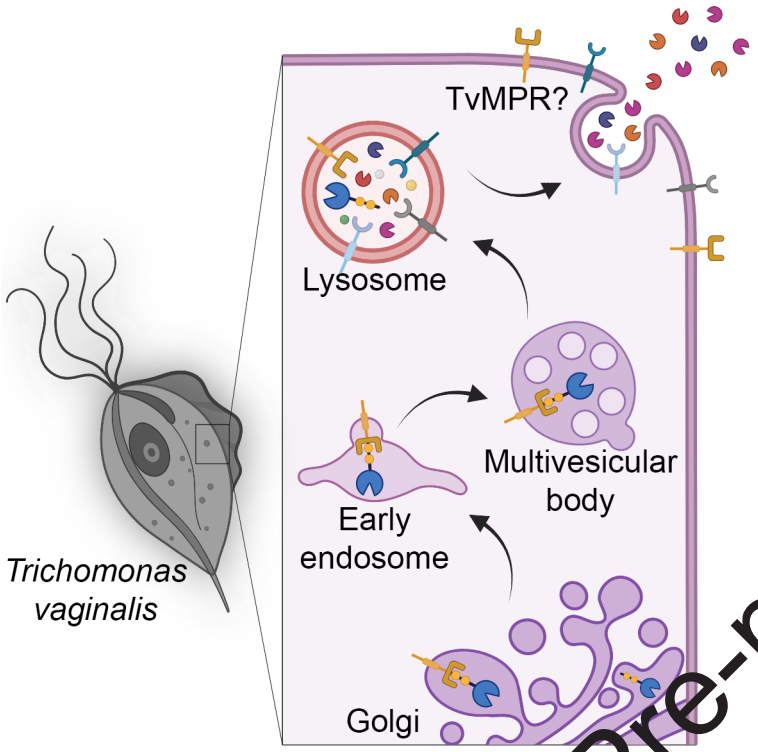

Proteomic analysis of *Trichomonas vaginalis* phagolysosome, lysosomal targeting, and unconventional secretion of cysteine peptidases

Nadine Zimmann[1], Petr Rada[1], Vojtěch Žárský[1], Tamara Smutná[1], Kristína Záhonová[1,2], Joel Dacks[2,3], Karel Harant[1], Ivan Hrdý[1], Jan Tachezy[1]*

[1]Department of Parasitology, Faculty of Science, Charles University, BIOCEV, Průmyslová 595, 252 50 Vestec, Czech Republic

[2]Institute of Parasitology, Biology Centre, Czech Academy of Sciences, České Budějovice, Czech Republic

[3]Division of Infectious Diseases, Department of Medicine, University of Alberta, Edmonton, Alberta, Canada

Running title: *T. vaginalis* lysosomal proteome and targeting

*To whom correspondence should be addressed: Jan Tachezy, e-mail jan.tachezy@natur.cuni.cz, Department of Parasitology, Faculty of Science, Charles University BIOCEV, Průmyslová 595, 252 50 Vestec, Czech Republic

Keywords: *Trichomonas vaginalis*, phagolysosome, proteome, cysteine peptidase, glycosylation, mannose-6-phosphate receptor

Abbreviations

AP	Acid phosphatase
BA	β-amylase
BBS	Borate buffered saline
BFA	Brefeldin A
bHX	β-hexosaminidase
CD-MPR	Cation dependent mannose-6-phosphate receptor
CI-MPR	Cation independent mannose-6-phosphate receptor
CLCP	Cathepsin L-like cysteine peptidase
CLQ	Chloroquine
CP	Cysteine protease
CPBF1	Cysteine protease binding protein family 1
DMAP	DNA methyltransferase-associated protein
EDC	1-ethyl-3-[3-dimethylaminopropyl] carbodiimide hydrochloride
ER	Endoplasmic reticulum
FITC	Fluorescein isothiocyanate
GGA	Golgi-localized, γ-ear-containing, ADP ribosylation factor-binding protein
GlcNAc-PT	N-acetylglucosamine-1-phosphotransferase
HA	Hemagglutinin
LAMP	Lysosome-associated membrane glycoprotein
LERP	Lysosomal Enzyme Receptor Protein

LF	Lactoferrin
LFQ MS	Label-free quantitative mass spectrometry
LGF	Large granule fraction
LTS	Lysosomal targeting sequence
M6P	Mannose-6-phosphate
mBA	Mutated β-amylase
mCLCP	Mutated cathepsin L-like cysteine peptidase
MES	2-[n-morpholino]-ethanesulfonic acid buffer
MPR	Mannose-6-phopshate receptor
MPR300	Mannose-6-phopshate receptor 300
MRH	Mannose 6-phosphate Receptor Homology
MS	Mass spectrometry
nanoLC-MS	Nano reverse phase liquid chromatography mass spectrometry
NHS	N-hydroxysuccinimide
PBS	Phosphate buffered saline
s-LTS	Lysosomal targeting sequence of soluble protein
SDC	Sodium deoxycholate
SNAP	Soluble N-ethylmaleimide-sensitive-factor attachment protein
SNARE	SNAP receptor
ST	Sucrose-tris buffer
t-LTS	Lysosomal targeting sequence of transmembrane protein
TBSR	*Trichomonas* Beta-Sandwich Repeat protein

TCA	Trichloracetic acid
TEAB	Triethylammonium bicarbonate
TGN	Trans Golgi network
TLCK	Tosyl-L-lysyl-chloromethane hydrochloride
TMD	Transmembrane domain
TSP	Tetraspanin
TYM	Tryptone-yeast extract-maltose medium
UCE	Uncovering enzyme, N-acetylglucosamine-1-phosphodiester α-N-acetylglucosaminidase
vATPase	vacuolar ATPase

Abstract

The lysosome represents a central degradative compartment of eukaryote cells, yet little is known about the biogenesis and function of this organelle in parasitic protists. Whereas the mannose 6-phosphate (M6P)-dependent system is dominant for lysosomal targeting in metazoans, oligosaccharide-independent sorting has been reported in other eukaryotes. In this study, we investigated the phagolysosomal proteome of the human parasite *Trichomonas vaginalis*, its protein targeting and the involvement of lysosomes in hydrolase secretion. The organelles were purified using Percoll and OptiPrep gradient centrifugation and a novel purification protocol based on the phagocytosis of lactoferrin-covered magnetic nanoparticles. The analysis resulted in a lysosomal proteome of 468 proteins, which were sorted into 21 classes. Hydrolases represented the largest functional class and included proteases, lipases, phosphatases, and glycosidases. Identification of a large set of proteins involved in vesicular trafficking (80) and turnover of actin cytoskeleton rearrangement (29) indicate a dynamic phagolysosomal compartment. Several cysteine proteases such as TvCP2 were previously shown to be secreted. Our experiments showed that secretion of TvCP2 was strongly inhibited by chloroquine, which increases intralysosomal pH, thus indicating that TvCP2 secretion occurs through lysosomes rather than the classical secretory pathway. Unexpectedly, we identified divergent homologues of the M6P receptor TvMPR in the phagolysosomal proteome, although *T. vaginalis* lacks enzymes for M6P formation. To test whether oligosaccharides are involved in lysosomal targeting, we selected the lysosome-resident cysteine protease CLCP, which possesses two glycosylation sites. Mutation of any of the sites redirected CLCP to the secretory pathway. Similarly, the introduction of glycosylation sites to secreted β-amylase redirected this

protein to lysosomes. Thus, unlike other parasitic protists, *T. vaginalis* seems to utilize glycosylation as a recognition marker for lysosomal hydrolases. Our findings provide the first insight into the complexity of *T. vaginalis* phagolysosomes, their biogenesis and role in the unconventional secretion of cysteine peptidases.

Introduction

Trichomonas vaginalis is a flagellated parasitic protist that causes the most common non-viral sexually transmitted disease, with 276 million new infections annually (1). In women, the parasite can cause vaginitis and increase the risk of HIV transmission, preterm delivery, low birth weight, and cervical cancer. Most infected men are asymptomatic, but long-term infections increase the risk of prostate cancer development (2–5). In the vaginal mucosa, *T. vaginalis* parasites actively phagocytose host cells such as epithelial cells, lymphocytes, erythrocytes, as well as cell debris and microbes, including yeast and bacteria (6–9). Moreover, *T. vaginalis* secretes a large number of biologically active molecules, such as adhesins for cytoadherence, cytotoxic cysteine proteases (CPs), amylases and glycosidases to metabolize available glycogen (4, 10), and peptidoglycan hydrolases that are active against the bacterial cell wall (11). *T. vaginalis* secretes proteins through the classical secretory pathway (10) or unconventionally via exosomes, which are derived from the endolysosomal pathway (12). Vesicles with engulfed material fuse with lysosomes to form phagolysosomes, which are acidic organelles specializing in the breakdown of a broad range of biomolecules (13–16). In addition, lysosomes participate in various other cellular processes, such as autophagy (17, 18), secretion, and degradation of misfolded proteins within the secretory pathway (19).

The biogenesis of lysosomes depends on the delivery of newly synthesized proteins from the trans-Golgi network (TGN) via the transport vesicles that deliver cargo within the cell and through the endosomal pathway that imports proteins from the plasma membrane (20, 21). Lysosomes are supplied with over 60 hydrolases (15, 22), as well as other proteins such as acidifying vacuolar ATPases (vATPases), lysosome-associated membrane glycoproteins (LAMPs), and over 50 lysosomal channel proteins and transporters (14, 15).

In metazoans, the sorting of most lysosomal hydrolases depends on the mannose-6-phosphate (M6P) pathway (23). Soluble lysosomal proteins are glycosylated on asparagine residues within the sequence Asn-X-[Ser/Thr] (soluble lysosomal targeting sequence, s-LTS) in the endoplasmic reticulum (ER) (23, 24). Then, in the Golgi body, N-acetylglucosamine-1-phosphotransferase (GlcNAc-PT) and N-acetylglucosamine-1-phosphodiester α-N-acetylglucosaminidase ('uncovering enzyme', UCE) form M6P for interaction with M6P receptors (MPRs). Two MPRs, a cation-dependent (CD-MPR) and cation-independent MPR (CI-MPR), have been identified (22, 23, 25). Other lysosomal sorting receptors have also been described, including LIMP-2 (mammals), VSR (plants, algae, alveolates), and sortilin/Vps10, which were studied in mammals and yeast; however, sortilin homologues have been identified in members of all eukaryotic groups (23). Novel receptors for the delivery of CPs to lysosomes (CP-binding protein family 1) were identified in *Entamoeba histolytica* (26).

Receptors involved in protein delivery to lysosomes consist of a luminal domain that binds cargo in the Golgi body, at least one transmembrane domain, and a C-terminal tail that contains a lysosomal targeting sequence (LTS) facing the cytosol. LTSs of transmembrane proteins and receptors (t-LTS) are most frequently dileucine-based ([DE]xxxL[LI], DxxLL) or

tyrosine-based (YxxØ) (24) and regulate endosomal/lysosomal sorting and internalization from the plasma membrane (27). T-LTSs are bound by cytosolic Golgi-localized, γ-ear-containing, ADP ribosylation factor-binding proteins (GGAs) that mediate sorting at the TGN, which is further facilitated by adaptor proteins. Cargo is released into acidified endosomes, and receptors are recycled. However, GGAs are known to be opisthokont-specific innovations while adaptor protein complexes that recognize the same LTSs are found across eukaryotes and are known to be involved in trafficking throughout the endolysosomal system (23–25, 28–31).

Little is known about the lysosomal proteome, its biogenesis, and function in *T. vaginalis*. The genome of this protist encodes 447 proteases; thus, a high number of these proteins can be expected in lysosomes (32). Indeed, some cysteine proteases involved in *T. vaginalis* pathogenesis, such as TvCP4, have been shown to reside partially in lysosomes (33–35). The secretome of *T. vaginalis* revealed active secretion of almost 90 proteins, including over 20 hydrolases (10). Moreover, the genome of *T. vaginalis* encodes an extensive complement of at least 72 adaptin subunit genes implying their role in the endolysosomal system (32). However, these data did not clarify the role of lysosomes in secretion, nor has lysosomal protein targeting been studied in this organism.

Considering the highly complex lysosomal content originating from external and internal sources and the high sensitivity of mass spectrometry (MS), the major challenge is to distinguish the actual lysosomal proteome from contaminants. Therefore, we used three different methods to isolate phagolysosomes and lysosome-enriched samples, which were analysed by MS to estimate the phagolysosomal proteome. To uncover the mode of *T. vaginalis* lysosomal targeting, we evaluated the role of specific glycosylation. Furthermore, we

demonstrated that lysosomes are involved in the unconventional secretion of a papain-like cysteine peptidase. These studies provide the first insights into the phagolysosomal composition and the endolysosomal route of *T. vaginalis*.

Experimental Procedures

Cell cultivation

The *T. vaginalis* strains T1 (36) and TV17-48 (37) were cultured axenically in tryptone-yeast extract-maltose medium (TYM; pH 6.2) with 10% (v/v) heat-inactivated horse serum. The culture medium was supplemented with 200 µg/ml Geneticin G418 (single transfectants) or with both 200 µg/ml G418 and 40 µg/ml puromycin (double transfectants) for transfectant selection (10). Cultures were grown at 37°C.

Gene cloning and *T. vaginalis* transfection

The genes encoding Rab7a (TVAG_159730), acid phosphatase (AP, TVAG_169070), Trichomonas beta-sandwich repeat protein 5 (TBSR5, TVAG_340570), β-hexosaminidase (bHX, TVAG_110660), MPR-2 (TVAG_317730), MPR-3 (TVAG_498650), β-amylase 2 (BA2, TVAG_080000) and mutated BA2 (mBA2), and the cysteine peptidases TvCP2 (TVAG_057000), CLCP (TVAG_485880), and mutated CLCP (mCLCP) were cloned into the vector pTagVag-HA-Neo (38), enabling the expression of these proteins with a C-terminal haemagglutinin (HA) tag. The gene encoding BA1 (TVAG_436700) was cloned into the vector pTagVag-V5-Pur (10), fusing the protein to a V5 tag at the C-terminus. Genes were expressed with their respective native promotor (300 bp upstream of coding sequence). The plasmids were transfected into trichomonads by nucleofection using the Human T Cell Nucleofector™ Kit (Lonza, Basel, Switzerland). Approximately 4 ml of cells in the logarithmic growth phase (1.5 x 10^6 cells/ml) were harvested and resuspended gently in 82 µl Nucleofector Solution and 18 µl Supplement 1.

Then, 10 µg of plasmid was added, and the mixture was incubated at room temperature for 10 min. The manufacturer's program U.033 was used for transfection (39). For double transfection, the cells were consecutively transfected with pTagVag-HA-Neo and pTagVag-V5-Pur. All primers used for gene amplification and cloning are listed in Table S1.

Isolation of lysosomal fractions

Lysosomes were isolated by three approaches. (i) For density gradient centrifugation in Percoll, we used a modified procedure based on the protocol by Bradley et al. 1997 (40). Briefly, 1 l of TV17-48 expressing HA-tagged TvRab7a (TV17-48-Rab7a) ($1.5x10^6$ cells/ml) was harvested by centrifugation (1,200 x g, 10 min, 4°C) and washed twice with phosphate-buffered saline (PBS) and once with sucrose-tris (ST) buffer (500 mM sucrose, 20 mM Tris, 1 mM KCl, pH 7.2). The cells were resuspended in 7.5 ml of ST buffer with 10 µg/ml leupeptin and 50 µg/ml tosyl-L-lysyl-chloromethane hydrochloride (TLCK). The cells were disintegrated by sonication on ice, and unbroken cells were removed by centrifugation at 800 x g for 10 min at 4°C. The supernatant was centrifuged at 14,000 x g for 20 min at 4°C. The top white layer of the pellet was separated from a brown layer of hydrogenosomes, gently resuspended in 7.5 ml of ST buffer and centrifuged again under the same conditions. The white pellet was collected and resuspended in 2 ml of ST buffer with protease inhibitors as described above (large granule fraction, LGF) and centrifuged in a 45% Percoll gradient at 30,000 rpm for 30 min at 4°C using a Beckman Optima XPN-90 ultracentrifuge and a Ti70 rotor. Deceleration was set to 9 to avoid disruption of the gradient. The upper lysosomal fraction was collected and centrifuged again in a 45% Percoll gradient under the same conditions. The final lysosomal fraction was washed

twice with ST buffer at 14,000 x g for 20 min at 4°C, resuspended in 500 µl ST buffer with protease inhibitors and frozen before further processing.

(ii) Density gradient centrifugation using Optiprep. The LGF of TV17-48-Rab7a was obtained as above and resuspended in 800 µl of a buffer consisting of 0.25 M sucrose, 1 mM EDTA, and 10 mM Tris-HCl, pH 7.4. The suspension was loaded into a 5% to 50% continuous Optiprep gradient and centrifuged at 200,000 x g for 2 h at 4°C using a Beckman Optima XPN-90 ultracentrifuge with an SW 41 Ti rotor. Acceleration was set to 4 and deceleration to 9. Three fractions corresponding to three visible bands were collected, washed and frozen.

(iii) Phagolysosomes were isolated using lactoferrin (Lf)-coupled Dynabeads. Lf was coupled with fluorescein isothiocyanate (FITC) in one volume PBS and two volumes borate buffered saline (BBS, pH 9) at a final concentration of 100 ng FITC/1 µg Lf. Then, the PBS-BBS solution was exchanged for 25 mM 2-[n-morpholino]-ethanesulfonic acid (MES) buffer (pH 6) using Amicon Ultra-4 30K Centrifugal Filters (Millipore). Magnetic Dynabeads MyOne Carboxylic Acid (Invitrogen) of 1 µm in diameter were coupled with the FITC-Lf in MES buffer according to Invitrogen's two-step protocol using 1-ethyl-3-[3-dimethylaminopropyl] carbodiimide hydrochloride (EDC) and N-hydroxysuccinimide (NHS). Subsequently, FITC-Lf-coupled Dynabeads were incubated with 300 µl of 50 mM Tris, pH 7.4, for 15 min to quench non-reacted activated carboxylic acid groups. The FITC-Lf-coupled Dynabeads were washed four times with Tris for 5 min and resuspended in 100 µl PBS. For the isolation of phagolysosomes, 1 l of TV17-48-Rab7a cells ($1.5x10^6$ cells/ml) was harvested. The cells were resuspended in 20 ml TYM medium and incubated with 100 µl of FITC-Lf-coupled Dynabeads in a 150 ml tissue culture flask for 1 h at 37°C. After incubation, the cells were gently disintegrated by sonication on ice.

Lysis was evaluated under a microscope at 30-sec intervals. Leupeptin and TLCK were added as before to avoid protein degradation. The lysosomes containing Dynabeads were washed three times with PBS by applying a magnet for 15 min after each wash and then filtering them through a 3 µm pore size filter (Whatman, GE Healthcare). Then, the lysosomes were treated with 0.1% Triton X-100 to release the Dynabeads. A magnet was applied, and the supernatant containing the lysosomal content was transferred to a new tube and frozen.

Immunoblot analysis

The presence of marker proteins in cellular fractions was tested by immunoblotting using mouse monoclonal anti(α)-HA antibody (Exbio, Vestec, Czech Republic) against HA-tagged TvRab7a (lysosomes) and rat polyclonal α-OsmC antibody (hydrogenosomes) (41). Rat polyclonal α-soluble protein disulphide-isomerase (sPDI) antibody (endoplasmic reticulum) was raised against a recombinant PDI produced in E. coli BL21 DE. The sPDI gene (TVAG_267400) was cloned into the bacterial expression vector pET42b, and the His-tagged protein was isolated by Ni-NTA agarose affinity chromatography (Qiagen). Anti-mouse or anti-rat polyclonal antibodies coupled with peroxidase were used as secondary antibodies (Sigma-Aldrich). Visualization was performed with chemiluminescence (Immobilon Forte, Merck, St. Louis, MO, USA) and images were obtained using the Amersham Imager 600 (GE Healthcare), and signals quantified using ImageJ/Fiji software (42).

Fluorescence microscopy

T. vaginalis cells were incubated with 2.5 µM LysoTracker Deep Red (Thermo Fisher Scientific) for 5 min or with 5% FITC-Lf (v/v) for 30 min at 37°C. Then, the cells were washed in PBS, fixed with 2% formaldehyde, and processed as described (43). Transfectants were stained using mouse monoclonal α-HA antibody (Exbio) and the secondary donkey α-mouse antibody conjugated to Alexa Fluor 488 or 594 (Life Technologies), and rabbit polyclonal α-V5 antibody (Abcam) and Alexa Fluor 594 donkey α-rabbit (Life Technologies). To observe *T. vaginalis* phagocytosis, TV17-48 cells expressing HA-tagged TvRab7a were incubated with FITC-Lf coupled Dynabeads for 40 min at 37°C, washed in PBS, and processed as before with TvRab7a labelled with Alexa Fluor 594. Slides were observed with a Leica TCS SP8 confocal laser scanning microscope (Leica Microsystems, Germany). Images were processed using Huygens Professional version 19.10 (Scientific Volume Imaging, The Netherlands) and further processed using ImageJ/Fiji software (42) and the Imaris 9.7.2 Package for Cell Biologists (Bitplane AG, Zurich, Switzerland). Voxel-based colocalization was performed using ImarisColoc. Costes's automatic thresholding was applied to the images in the Z stack, and Pearson's correlation coefficient (PCC) in colocalized volume was calculated.

Protein preparation

Protein samples were precipitated with trichloroacetic acid (TCA) for 1 h at -20°C (44), pelleted at 21,000 x g for 5 min at 4°C, washed twice with cold acetone, dried for 5 min at 95°C and stored at -80°C. LFQ MS analysis was performed as described previously (10). Briefly, proteins were dissolved in 100 mM TEAB with 1% sodium deoxycholate (SDC). Samples were digested with trypsin, and detergent was removed by liquid-liquid extraction (45).

Mass spectrometry data acquisition

Tryptic peptides were injected on a nano reverse-phase liquid chromatograph (UltiMate 3000 RSLC, Thermo Scientific) coupled with MS (nanoLC-MS) using a Orbitrap Fusion Tribrid mass spectrometer (Thermo Scientific) as described previously (10). Briefly, peptides were loaded onto an Acclaim PepMap300 trap column (300 µm x 5 mm) packed with C18 (5 µm, 300 Å) in loading buffer (0.1% trifluoroacetic acid in 2% acetonitrile) for 4 min at a flow rate of 15 µL/min and then separated on an EASY-Spray column (75 µm x 50 cm) packed with C18 (2 µm, 100 Å, Thermo Scientific) at a flow rate of 300 nl/min. Mobile phase A (0.1% formic acid in water) and mobile phase B (0.1% formic acid in acetonitrile) were used to establish a 60-min gradient from 4% to 35% B. Eluted peptides were ionized by electrospray. The full MS spectrum (350-1,400 m/z range) was acquired at a resolution of 120,000 at m/z 200 and a maximum ion accumulation time of 100 ms. Dynamic exclusion was set to 60 s. Higher-energy collisional dissociation (HCD) MS/MS spectra were acquired in iontrap in rapid mode and the normalized collision energy was set to 30% with a maximum ion accumulation time of 35 ms. An isolation width of 1.6 m/z units was used for MS 2.

Analysis of MS data

Raw data were processed using MaxQuant version 1.6.2.0 (Max-Planck-Institute of Biochemistry, Planegg, Germany) (46). Searches were performed using the *Trichomonas vaginalis* database from EUpathDB (47) (release 2020-05-27, 60,330 entries). Trypsin cleaving specificity was used to generate the peptides, and two missed cleavages were allowed. The

protein modifications were set as follows: cysteine (unimod nr: 39) as static and methionine oxidation (unimod: 1384) and protein N-terminus acetylation (unimod: 1) as variable. The false discovery rates for peptides and proteins were set to 1%. Search mass tolerances were used in MaxQuant default settings for Orbitrap and Iontrap. The precursor ion mass tolerance in the initial search was 20 ppm, the tolerance in the main search was 4.5 ppm, and the fragment ion mass tolerance was 0.5 Da.

Experimental design and statistical rationale

Three different isolation methods were used, three independent biological experiments were performed for each method, and each biological sample was analysed by MS in three technical replicates. The lysosomal proteome identifications were filtered using following criteria: (i) the protein identification was supported by at least three peptides, (ii) the protein was identified in at least two out of three biological replicates, and (iii) the protein was identified by all three methods for organelle isolation.

Bioinformatics

For each protein identified in the lysosomal proteome, targeting to the secretory pathway was predicted using the SignalP 4.1 server (http://www.cbs.dtu.dk/services/SignalP-4.1/), the TargetP 2.0 server (http://www.cbs.dtu.dk/services/TargetP/), and the SecretomeP 2.0 server (http://www.cbs.dtu.dk/services/SecretomeP/). Transmembrane domains were predicted using the TMHMM server v. 2.0 (http://www.cbs.dtu.dk/services/TMHMM/). Conserved domains were predicted using the Pfam 34.0 database (http://pfam.xfam.org, 19,179 entries). Identified proteins were annotated and sorted based on TrichDB annotation

(https://trichdb.org/trichdb/), Pfam database, consensus of BLASTp top hits against the refseq database for the vesicle-trafficking specific proteins, and molecular function gene ontology (http://geneontology.org/docs/ontology-documentation/). Putative lysosomal targeting motifs were detected using the Protein Motif Pattern tool (https://trichdb.org/trichdb/app/search/transcript/GenesByMotifSearch). For sequence alignments, Clustal Omega 1.2.4 was used (48).

Site-directed mutagenesis

Q5 Site-Directed Mutagenesis Kit (New England Biolabs, Inc.) was used alongside its high-efficiency 5-alpha competent E. coli to introduce mutations into the CLCP gene. NEBaseChanger was used to design primers (Table S1), and mutagenesis was performed according to the manufacturer's protocol.

Monitoring of protein secretion

T. vaginalis T1 cells (50 ml, approximately $7.5x10^7$ cells) were harvested by centrifugation and washed three times with TYM without horse serum. The cells were resuspended in 2 ml TYM without horse serum and incubated for 60 min at 37°C. The cells were removed by centrifugation at 1,200 x g for 10 min at 4°C, and then the supernatant was centrifuged at 10,000 x g for 10 min at 4°C to remove cell debris, followed by filtration through a 0.2 µm pore size filter (Whatman, GE Healthcare). Proteins in the supernatant were precipitated with TCA as described previously (44) and analysed by immunoblotting as above. Alternatively, cells were

incubated with 1 µM chloroquine (Sigma-Aldrich) or 50 µg/ml brefeldin A (Sigma-Aldrich) for 15 min or 45 min prior to protein isolation from the supernatant.

Results

Lysosomal localization of TvRab7a

Before the separation of *T. vaginalis* phagolysosomes, we selected Rab7 as a potential phagolysosomal protein marker. There are three Rab7 paralogues in the *T. vaginalis* genome, of which we selected TvRab7a (49), which displayed the highest pairwise protein sequence identity with human Rab7 (45.5%). To verify its lysosomal localization in *T. vaginalis*, FITC-Lf and LysoTracker Deep Red were used as lysosomal markers. Extracellular Lf is known to be imported by trichomonads via receptor-mediated endocytosis; thus, TV17-48-Rab7a cells were incubated with FITC-Lf prior to slide preparation to allow for FITC-Lf internalization. FITC-Lf appeared in a few small but mainly larger vesicles corresponding to endosomes and lysosomes (Fig. 1A). TvRab7a and LysoTracker appeared in numerous small- to larger-sized vesicles scattered throughout the cell (Fig. 1B). Colocalization of TvRab7a with FITC-Lf was found mainly in the larger vesicles (Fig. 1A). Similarly, LysoTracker colocalized with TvRab7a mainly in larger vesicles, which further supports that these vesicles represent lysosomes (Fig. 1B).

Proof of principle of lysosomal isolation methods

Three different methods were used for the isolation of lysosomes/phagolysosomes. First, we employed 45% Percoll gradient centrifugation as previously described (40), which resulted in the separation of a brown hydrogenosomal fraction (lower band) and a white upper lysosome-enriched fraction (Fig. 2A). The lysosomal fraction was subsequently repurified on a second 45% Percoll gradient. Using the OsmC protein as a marker (41), immunoblot analyses confirmed a

clear separation of hydrogenosomes from the lysosomal fraction with TvRab7a; however, the lysosomal fraction also contained a weaker sPDI signal, suggesting the presence of ER-derived vesicles (Fig. 2B). Next, we employed an OptiPrep density gradient, which appeared to be more favourable to the isolation of *T. vaginalis* hydrogenosomes compared to the Percoll gradient (50). Separation of the LGF using OptiPrep resulted in the formation of three visible bands (Fig. 2C), and immunoblot analyses revealed that lysosomes were present in the uppermost band with a strong TvRab7a signal and a low sPDI signal (Fig. 2D). Hydrogenosomes detected by OsmC were clearly separate from the lysosomal fraction. Finally, we employed a method based on *T. vaginalis* phagocytic activity. TV17-48-Rab7a cells were incubated with magnetic beads coupled with Lf that were ingested by phagocytosis. Fluorescence microscopy confirmed the uptake of beads into phagolysosomes colocalizing with TvRab7a (Fig. 2E). Phagolysosomes containing beads were then separated by a magnet. This approach resulted in the separation of a phagolysosomal fraction with the TvRab7a marker that was free of OsmC and sPDI (Fig. 2F). Lysosomal fractions obtained by all three methods were submitted for MS.

Proteomic analysis

The total number of proteins identified by MS was 3,442 in the Percoll purified fraction, 4,055 using the OptiPrep gradient, and 1,351 in the fraction obtained with magnetic beads (Table S2-S4). The initial dataset was filtered using two parameters: the protein must be identified in at least two out of three biological experiments, and the protein identification must be supported by at least three peptides. Therefore, we obtained 1,758 (Percoll), 2,748 (Optiprep), and 748 (Dynabeads) proteins. These datasets overlapped in 550 proteins of which eighty-eight proteins

were considered contaminants based on their annotation and known cellular localization and the remaining 462 proteins were considered to represent phagolysosomal proteins. These proteins were sorted into 21 functional groups considering TrichDB annotations, Pfam domain identifications, and molecular function gene ontology (Fig. 3, Table S5). Seventy-six percent (351 proteins) appeared to be soluble proteins, and the remaining 24% (111 proteins) possessed one or more transmembrane domains (TMDs), with the majority (75 proteins) possessing a single TMD. Hydrolases, including proteases, phosphatases, lipases, and glycosidases, represented the largest functional class in the phagolysosomal proteome. Cysteine proteases formed the largest protease set (13 proteins). They included TvCP2, TvCP3, TvCP4, and TvCPT, which were previously shown to be secreted by *T. vaginalis* (51); the legumain-like protease TvLEGU-1 (52); 10 metallopeptidases (53); and eight serine peptidases (10, 54). The other typical lysosomal hydrolase was represented by a β-hexosaminidase that was present as two paralogues. In the category of carbohydrate metabolism, we identified 17 proteins, including a putative glycogen debranching enzyme (TVAG_150430) and three paralogues of 4-α-glucanotransferase. Another class of typical lysosomal proteins are the vATPases, of which we identified six, with two of them possessing seven TMDs. One vATPase (TVAG_075320) has also been found on the surface (54). Among the channel proteins, we found three ABC transporters, a class of proteins known to couple ATP hydrolysis with the transport of substrates across membranes. Interestingly, we identified one Piezo channel (TVAG_223490) with 37 TMDs. In Dictyostelium, this group of proteins is proposed to act as a pressure sensor to regulate cell movement (55).

In the vesicular trafficking group, we identified 43 Rab proteins, including multiple paralogues in most categories. Of these, six Rabs were assigned to known categories based on orthology searches (Fig. 4, Table S5). As expected, we identified Rab7a, which controls transport to late endosomes and lysosomes and is required for phagosomal maturation (56). We also identified three paralogues of Rab32 that are known to promote the fusion of phagosomes with lysosomes (57) and Rab 6 which has been shown to play a role in targeting material to lysosome related organelles in mammalian systems (58). Furthermore, we identified Rabs 21 and notably Rab1. The metazoan-specific paralogue of Rab 1, Rab 35 is well-established to play a role in regulating phagosomal maturation (59, 60). Finally, we identified Rab11 which although not directly lysosomal is a well-known marker of the recycling endosome, an upstream endocytic compartment (61). Five Rabs were present with less supported classifications, including Rab4, Rab8, Rab14, Rab22 and Rab24, and interestingly, 18 Rabs with no clear classification. An overview of the identified Rab proteins is given in Fig. 4. In addition to Rabs, we identified components of the retromer complex (Vps35), of the lysosome-associated HOPS complex (Vps16, 33, 39), of the late endosomal/multi-vesicular body associated ESCRT complexes (SNF7) and several other endosomally-associated Vps proteins (eg. Vps9). We also identified SNARE proteins, notably syntaxin 16, Vta1, and several Vamp7 homologues, all of which mediate endolysosomal trafficking and cargo delivery. Additional proteins associated with endocytic vesicle formation included a single enthoprotin, and three dynamins. Finally, we found clathrin and six subunits of adaptor complexes including a near complete AP4 complex (missing only the sigma subunit) and mu subunits for AP1, AP2, and AP4. It is the mu subunit that binds the YXXØ motif in proteins during lysosomal trafficking (62).

Another striking category was the cytoskeleton, for which we identified 29 proteins. These proteins included two actins and other actin-interacting proteins such as two actinins, three profilins, two gelsolins, and one twinfilin. The identification of proteins involved in vesicular trafficking and proteins associated with the cytoskeleton in the lysosomal proteome is in line with the established model of endolysosomal trafficking and organellar movement along the cytoskeleton (63–65).

A total of 55 proteins in the phagolysosomal proteome overlap with the surface proteome (54) (Fig. 5), of which 45 are TM proteins. These proteins include two putative adhesins of the BspA family, and in our phagolysosomal proteome, we identified three more BspA members, the tetraspanin protein TSP1 (TVAG_019180), which is associated with multivesicular bodies (12), and five paralogues of the *Trichomonas* β-sandwich repeat protein (TBSR). A relatively small number of TM proteins overlapping with the surface proteome possess an internalization motif in the cytosolic tail; a single protein contains the classical NPxY signal (TBSR-5, TVAG_340670), five proteins harbour the [DE]xxxL[LI] motif, and 16 proteins possess the YxxØ signal (Table S5). The phagolysosomal proteome and the *T. vaginalis* secretome overlapped with only 26 proteins, eight of which are hydrolases, including β-hexosaminidase, an acid phosphatase, a serine and two cysteine peptidases, two phospholipases, and a glucosaminidase (Fig. 5) (10). A relatively low level of overlap between phagolysosomal proteome and previously reported proteomes of the secreted proteins, and the surface proteome supports the successful separation of the phagolysosomal fraction. However, it also indicates an expected engulfment of some surface proteins and their transport

to the lysosomes, and conversely, possible participation of lysosomes in unconventional protein secretion.

Experimental cellular localization of selected proteins

Acid phosphatase (AP, TVAG_169070), TBSR-5 (TVAG_340570), β-hexosaminidase (bHX, TVAG_110660), TvCP2 (TVAG_057000), and CLCP (TVAG_485880) were selected for experimental verification of their cellular localization. AP and bHX are known to reside in lysosomes in other organisms and may serve as lysosomal markers (66), TBSR-5 was selected as an example of a membrane protein with C-terminal NPIY signal for endocytic internalization (Table S5), TvCP2 is known to be secreted as an important virulence factor (67), while CLCP represents a new resident cysteine protease that was not identified in other *T. vaginalis* proteomes, thus far. The corresponding genes were expressed in *T. vaginalis* under the control of their respective native promotors and with a C-terminal HA-tag and investigated by confocal microscopy. Colocalization with LysoTracker supported their lysosomal localization in large vesicles, whereas limited colocalization was observed in smaller vesicles (Fig. 6, Fig. 7A WT). The PCC in colocalized volume ranged from low (PCC r = 0.290, AP) to moderate (PCC r = 0.633, TvCP2) values (Fig. 6, Fig. 7C).

Mannose-6-phosphate-like receptors

Four transmembrane proteins identified in phagolysosomes appear to be homologues of mammalian cation-independent mannose-6-phosphate receptor 300 (MPR300). These proteins were named TvMPR-1 (TVAG_177320), TvMPR-2 (TVAG_351790), TvMPR-3 (TVAG_498650),

and TvMPR-4 (TVAG_166760). In addition, we identified two more paralogues, TvMPR-5 (TVAG_160180) and TvMPR-6 (TVAG_445110), in the *T. vaginalis* genome, which are between 882 and 991 amino acids long. Their N-terminal domains range in length between 809 and 924 amino acid residues, and their C-terminal tails are between eight and 49 amino acids long. Human MPR300 (hMRP300) consists of 15 characteristic mannose 6-phosphate receptor homology (MRH) domains in the N-terminus (Fig. 8), of which MRH3, 5, and 9 were implicated in binding M6P and MRH11 has been implicated in binding insulin-like growth factor II (IGF2) (23, 68). Each MRH domain consists of approximately 150 amino acid residues with eight conserved cysteine residues. Interestingly, *T. vaginalis* MPRs consist of only five MRH domains, which aligned with MRH9 to MRH13 of hMPR300 (Fig. 8). Although the protein sequence similarity of *T. vaginalis* MRH domains to MRH of hMPR300 appeared to be rather low (7.2% to 35.2%), most of the conserved cysteine residues are present. TvMPR structure is similar to the Drosophila lysosomal enzyme receptor protein (LERP), which also possesses five MRH domains (Fig. S1). Moreover, similar to LERP, TvMPR proteins lack most residues in hMPR300 that are essential for the binding of M6P and IGF2. All TvMPR proteins possess either the YxxØ or DxxL[LI] sorting motif for recognition by adaptor proteins (Fig. 8, Fig. S1). However, only three of them, TvMPR-1, TvMPR-4, and TvMPR-5, were predicted to be type I glycoproteins with a single TMD, similar to hMPR300 and LERP, which is consistent with the cytosolic topology of their sorting signal (Fig. 8). The other three TvMPR proteins were predicted to possess two TMDs, resulting in the C-terminal YxxØ motif most likely being in the same compartment as the N-terminal domain. Although we found TvMPR proteins in the phagolysosomal proteome and previously identified them in the secretome and surface proteome, the expression of HA-

tagged TvMPR-2 and TvMPR-3 revealed that they localize predominantly to the structures of the ER and Golgi body (Fig. 9). V5-tagged β-amylase 1 was used as a marker for the ER/Golgi body (10) that was co-expressed in double *T. vaginalis* transfectants and colocalized with TvMPR-2 and TvMPR-3 (Fig. 9).

Glycosylation dependent targeting to lysosomes

The observed localization of TvMPR proteins is consistent with the model of the M6P-dependent signalling pathway that is initiated in the ER, where lysosomal cargo is glycosylated on the asparagine of the s-LTS motif Asn-X-[Ser/Thr] and subsequently modified in the Golgi body to be recognized by MPR. However, as TvMPR proteins lack most residues required for M6P-dependent recognition, M6P signalling is unlikely. Moreover, the generation of M6P on N-linked glycans requires the consecutive activity of GlcNAc-PT and UCE. Thus, we searched for corresponding homologues in the *T. vaginalis* database using the human α/β GlcNAc-PT (Q3T906) and UCE (Q9UKZ3) amino acid sequences as queries. We identified the protein TVAG_166090 with only limited homology to one of four characteristic GlcNAc-PT stealth domains (69), and we did not identify any UCE homologues, which further supports the absence of M6P signalling. Thus, we hypothesized that another M6P-independent feature, such as a peptide structure or glycans, may serve as a signal. To test whether glycosylation is involved in the protein targeting of *T. vaginalis* lysosomes, we selected phagolysosome-resident CLCP. This protein is composed of 452 amino acid residues and possesses two putative s-LTSs, Asn-Ser-Thr at position 188-190 (LTS1) and Asn-Arg-Ser at position 268-270 (LTS2). A series of CLCPs with mutated s-LTSs (mCLCP) was prepared in which asparagine was replaced by serine or glutamine

(Fig. 7B). Whereas wild-type CLCP was observed in lysosomes with a PCC r = 0.512 ± 0.1 (n = 16) (Fig. 7C), all mCLCP variants accumulated predominantly around the nucleus (Fig. 7A). Some mCLCP variants were observed in vesicles scattered throughout the cell, in which cases the mCLCP signal exceptionally colocalized with LysoTracker. The PCC of mCLCP was below r = 0.1 (Fig. 7C). Next, we were interested in whether mCLCP is arrested in the ER or secreted into the cell environment. Thus, the cells were incubated for 1 h at 37°C in TYM, and secreted mCLCP was detected by immunoblotting. Whereas wild-type CLCP was not secreted, which is consistent with its absence in the secretome (10), all mutated LTSs versions of mCLCP were secreted (Fig. 7D).

To further test the ability of the CLCP LTS1 and LTS2 sequences to target a protein to lysosomes, we introduced both motifs into BA2 (mBA2), a non-lysosomal protein that does not possess any glycosylation sites and expressed the protein with a C-terminal HA tag. LTS1 was introduced at positions 232-234 and LTS2 at positions 312-314, thereby maintaining the same distance of 78 amino acids between the signals as in CLCP (Fig. 10B). The active sites of BA2 are located at positions 133 and 330 and thus were not altered by the insertions. While wild-type BA2 did not localize to lysosomes (PCC r = 0.051 ± 0.029, n = 29, Fig. 10) but labelled ER structures surrounding the nucleus as demonstrated previously (10), cells expressing mBA2 showed significant colocalization with LysoTracker in lysosomes (Fig. 10A) with a PCC r = 0.556 ± 0.07 (n = 22, Fig. 10C), whereas no accumulation in the ER/Golgi was observed. Next, we were interested in whether the insertion of LTS1 and LTS2 into BA2 influences protein secretion. Therefore, the cells were incubated in TYM as before, and the conditioned medium was analysed by immunoblotting. Whereas wild-type BA2 was secreted, mBA2 was associated

exclusively with cells, and no secretion was observed (Fig. 10D). These experiments demonstrated that the tandem N-glycosylation sites were decisive for protein sorting, they represent the s-LTS of CLCP, and they are essential for protein delivery to lysosomes. The screening of the lysosomal proteome for tandem N-glycosylation sites that have a similar distance to one another as in CLCP (78 amino acids ± 20 amino acid range) revealed 27% of soluble proteins with such a motif (Table S5). Interestingly, within the soluble proteases, 44% contain this motif. These results suggest that the tandem glycosylation sites might be a general motif for lysosomal delivery in *T. vaginalis*, however, such an assumption needs experimental verification in future. Moreover, the distance between the glycosylation sites in different proteins might not be conserved because the steric position of glycans that are recognized by receptors is likely dependent on the protein conformation. Further studies are needed to establish which and how lysosomal receptor recognizes this s-LTS for which TvMPR proteins are the best candidates.

Lysosomes are involved in unconventional secretion of CP

A few proteins were observed in the phagolysosomal proteome as well as in the secretome. This phenomenon prompted us to test whether lysosomes are involved in protein secretion in addition to the classical ER-Golgi secretory pathway. We selected the two proteins TvCP2 and AP that were found in the phagolysosome and secretome and BA2 as a control for classical secretion (10). The proteins were expressed with an HA-tag and transfected trichomonads were incubated in TYM medium with either 1 µM chloroquine (CLQ) or 50 µg/ml brefeldin A (BFA). CLQ blocks the endolysosomal pathway by increasing lysosomal pH (70, 71), while BFA inhibits

classical secretion via stimulation of retrograde transport from the Golgi body to the ER (10, 72). The secretion of TvCP2 was strongly decreased by both CLQ and BFA, while the secretion of BA2 and AP was inhibited only by BFA (Fig. 11). These results indicated that lysosomes were involved in the unconventional secretion of TvCP2, as opposed to BA2 and AP, which are secreted through the classical secretory pathway, and AP is eventually delivered to lysosomes via endocytosis (Fig. 11).

Discussion

Lysosomes play a key role in the pathogenicity and virulence of parasitic protists (73). However, little is known about their biogenesis, lysosomal protein targeting and composition outside of classical mammalian and yeast models. In this paper, we characterized the proteome of *T. vaginalis* phagolysosomes, showed that glycosylation is involved in lysosomal targeting of CLCP and that lysosomes are involved in protease secretion. Unexpectedly, we identified homologues of the M6P receptor, TvMPRs. While this protein has bioinformatically been identified across eukaryotes, it is inconsistently conserved and to our knowledge only functionally characterized in metazoans and fungi (31).

To separate the *T. vaginalis* lysosome-enriched fraction, we initially employed a method based on differential and gradient centrifugation using two different isoosmotic gradient media, Percoll and Optiprep. MS analysis identified 1,758 (Percoll) and 2,748 (Optiprep) reproducibly enriched proteins in these preparations, which is comparable to the 3,703 proteins identified in the macrophage lysosome-enriched fraction using a similar approach (74). Although these methods are widely applied, lysosomes tend to co-purify with other organelles, typically the endoplasmic reticulum, Golgi, and mitochondria (74, 75), or may contain proteins of other compartments due to autophagy (18). Indeed, we observed the presence of the PDI ER marker in samples of the lysosome-enriched fractions using immunoblotting, and contaminants were apparent from the annotations of identified proteins. Therefore, we developed a new experimental protocol for phagolysosome purification based on the ingestion of magnetic

nanobeads by *T. vaginalis*. To increase the specific binding of the nanobeads, we covered the beads with Lf, which binds to trichomonad receptors on the surface (76). This analysis identified 748 proteins and resulted in a set of 462 phagolysosomal proteins when combined with the previous proteomic datasets. The obtained size of the trichomonad phagolysosomal proteome is close to the approximately 450 lysosomal proteins identified in the lysosomes of mouse embryonic fibroblasts isolated using magnetite solution (77).

Comparisons of the phagolysosomal proteome with previous proteomic studies of *T. vaginalis* surface membrane proteins (54), secretome (10), and exosomes (12) allow us to estimate the purity of our preparation and detect proteins with multiple localizations. Indeed, there was a very low overlap with these compartments that corroborated efficient organellar separation. The highest number of shared proteins (55) was found with the surface proteome. However, multiple localizations are expected for membrane proteins and this is consistent with the endocytic pathways of some lysosomal proteins that are expressed on the plasma membrane as receptors, adhesins or proteases and subsequently internalized via endocytosis/phagocytosis and transported to lysosomes. These shared proteins included the leucine-rich repeat protein BspA (78), β-hexosaminidase, and the surface adhesin TvAD1, which is also associated with exosomes (79). Moreover, there were nineteen conserved membrane proteins of unknown function, which provide interesting targets for future studies.

Proteases have been repeatedly implicated in *T. vaginalis* virulence (33, 80), however, their cellular localization is mostly unknown. A comparison of the lysosomal proteome that included 38 peptidases with previous studies allowed us to distinguish three groups. The first

and the major group includes primary lysosomal resident peptidases (34) that have not been detected in other cellular compartments. This group included seven new CPs, such as CLCP, in addition to four CPs (TvCP3, TvCP4, TvCPT, and TvLEGU-1) that have been previously recognized in trichomonad cellular lysates (81). TvLEGU-1 has been observed in lysosomes, the Golgi complex, and on the trichomonad surface using immunofluorescence and immunoelectron microscopy (52), whereas it has been absent from the secretome and the surface proteome (10, 54). However, the expression of TvLEGU-1 seems to be strongly dependent on the iron level, which may explain the observed differences in cellular localization (52). The first group further included seven serine peptidases and nine metallopeptidases of different families (M1, 8, 16, 20, 24, 28, 67) that had not been characterized thus far. The second group consists of two soluble CPs that are secreted (10) including TvCP2, an important virulence factor (67), whereas leishmanolysin-like metallopeptidase (GP63 like) and subtilisin-like serine peptidase (SUB1) were two membrane proteases of the third group, which were shared with the surface proteome (54). Previous cellular localization of SUB1 using fluorescence microscopy suggested its presence in intracellular vesicles and on the plasma membrane, which supports our proteomic data (82). In pathogenic fungi, subtilisin proteases have been shown to be important for host invasion (83, 84), however, their role in *T. vaginalis* has not been established. Another hydrolase group that we found in the lysosomal proteome was phospholipase B, of which we identified eight paralogues, two of which are secreted (TVAG_215920, TVAG_333010). Phospholipase B belongs to the group of acyl esterases and represents an important lysosomal component to hydrolyse glycerophospholipids (85). Secreted phospholipases have been shown to kill bacteria (86) and display antiviral activity (87), however, have not been studied in

trichomonads. Finally, β-hexosaminidase is a typical lysosomal hydrolase that we identified two copies of. Interestingly, one copy (TVAG_110660) possesses a single TMD and was shared between the secretome and the surface proteome. Its cell membrane localization and previously determined N-acetyl-β-D-glucosaminidase activity in *T. vaginalis* (88) suggest that β-hexosaminidase may participate in *T. vaginalis* virulence via host mucin degradation. Interestingly, in *E. histolytica*, β-hexosaminidase is transported to the phagolysosome by a unique cysteine protease binding protein family 8 (CPBF8) receptor that is not present in *T. vaginalis* (26).

The model of protein delivery to lysosome and secretion in *T. vaginalis*, which is based on our results, is provided in Fig. 11. In metazoans, most lysosomal proteins are typically targeted via M6P-dependent pathways, whereas in other eukaryotic lineages, sorting of hydrolases was not reported to depend on oligosaccharides. Alternative receptors such as sortilins/Vps10 and plant vacuolar sorting receptors (VSRs) directly recognize the polypeptide motifs of cargo (23). Vsp10 is conserved in most eukaryotic lineages (31), and its function as a sorting receptor was shown in *Giardia intestinalis* (89) and *Toxoplasma gondii* (90). However, there is no obvious orthologue of Vsp10 in the *T. vaginalis* genome (31). Surprisingly, we identified four paralogues of the putative M6P receptor TvMPR in the lysosomal proteome and two other paralogues in the genome. These proteins contain the characteristic N-terminal domain repeats with typical cysteines (22) that are mostly conserved in TvMRPs. However, unlike the mammalian CI-MPR with 15 domains, TvMPRs contain only 5 domains, which resembles the structure of the MPR-like protein LERP in Drosophila (91). Moreover, TvMPR1, TvMPR4, and TvMPR5 possess a single TMD and the endocytic sorting signal YxxØ or a dileucine

motif (DXXLI]) in their C-termini, which further supports their role as receptors and is consistent with the presence of adaptin complex proteins, particularly the mu subunits that we identified. Interestingly, TvMPR2, 3 and 6 were predicted to possess double TMDs at their C-termini, which may indicate a different topology of their N-terminal domains. Similar to Drosophila, TvMPRs lack most of the residues involved in M6P binding and the two enzymes (GlcNAc-PT and UCE) required for the formation of M6P recognition markers. Interestingly, LERP has been shown to rescue the missorting of lysosomal proteins in MPR-deficient mouse cells in an M6P-independent manner, although it is not known whether LERP recognizes a glycan or a peptide structure (91). Thus, the identification of LERP-like TvMPR prompted us to test whether glycans are involved in lysosomal targeting in *T. vaginalis*. Indeed, we demonstrated that two sites for N-glycosylation of the Nx[ST] motif within the lysosomal resident CLCP are essential for its lysosomal localization. Moreover, introducing the two Nx[ST] motifs into non-glycosylated BA2, which is secreted by the classical ER-Golgi pathway (10), redirected this protein from the secretory pathway to lysosomes (Fig. 12). However, glycosylation apparently needs a specific structure/conformation to provide the lysosomal signal. First, we demonstrated that both Nx[ST] motifs in CLCP are needed for correct targeting, as mutation of a single site mistargeted CLCP to the secretory pathway. Second, a number of other glycosylated proteins, such as BA1, that possess multiple Nx[ST] motifs are predominantly secreted (10) (Fig. 12). For future investigations of recognition markers, it also needs to be considered that *T. vaginalis* possesses a limited set of glycosyltransferases available for glycan synthesis in the ER, producing a simplified glycan structure consisting of two N-acetyl glucosamines and only five mannose residues, as opposed to $GlcNAc_2Man_9Glu_3$ in the majority of eukaryotes (10, 92). Collectively,

these results indicate that glycosylation is required for the recognition and targeting of lysosomal proteins in *T. vaginalis*; however, whether TvMPRs or other possible receptors are involved in this process and the precise structure of the lysosomal recognition marker need to be clarified in future studies.

The secretion of TvCP2 has been shown to contribute to the host cell cytotoxicity caused by *T. vaginalis*. It has been suggested that this hydrolase is not a lysosomal protein and is secreted via secretory vesicles (67). However, the presence of TvCP2 in lysosomes, which was supported by immunofluorescence microscopy and the proteomic analysis in this study, suggested that TvCP2 might be secreted by an unconventional secretory pathway (USP) via lysosomes (Fig. 12) (93). The involvement of acidic organelles in TvCP2 secretion supported the treatment of *T. vaginalis* with the lysosomotropic amine chloroquine, which is known to increase the intralysosomal pH and inhibit lysosomal function (70, 71). The secretion of TvCP2 under chloroquine treatment was strongly inhibited, whereas no inhibition was observed for the secretion of non-lysosomal BA2. Secretion of both proteins was inhibited by brefeldin A, which impairs transport between the ER and Golgi (10, 72). Unlike TvCP2, secretion of lysosomal acid phosphatase (TVAG_169070) was insensitive to chloroquine, suggesting that this soluble protein is released via the secretory pathway as BA2 and possibly internalized via endocytosis. Interestingly, chloroquine was observed to have the opposite effect on lysosomal protein secretion in human cells that employed the M6P recognition marker. Treatment with chloroquine resulted in enhanced secretion of lysosomal proteins via the secretory pathway. In these cells, MPR proteins bind lysosomal cargo in the TGN and deliver the cargo through the intracellular pathway or via the plasma membrane to acidic vesicles, where the cargo

dissociates and MPRs are recycled. Enhanced secretion of lysosomal proteins was explained by the inhibition of MPR recycling and consequently the decreased capacity to bind M6P (24, 70). The striking differences in the effect of chloroquine on lysosomal protein secretion and the absence of the M6P-dependent pathway in *T. vaginalis* suggest that the parasite employs specific unconventional mechanisms for the secretion of virulence factors such as TvCP2.

In conclusion, our proteomics study provided an extensive dataset of phagolysosmal proteins, including known and potentially novel virulence factors. Future investigations need to be performed to elucidate their functions and, in particular, to decipher the molecular mechanism of lysosomal sorting, which may provide an interesting target for the development of new antiparasitic strategies.

Acknowledgements

This work was supported by the Charles University Grant Agency, project number 18218 (NZ), the Czech Science Foundation (19-18773J) (JT), European Regional Development Funds project CePaViP (02.1.01/0.0/0.0/16_019/0000759) (JT), and H2020 Spreading Excellence and Widening Participation MICOBION (H2020 No 81022) (JT). We acknowledge Imaging Methods Core Facility at BIOCEV, an institution supported by the MEYS CR (Large RI Project LM2018129 Czech-BioImaging); the OMICS Proteomics of BIOCEV for mass spectrometry analysis; and Michaela Marcinčiková for technical assistance. We also thank BioRender.com, which was used to create Figs. 4, 12, and the graphical abstract.

Data availability

The mass spectrometry proteomics data have been deposited to the ProteomeXchange Consortium via the PRIDE (94) partner repository with the dataset identifier PXD029152

Declaration of interest

There are no conflicts of interest to disclose.

Supplemental data

This article contains supplemental data.

References

1. World Health Organisation (2012) Global incidence and prevalence of selected curable sexually transmitted infections 2008. WHO Press, World Health Organization, Geneva, Switzerland

2. Twu, O., Dessí, D., Vu, A., Mercer, F., Stevens, G. C., De Miguel, N., Rappelli, P., Cocco, A. R., Clubb, R. T., Fiori, P. L., and Johnson, P. J. (2014) *Trichomonas vaginalis* homolog of macrophage migration inhibitory factor induces prostate cell growth, invasiveness, and inflammatory responses. Proc. Natl. Acad. Sci. U. S. A. 111, 8179–8184

3. Kissinger, P. (2015) *Trichomonas vaginalis*: A review of epidemiologic, clinical and treatment issues. BMC Infect. Dis. 15. doi: 10.1186/s12879-015-1055-0

4. Petrin, D., Delgaty, K., Bhatt, R., and Garber, G. (1998) Clinical and microbiological aspects of *Trichomonas vaginalis*. Clin. Microbiol. Rev. 11, 300–317

5. Kissinger, P., and Adamski, A. (2013) Trichomoniasis and HIV interactions: A review. Sex. Transm. Infect. 89, 426–433

6. Benchimol, M., De Andrade Rosa, I., Da Silva Fontes, R., and Burla Dias, Â. J. (2008) *Trichomonas* adhere and phagocytose sperm cells: Adhesion seems to be a prominent stage during interaction. Parasitol. Res. 102, 597–604

7. Midlej, V., and Benchimol, M. (2010) *Trichomonas vaginalis* kills and eats - Evidence for phagocytic activity as a cytopathic effect. Parasitology 137, 65–76

8. Pereira-Neves, A., and Benchimol, M. (2007) Phagocytosis by *Trichomonas vaginalis*: new insights. Biol. Cell 99, 87–101

9. Rendón-Maldonado, J. G., Espinosa-Cantellano, M., González-Robles, A., and Martínez-Palomo, A. (1998) *Trichomonas vaginalis*: In vitro phagocytosis of lactobacilli, vaginal epithelial cells, leukocytes, and erythrocytes. Exp. Parasitol. 89, 241–250

10. Štáfková, J., Rada, P., Meloni, D., Zárský, V., Smutná, T., Zimmann, N., Harant, K., Pompach, P., Hrdý, I., and Tachezy, J. (2018) Dynamic secretome of *Trichomonas vaginalis*: Case study of β-amylases. Mol. Cell. Proteomics 17, 304–320

11. Pinheiro, J., Biboy, J., Vollmer, W., Hirt, R. P., Keown, J. R., Artuyants, A., Black, M. M., Goldstone, D. C., and Simoes-Barbosa, A. (2018) The protozoan *Trichomonas vaginalis* targets bacteria with laterally acquired NlpC/P60 peptidoglycan hydrolases. MBio 9, doi: 10.1128/mBio.01784-18

12. Twu, O., de Miguel, N., Lustig, G., Stevens, G. C., Vashisht, A. A., Wohlschlegel, J. A., and Johnson, P. J. (2013) *Trichomonas vaginalis* exosomes deliver cargo to host cells and mediate host:parasite interactions. PLoS Pathog. 9, e1003482

13. Hyttinen, J. M. T., Niittykoski, M., Salminen, A., and Kaarniranta, K. (2013) Maturation of autophagosomes and endosomes: A key role for Rab7. Biochim. Biophys. Acta - Mol. Cell Res. 1833, 503–510

14. Ganley, I. G. (2013) Autophagosome maturation and lysosomal fusion. Essays Biochem. 55, 65–78

15. Xu, H., and Ren, D. (2015) Lysosomal physiology. Annu. Rev. Physiol. 77, 57–80

16. Kinchen, J. M., and Ravichandran, K. S. (2008) Phagosome maturation: Going through the acid test. Nat. Rev. Mol. Cell Biol. 9, 781–795

17. Yu, L., Chen, Y., and Tooze, S. A. (2018) Autophagy pathway: Cellular and molecular mechanisms. Autophagy 14, 207–215

18. Benchimol, M. (1999) Hydrogenosome autophagy: An ultrastructural and cytochemical study. Biol. Cell 91, 165–174

19. Sun, Z., and Brodsky, J. L. (2019) Protein quality control in the secretory pathway. J. Cell Biol. 218, 3171–3187

20. Peden, A. A., Oorschot, V., Hesser, B. A., Austin, C. D., Scheller, R. H., and Klumperman, J. (2004) Localization of the AP-3 adaptor complex defines a novel endosomal exit site for lysosomal membrane proteins. J. Cell Biol. 164, 1065–1076

21. Janvier, K., and Bonifacino, J. S. (2005) Role of the endocytic machinery in the sorting of lysosome-associated membrane proteins. Mol. Biol. Cell 16, 4231–4242

22. Castonguay, A. C., Lasanajak, Y., Song, X., Olson, L. J., Cummings, R. D., Smith, D. F., and Dahms, N. M. (2012) The glycan-binding properties of the cation-independent mannose 6-phosphate receptor are evolutionary conserved in vertebrates. Glycobiology 22, 983–996

23. Lousa, C. D. M., and Denecke, J. (2016) Lysosomal and vacuolar sorting: Not so different after all! Biochem. Soc. Trans. 44, 891–897

24. Braulke, T., and Bonifacino, J. S. (2009) Sorting of lysosomal proteins. Biochim. Biophys. Acta - Mol. Cell Res. 1793, 605–614

25. Coutinho, M. F., Prata, M. J., and Alves, S. (2012) Mannose-6-phosphate pathway: A review on its role in lysosomal function and dysfunction. Mol. Genet. Metab. 105, 542–550

26. Nakada-Tsukui, K., Tsuboi, K., Furukawa, A., Yamada, Y., and Nozaki, T. (2012) A novel class of cysteine protease receptors that mediate lysosomal transport. Cell. Microbiol. 14, 1299–1317

27. Bonifacino, J. S., and Traub, L. M. (2003) Signals for sorting of transmembrane proteins to endosomes and lysosomes. Annu. Rev. Biochem. 72, 395–447

28. Puertollano, R., Aguilar, R. C., Gorshkova, I., Crouch, R. J., and Bonifacino, J. S. (2001) Sorting of mannose 6-phosphate receptors mediated by the GGAs. Science. 292, 1712–1716

29. Höning, S., Sandoval, I., and Von Figura, K. (1998) A di-leucine-based motif in the cytoplasmic tail of LIMP-II and tyrosinase mediates selective binding of AP-3. EMBO J. 17, 1304–1314

30. Kyttälä, A., Yliannala, K., Schu, P., Jalanko, A., and Luzio, J. P. (2005) AP-1 and AP-3 facilitate lysosomal targeting of Batten disease protein CLN3 via its dileucine motif. J. Biol. Chem. 280, 10277–10283

31. Koumandou, V. L., Klute, M. J., Herman, E. K., Nunez-Miguel, R., Dacks, J. B., and Field, M. C. (2011) Evolutionary reconstruction of the retromer complex and its function in *Trypanosoma brucei*. J. Cell Sci. 124, 1496–1509

32. Carlton, J. M., Hirt, R. P., Silva, J. C., Delcher, A. L., Schatz, M., Zhao, Q., Wortman, J. R., Bidwell, S. L., Alsmark, U. C. M., Besteiro, S., Sicheritz-Ponten, T., Noel, C. J., Dacks, J. B., Foster, P. G., Simillion, C., Van De Peer, Y., Miranda-Saavedra, D., Barton, G. J., Westrop, G. D., Müller, S., Dessi, D., Fiori, P. L., Ren, Q., Paulsen, I., Zhang, H., Bastida-Corcuera, F. D., Simoes-Barbosa, A., Brown, M. T., Hayes, R. D., Mukherjee, M., Okumura, C. Y., Schneider, R., Smith, A. J., Vanacova, S., Villalvazo, M., Haas, B. J., Pertea, M., Feldblyum, T. V., Utterback, T. R., Shu, C. L., Osoegawa, K., De Jong, P. J., Hrdy, I., Horvathova, L., Zubacova, Z., Dolezal, P., Malik, S. B., Logsdon, J. M., Henze, K., Gupta, A., Wang, C. C., Dunne, R. L., Upcroft, J. A., Upcroft, P., White, O., Salzberg, S. L., Tang, P., Chiu, C. H., Lee, Y. S., Embley, T. M., Coombs, G. H., Mottram, J. C., Tachezy, J., Fraser-Liggett, C. M., and Johnson, P. J. (2007) Draft genome sequence of the sexually transmitted pathogen *Trichomonas vaginalis*. Science. 315, 207–212

33. Hernández, H. M., Marcet, R., and Sarracent, J. (2014) Biological roles of cysteine proteinases in the pathogenesis of *Trichomonas vaginalis*. Parasite 21, doi: 10.1051/parasite/2014054

34. Scott, D. A., North, M. J., and Coombs, G. H. (1995) The pathway of secretion of proteinases in *Trichomonas vaginalis*. Int. J. Parasitol. 25, 657–666

35. Cárdenas-Guerra, R. E., Arroyo, R., Rosa de Andrade, I., Benchimol, M., and Ortega-López, J. (2013) The iron-induced cysteine proteinase TvCP4 plays a key role in *Trichomonas vaginalis* haemolysis. Microbes Infect. 15, 958–968

36. Tai, J. H., Su, H. M., Tsai, J., Shaio, M. F., and Wang, C. C. (1993) The divergence of *Trichomonas vaginalis* virus RNAs among various isolates of *Trichomonas vaginalis*. Exp. Parasitol. 76, 278–286

37. Kulda, J., Vojtechovska, M., Tachezy, J., Demes, P., and Kunzova, E. (1982) Metronidazole resistance of *Trichomonas vaginalis* as a cause of treatment failure in trichomoniasis. A case report. Br. J. Vener. Dis. 58, doi: 10.1136/sti.58.6.394

38. Hrdy, I., Hirt, R. P., Dolezal, P., Bardonová, L., Foster, P. G., Tachezy, J., and Embley, T. M. (2004) Trichomonas hydrogenosomes contain the NADH dehydrogenase module of mitochondrial complex I. Nature 432, 618–622

39. Janssen, B. D., Chen, Y. P., Molgora, B. M., Wang, S. E., Simoes-Barbosa, A., and Johnson, P. J. (2018) CRISPR/Cas9-mediated gene modification and gene knock out in the human-infective parasite *Trichomonas vaginalis*. Sci. Rep. 8, doi: 10.1038/s41598-017-18442-3

40. Bradley, P. J., Lahti, C. J., Plumper, E., and Johnson, P. J. (1997) Targeting and translocation of proteins into the hydrogenosome of the protist Trichomonas: similarities with mitochondrial protein import. EMBO J. 16, 3484–3493

41. Nývltová, E., Smutná, T., Tachezy, J., and Hrdý, I. (2016) OsmC and incomplete glycine decarboxylase complex mediate reductive detoxification of peroxides in hydrogenosomes of *Trichomonas vaginalis*. Mol. Biochem. Parasitol. 206, 29–38

42. Schindelin, J., Arganda-Carreras, I., Frise, E., Kaynig, V., Longair, M., Pietzsch, T., Preibisch, S., Rueden, C., Saalfeld, S., Schmid, B., Tinevez, J. Y., White, D. J., Hartenstein, V., Eliceiri, K., Tomancak, P., and Cardona, A. (2012) Fiji: An open-source platform for biological-image analysis. Nat. Methods 9, 676-82

43. Woessner, D. J., and Dawson, S. C. (2012) The *Giardia* median body protein is a ventral disc protein that is critical for maintaining a domed disc conformation during attachment. Eukaryot. Cell 11, 292-301

44. Méchin, V., Damerval, C., and Zivy, M. (2007) Total protein extraction with TCA-acetone. Methods Mol. Biol. 355, 1–8

45. Masuda, T., Tomita, M., and Ishihama, Y. (2008) Phase transfer surfactant-aided trypsin digestion for membrane proteome analysis. J.Proteome.Res. 7, 731–740

46. Cox, J., Hein, M. Y., Luber, C. A., Paron, I., Nagaraj, N., and Mann, M. (2014) Accurate proteome-wide label-free quantification by delayed normalization and maximal peptide ratio extraction, Termed MaxLFQ. Mol. Cell. Proteomics 13, 2513–2526

47. Warrenfeltz, S., Basenko, E., Crouch, K., Harb, O., Kissinger, J., Roos, D., Shanmugasundram, A., and Silva-Franco, F. (2018) EuPathDB: The eukaryotic pathogen genomics database resource. Methods Mol. Biol. 1757, 69–113

48. Madeira, F., Park, Y. M., Lee, J., Buso, N., Gur, T., Madhusoodanan, N., Basutkar, P., Tivey, A. R. N., Potter, S. C., Finn, R. D., and Lopez, R. (2019) The EMBL-EBI search and sequence analysis tools APIs in 2019. Nucleic Acids Res. 47, W636–W641

49. Lal, K., Field, M. C., Carlton, J. M., Warwicker, J., and Hirt, R. P. (2005) Identification of a very large Rab GTPase family in the parasitic protozoan *Trichomonas vaginalis*. Mol. Biochem. Parasitol. 143, 226-235

50. Beltrán, N. C., Horváthová, L., Jedelsky, P. L., Šedinová, M., Rada, P., Marcinčiková, M., Hrdý, I., and Tachezy, J. (2013) Iron-induced changes in the proteome of *Trichomonas vaginalis* hydrogenosomes. PLoS One 8, e65148

51. Sommer, U., Costello, C. E., Hayes, G. R., Beach, D. H., Gilbert, R. O., Lucas, J. J., and Singh, B. N. (2005) Identification of *Trichomonas vaginalis* cysteine proteases that induce apoptosis in human vaginal epithelial cells. J. Biol. Chem. 280, 23853–23860

52. Rendón-Gandarilla, F. J., Ramón-Luing, L. D. L. A., Ortega-López, J., Rosa De Andrade, I., Benchimol, M., and Arroyo, R. (2013) The TvLEGU-1, a legumain-like cysteine proteinase, plays a key role in *Trichomonas vaginalis* cytoadherence. Biomed Res. Int. 2013, doi.org/10.1155/2013/561979

53. Ma, L., Meng, Q., Cheng, W., Sung, Y., Tang, P., Hu, S., and Yu, J. (2011) Involvement of the GP63 protease in infection of *Trichomonas vaginalis*. Parasitol. Res. 109, 71–79

54. De Miguel, N., Lustig, G., Twu, O., Chattopadhyay, A., Wohlschlegel, J. A., and Johnson, P. J. (2010) Proteome analysis of the surface of *Trichomonas vaginalis* reveals novel proteins and strain-dependent differential expression. Mol. Cell. Proteomics 9, 1554–1566

55. Srivastava, N., Traynor, D., Piel, M., Kabla, A. J., and Kay, R. R. (2020) Pressure sensing through Piezo channels controls whether cells migrate with blebs or pseudopods. Proc. Natl. Acad. Sci. U. S. A. 117, 2506–2512

56. Guerra, F., and Bucci, C. (2016) Multiple Roles of the Small GTPase Rab7. Cells 5, 34

57. Hu, Z. Q., Rao, C. L., Tang, M. L., Zhang, Y., Lu, X. X., Chen, J. G., Mao, C., Deng, L., Li, Q., and Mao, X. H. (2019) Rab32 GTPase, as a direct target of miR-30b/c, controls the intracellular survival of *Burkholderia pseudomallei* by regulating phagosome maturation. PLoS Pathog. 15, e1007879

58. Patwardhan, A., Bardin, S., Miserey-Lenkei, S., Larue, L., Goud, B., Raposo, G., and Delevoye, C. (2017) Routing of the RAB6 secretory pathway towards the lysosome related organelle of melanocytes. Nat. Commun. 8, doi: 10.1038/ncomms15835

59. Egami, Y., Fukuda, M., and Araki, N. (2011) Rab35 regulates phagosome formation through recruitment of ACAP2 in macrophages during FcγR-mediated phagocytosis. J. Cell Sci. 124, 3557–3567

60. Verma, K., and Datta, S. (2017) The Monomeric GTPase Rab35 regulates phagocytic cup formation and phagosomal maturation in *Entamoeba histolytica*. J. Biol. Chem. 292, 4960-4975

61. Gutierrez, M. G. (2013) Functional role(s) of phagosomal Rab GTPases. Small GTPases 4, 148-158

62. Ohno, H., Stewart, J., Fournier, M. C., Bosshart, H., Rhee, I., Miyatake, S., Saito, T., Gallusser, A., Kirchhausen, T., and Bonifacino, J. S. (1995) Interaction of tyrosine-based sorting signals with clathrin-associated proteins. Science 269, 1872-1875.

63. Caviston, J. P., and Holzbaur, E. L. F. (2006) Microtubule motors at the intersection of trafficking and transport. Trends Cell Biol. 16, 530–537

64. Krendel, M., and Mooseker, M. S. (2005) Myosins: Tails (and heads) of functional diversity. Physiology 20, 239–251

65. Bálint, Š., Vilanova, I. V., Álvarez, Á. S., and Lakadamyali, M. (2013) Correlative live-cell and superresolution microscopy reveals cargo transport dynamics at microtubule intersections. Proc. Natl. Acad. Sci. U. S. A. 110, 3375–3380

66. Lübke, T., Lobel, P., and Sleat, D. E. (2009) Proteomics of the lysosome. Biochim. Biophys. Acta 1793, 625–635

67. Miranda-Ozuna, J. F. T., Rivera-Rivas, L. A., Cárdenas-Guerra, R. E., Hernández-García, M. S., Rodríguez-Cruz, S., González-Robles, A., Chavez-Munguía, B., and Arroyo, R. (2019) Glucose-restriction increases *Trichomonas vaginalis* cellular damage towards HeLa cells and

proteolytic activity of cysteine proteinases (CPs), such as TvCP2. Parasitology 146, 1156–1166

68. Dahms, N. M., and Hancock, M. K. (2002) P-type lectins. Biochim. Biophys. Acta 1572, 317–340

69. Liu, L., Lee, W. S., Doray, B., and Kornfeld, S. (2017) Role of spacer-1 in the maturation and function of GlcNAc-1-phosphotransferase. FEBS Lett. 591, 4755

70. Gonzalez-Noriega, A., Grubb, J. H., Talkad, V., and Sly, W. S. (1980) Chloroquine inhibits lysosomal enzyme pinocytosis and enhances lysosomal enzyme secretion by impairing receptor recycling. J. Cell Biol. 85, 839–852

71. Fedele, A. O., and Proud, C. G. (2020) Chloroquine and bafilomycin A mimic lysosomal storage disorders and impair mTORC1 signalling. Biosci. Rep. 40, doi: 10.1042/BSR20200905

72. Chardin, P., and McCormick, F. (1999) Brefeldin A: The advantage of being uncompetitive. Cell 97, 153–155

73. Doyle, P., Sajid, M., O'Brien, T., DuBois, K., Engel, J., Mackey, Z., and Reed, S. (2008) Drugs targeting parasite lysosomes. Curr. Pharm. Des. 14, 889–900

74. Gao, Y., Chen, Y., Zhan, S., Zhang, W., Xiong, F., and Ge, W. (2017) Comprehensive proteome analysis of lysosomes reveals the diverse function of macrophages in immune responses. Oncotarget 8, 7420–7440

75. Schröder, B. A., Wrocklage, C., Hasilik, A., and Saftig, P. (2010) The proteome of lysosomes. Proteomics 10, 4053–4076

76. Peterson, K. M., and Alderete, J. F. (1984) Iron uptake and increased intracellular enzyme activity follow host lactoferrin binding by *Trichomonas vaginalis* receptors. J. Exp. Med. 160, 398–410

77. Mosen, P., Sanner, A., Singh, J., and Winter, D. (2021) Targeted quantification of the lysosomal proteome in complex samples. Proteomes 9, 1–17

78. Noël, C. J., Diaz, N., Sicheritz-Ponten, T., Safarikova, L., Tachezy, J., Tang, P., Fiori, P. L., and Hirt, R. P. (2010) *Trichomonas vaginalis* vast BspA-like gene family: Evidence for functional diversity from structural organisation and transcriptomics. BMC Genomics 11, doi: 10.1186/1471-2164-11-99

79. Molgora, B. M., Rai, A. K., Sweredoski, M. J., Moradian, A., Hess, S., and Johnson, P. J. (2021) A novel *Trichomonas vaginalis* surface protein modulates parasite attachment via protein:Host cell proteoglycan interaction. MBio 12, 1–17

80. Arroyo, R., Cárdenas-Guerra, R. E., Figueroa-Angulo, E. E., Puente-Rivera, J., Zamudio-Prieto, O., and Ortega-López, J. (2015) *Trichomonas vaginalis* cysteine proteinases: Iron response in gene expression and proteolytic activity. Biomed Res. Int. 2015, doi: 10.1155/2015/946787

81. Ramón-Luing, L. A., Rendón-Gandarilla, F. J., Cárdenas-Guerra, R. E., Rodríguez-Cabrera, N. A., Ortega-López, J., Avila-González, L., Angel-Ortiz, C., Herrera-Sánchez, C. N., Mendoza-

García, M., and Arroyo, R. (2010) Immunoproteomics of the active degradome to identify biomarkers for *Trichomonas vaginalis*. Proteomics 10, 435–444

82. Hernández-Romano, P., Hernández, R., Arroyo, R., Alderete, J. F., and López-Villaseñor, I. (2010) Identification and characterization of a surface-associated, subtilisin-like serine protease in *Trichomonas vaginalis*. Parasitology 137, 1621–1635

83. Hu, G., and St. Leger, R. J. (2004) A phylogenomic approach to reconstructing the diversification of serine proteases in fungi. J. Evol. Biol. 17, 1204–1214

84. Li, J., Yu, L., Yang, J., Dong, L., Tian, B., Yu, Z., Liang, L., Zhang, Y., Wang, X., and Zhang, K. (2010) New insights into the evolution of subtilisin-like serine protease genes in Pezizomycotina. BMC Evol. Biol. 10, 1–14

85. Shayman, J. A., and Tesmer, J. J. G. (2019) Lysosomal phospholipase A2. Biochim. Biophys. Acta - Mol. Cell Biol. Lipids 1864, 932–940

86. Harwig, S. S. L., Tan, L., Qu, X. D., Cho, Y., Eisenhauer, P. B., and Lehrer, R. I. (1995) Bactericidal properties of murine intestinal phospholipase A2. J. Clin. Invest. 95, 603–610

87. Fenard, D., Lambeau, G., Valentin, E., Lefebvre, J. C., Lazdunski, M., and Doglio, A. (1999) Secreted phospholipases A2, a new class of HIV inhibitors that block virus entry into host cells. J. Clin. Invest. 104, 611–618

88. Sanon, A., Tournaire-Arellano, C., Younes El Hage, S., Bories, C., Caujolle, R., and Loiseau, P. M. (2005) N-acetyl-β-d-hexosaminidase from *Trichomonas vaginalis*: substrate specificity and activity of inhibitors. Biomed. Pharmacother. 59, 245–248

89. Rivero, M. R., Miras, S. L., Feliziani, C., Zamponi, N., Quiroga, R., Hayes, S. F., Rópolo, A. S., and Touz, M. C. (2012) Vacuolar protein sorting receptor in *Giardia lamblia*. PLoS One 7, e43712

90. Sloves, P. J., Delhaye, S., Mouveaux, T., Werkmeister, E., Slomianny, C., Hovasse, A., Dilezitoko Alayi, T., Callebaut, I., Gaji, R. Y., Schaeffer-Reiss, C., Van Dorsselear, A., Carruthers, V. B., and Tomavo, S. (2012) Toxoplasma sortilin-like receptor regulates protein transport and is essential for apical secretory organelle biogenesis and host infection. Cell Host Microbe 11, 515–527

91. Dennes, A., Cromme, C., Suresh, K., Kumar, N. S., Eble, J. A., Hahnenkamp, A., and Pohlmann, R. (2005) The novel *Drosophila* lysosomal enzyme receptor protein mediates lysosomal sorting in mammalian cells and binds mammalian and Drosophila GGA adaptors. J. Biol. Chem. 280, 12849–12857

92. Samuelson, J., Banerjee, S., Magnelli, P., Cui, J., Kelleher, D. J., Gilmore, R., and Robbins, P. W. (2005) The diversity of dolichol-linked precursors to Asn-linked glycans likely results from secondary loss of sets glycosyltranferases. Proc. Natl. Acad. Sci. U. S. A. 102, 1548–1553

93. Lee, J., and Ye, Y. (2018) The roles of endo-lysosomes in unconventional protein Secretion. Cells 7, doi: 10.3390/cells7110198

94. Perez-Riverol, Y., Csordas, A., Bai, J., Bernal-Llinares, M., Hewapathirana, S., Kundu, D., Inuganti, A., Griss, J., Mayer, G., Eisenacher, M., and Al., E. (2019) The PRIDE database and

related tools and resources in 2019: improving support for quantification data. Nucleic Acids Res. 47, D442–D450

Figure legends

Figure 1. Lysosomal localization of TvRab7a in *T. vaginalis* TV17-48. TvRab7a (Rab7) was visualized using mouse monoclonal α-HA antibody and (A) Alexa Fluor 594 (red) or (B) Alexa Fluor 488 (green) donkey α-mouse antibody. FITC-lactoferrin (A, green) or LysoTracker (B, red) was used as a lysosomal marker. BF, brightfield; Coloc, colocalization channel (Imaris software). Scale bar = 5 μm.

Figure 2. The isolation of lysosomes. (A) The Percoll gradient yielded two bands corresponding to hydrogenosomes (1) and lysosomes (2). (B) Western blot of Percoll fractions from three independent isolations. HA-tagged TvRab7a was enriched in fraction 2, where the ER marker sPDI was also present. Hydrogenosomal OscC was detected only in fraction 1. (C) The Optiprep gradient showed three fractions. (D) Western blot of Optiprep fractions. (E) Immunofluorescence microscopy of *T. vaginalis* TV17-48 with endocytosed Dynabeads. The beads covered with FITC-lactoferrin (green) colocalize with mouse monoclonal α-HA and Alexa Fluor 594 donkey α-mouse-labelled TvRab7a (red) in phagolysosomes. (F) Western blot of three isolations by Dynabeads. Scale bar = 5 μm.

Figure 3. Lysosomal proteome. The 462 proteins were sorted into 21 groups with the help of TrichDB annotations, Pfam motif identifications, and molecular function gene ontology.

Figure 4. Schematic of Rabs in the endomembrane system. Rabs displayed in colour were identified in the lysosomal proteome and annotated with high confidence. Rabs in grey were found, but their phylogenetic classifications were weakly supported. White Rabs have been previously described to be present in the respective organelle but were not found in our

lysosomal proteome. Rab7 (TvRab7a) was used in this study as lysosomal marker. Grey arrows indicate the transport of cargo to the cell surface and secretion. MVB, multivesicular body; ER, endoplasmic reticulum.

Figure 5. Overlap of the lysosomal proteome with the secretome (10) and the surface proteome (54). Fifteen proteins were found in all three proteomic studies. The lysosomal proteome and surface proteome had 55 overlapping proteins, and the lysosomal proteome and secretome had 26 overlapping proteins.

Figure 6. Immunofluorescence microscopy of selected proteins. The proteins were visualized using mouse monoclonal α-HA antibody and Alexa Fluor 488 donkey α-mouse (green). LysoTracker (red) was used as a lysosomal marker. (A) Acid phosphatase, (B) Trichomonas β-sandwich repeat protein 5, (C) β-hexosaminidase, (D) *Trichomonas vaginalis* cysteine protease 2. BF, brightfield; Coloc, colocalization channel (ImarisColoc software). Scale bar = 5 μm.

Figure 7. Effect of LTS mutations on CLCP localization. (A) Localization of wild-type CLCP (WT) and CLCP with mutated glycosylation motifs LTS1 and LTS2 (mCLCP) in *T. vaginalis* T1. WT CLCP and mCLCP versions were visualized using mouse monoclonal α-HA antibodies and Alexa Fluor 488 donkey α-mouse antibodies (green). BF, brightfield; Coloc, colocalization channel (ImarisColoc software). Scale bar = 5 μm. (B) Schematic illustration of the amino acid substitutions (in red) introduced into glycosylation motifs LTS1 and LTS2 of CLCP. (C) Boxplot chart of Pearson's correlation coefficient (PCC) in colocalized volume for WT CLCP and mCLCP versions with LysoTracker. WT CLCP and LysoTracker colocalized with PCC $r = 0.512 \pm 0.1$ (n = 16), whereas the PCCs of the mCLCP versions were below $r = 0.1$ (n = 12 cells per each version).

Error bars represent standard deviation. (D) Secretion of mutated and WT CLCP. CLCP with mutated LTS1 (SST, QST) and LTS2 (SRS, QRS) was secreted and detected in the extracellular supernatant after 1 h incubation at 37°C. WT CLCP was not secreted and was associated only with cells (Pellet). Each experiment was performed with biological triplicates.

Figure 8. Domain composition of human MPR300 (hMPR300) and *T. vaginalis* homologues (TvMPR). hMPR300 consists of 15 repeats, of which five are homologous to TvMPRs. Detected C-terminal signal sequence motifs DxxLL and YxxØ (Ø, hydrophobic amino acid residue), which are involved in the internalization and trafficking of membrane proteins is indicated. M6P and IGF2 binding sites are absent in TvMPRs; only TvMPR-5 possesses three M6P binding residues, and TvMPR-1 and TvMPR-6 contain a single residue. TvMPR-2 contains the isoleucine that is essential for IGF2 binding. No N-terminal signal peptide was predicted in TvMPRs. SP, signal peptide; TM, transmembrane.

Figure 9. Immunofluorescence microscopy of (A) TvMPR-2 and (B) TvMPR-3. The proteins were visualized using mouse monoclonal α-HA antibody and Alexa Fluor 488 donkey α-mouse (green) in *T. vaginalis* T1. BA1 was used as an ER marker and was stained with rabbit polyclonal α-V5 antibody and Alexa Fluor 594 donkey α-rabbit (red). TvMPR-2 and TvMPR-3 strongly colocalized with BA1 in the ER and possibly Golgi body (asterisk). Some TvMPR-2 and TvMPR-3 appeared in small vesicles not colocalizing with BA1 (arrows). BA1, β-amylase 1; TvMPR, *Trichomonas vaginalis* mannose 6-phosphate receptor; BF, brightfield; Coloc, colocalization channel (ImarisColoc software). Scale bar = 5 µm.

Figure 10. Effect of LTS on BA2 localization. (A) Localization of wild-type and mutated BA2 (mBA2) in *T. vaginalis* T1 transformants. Both were visualized using mouse monoclonal α-HA antibodies and Alexa Fluor 488 donkey α-mouse antibodies (green). LysoTracker (red) was used as endolysosomal marker. BF, brightfield; Coloc, colocalization channel (Imaris software). Scale bar = 5 μm. (B) Schematic illustration of LTS1 and LTS2 insertions introduced into BA2. (C) Boxplot chart of Pearson's correlation coefficient (PCC) in colocalized volume for BA2 and mBA2 with LysoTracker. BA2 and LysoTracker did not colocalize with a PCC $r = 0.051 \pm 0.029$ (n = 29), whereas the PCC of mBA2 was $r = 0.556 \pm 0.07$ (n = 22). Error bars represent standard deviation. (D) Secretion of BA2 and mBA2. BA2 is secreted and can be detected in the extracellular supernatant and in cells (pellet) after 1h incubation at 37°C, whereas mBA2 was not secreted. Each experiment was performed with biological triplicates.

Figure 11. pH-dependent secretion of TvCP2. (A) Western blot of secreted TvCP2, acid phosphatase (AP), and β-amylase 2 (BA2) after 15 min and 45 min incubation at 37°C. Both chloroquine (CLQ) and brefeldin A (BFA) inhibited secretion of TvCP2 compared to the untreated control. Secretion of AP and BA2 was inhibited upon incubation with BFA compared to the untreated controls, but no change in secretion was observed upon treatment with CLQ. Each experiment was performed with biological triplicates. (B) Quantification of western blots using densitometry that shows the relative amounts of secreted TvCP2, AP, and BA2 from three biological replicates. Error bars indicate standard deviation. a. u., arbitrary unit; untr, untreated.

Figure 12. Hypothetical protein delivery to lysosomes and secretion in *T. vaginalis*. CLCP is a resident lysosomal peptidase, delivery of which is dependent on a glycosylation signal. Upon signal mutation (mCLCP), the protein is secreted. BA1, BA2, AP, and mCLCP are secreted via the

classical ER-Golgi secretory pathway that is inhibited by brefeldin A but not chloroquine. They are delivered by secretory vesicles directly to the plasma membrane and released to the extracellular space. AP is eventually endocytosed and transported to lysosomes. Introduction of CLCP glycosylation signal into BA2 (mBA2) redirected this protein to lysosomes. TvCP2 is a lysosomal peptidase, which is secreted. Inhibition of acidification by chloroquine inhibited TvCP2 secretion, which indicates that this peptidase is secreted via unconventional lysosomal pathway (UPS). AP, acid phosphatase; TvCP2, *Trichomonas vaginalis* cysteine protease 2; BA, β-amylase; TvMPR, *T. vaginalis* mannose 6-phosphate receptor; ER, endoplasmic reticulum; LE, late endosome; MVB, multivesicular body; CLQ, chloroquine; BFA, brefeldin A. Arrows indicate possible directions of the transport.

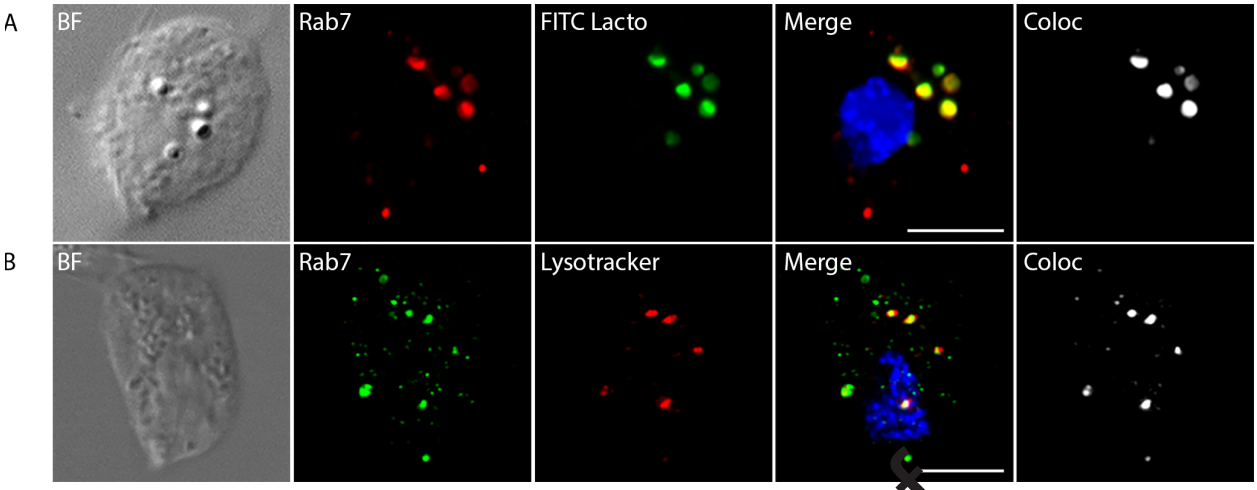

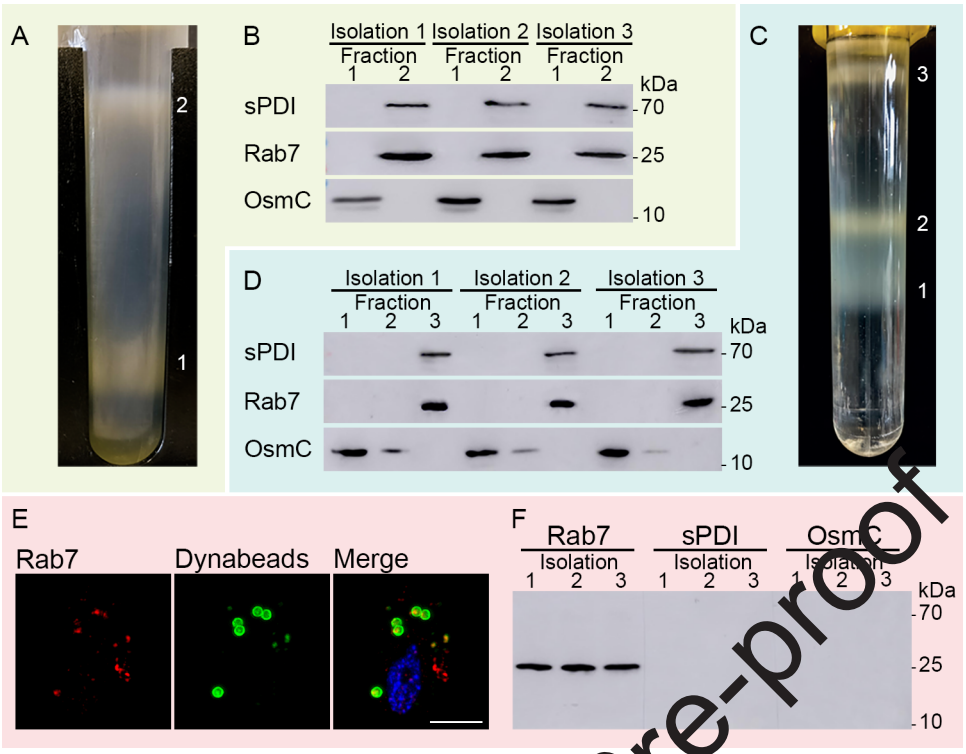

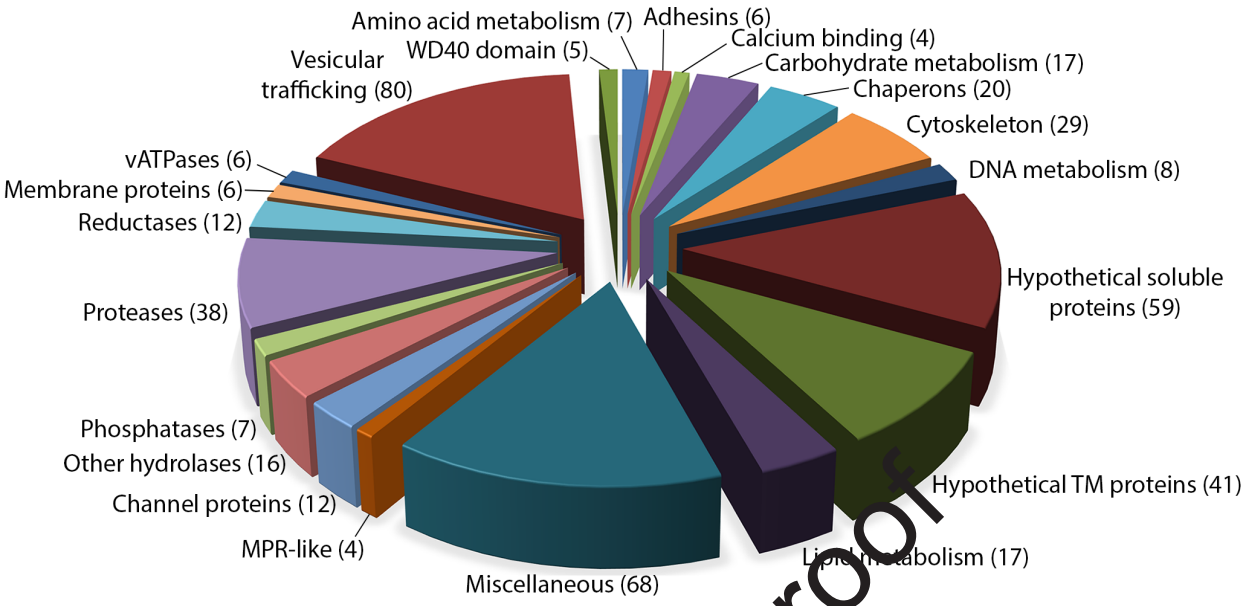

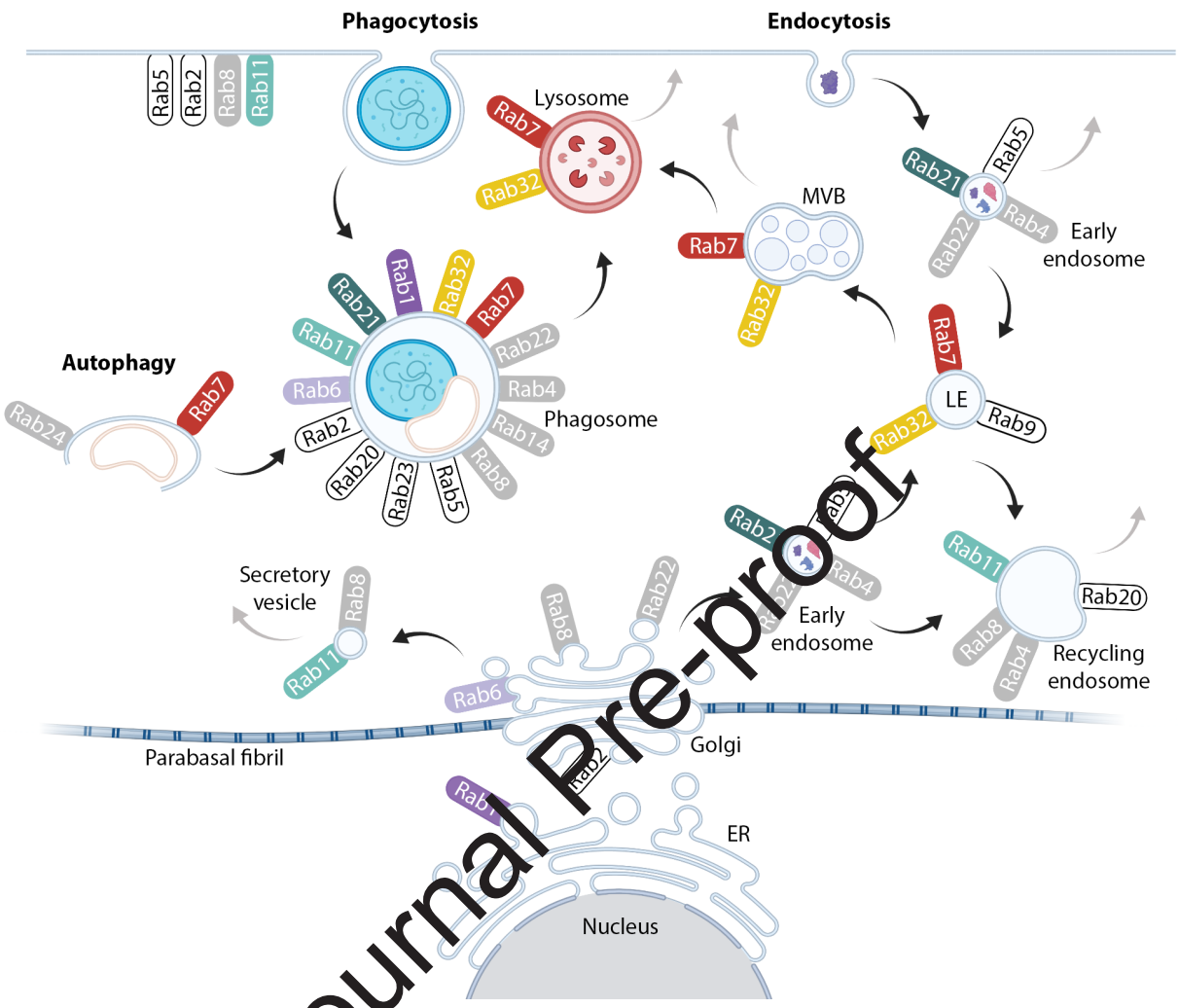

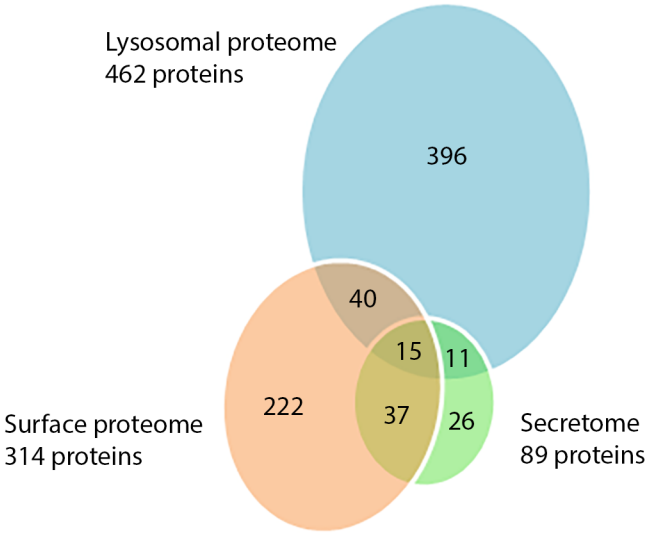

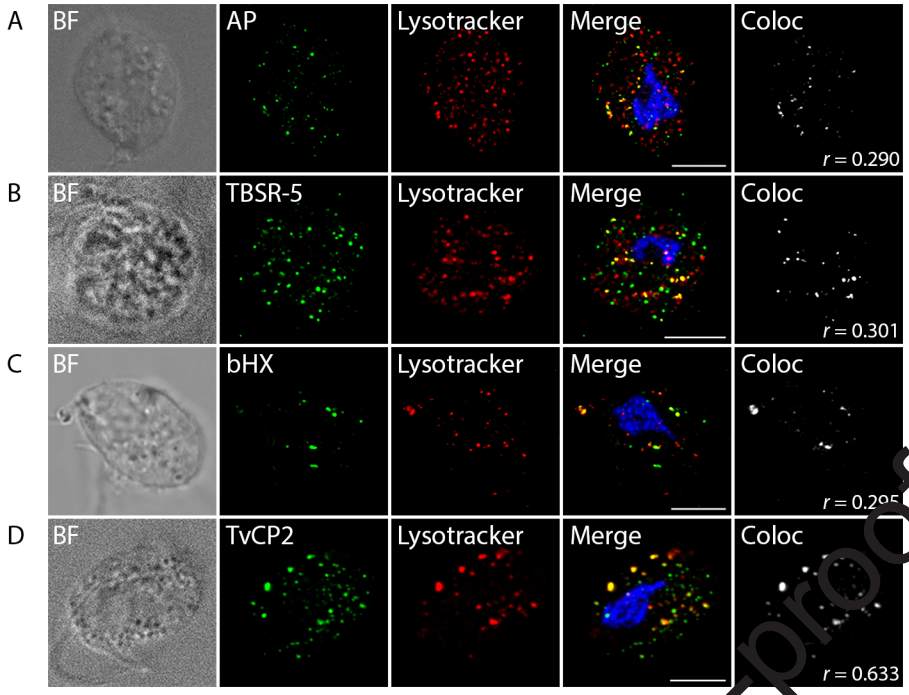

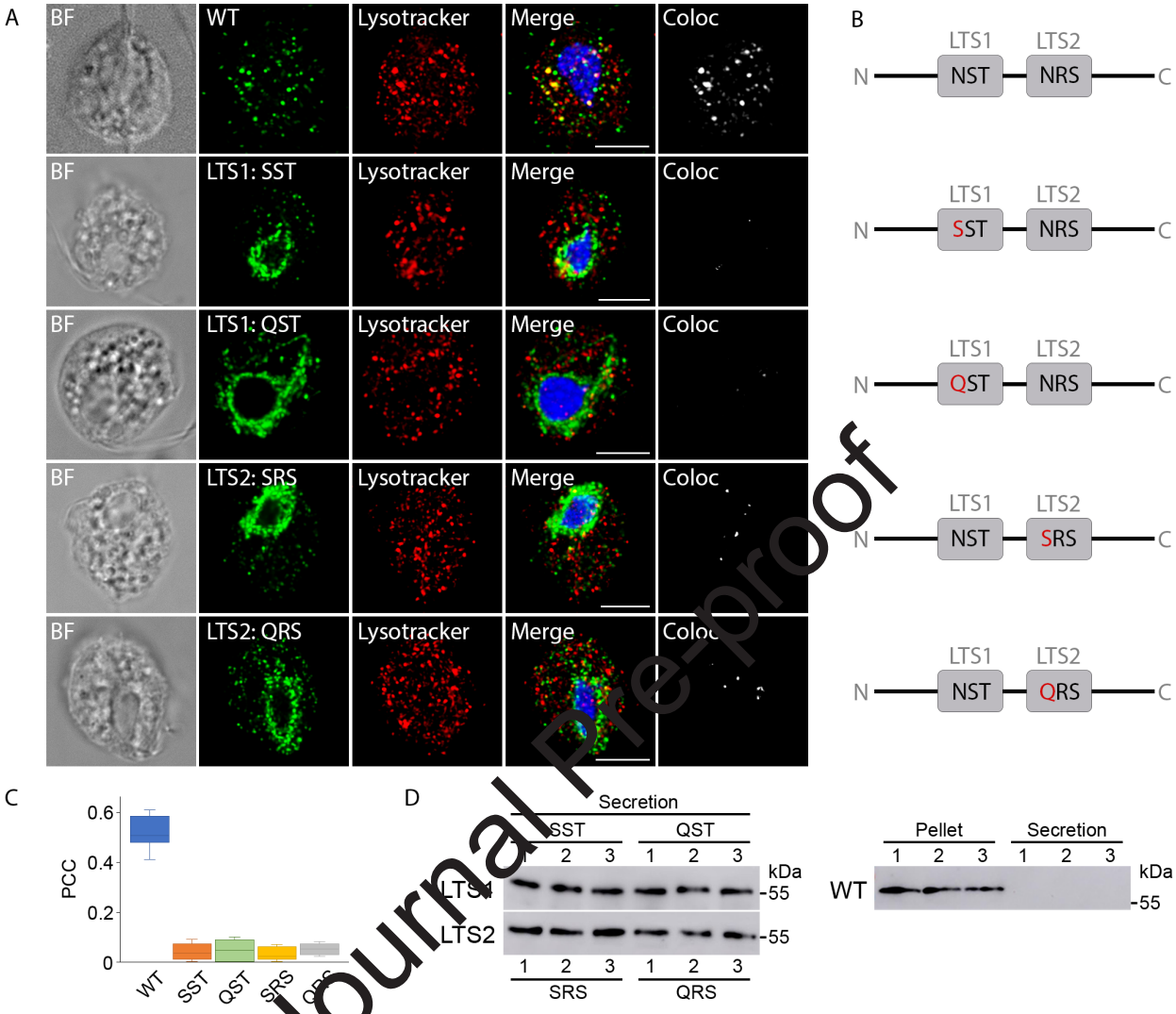

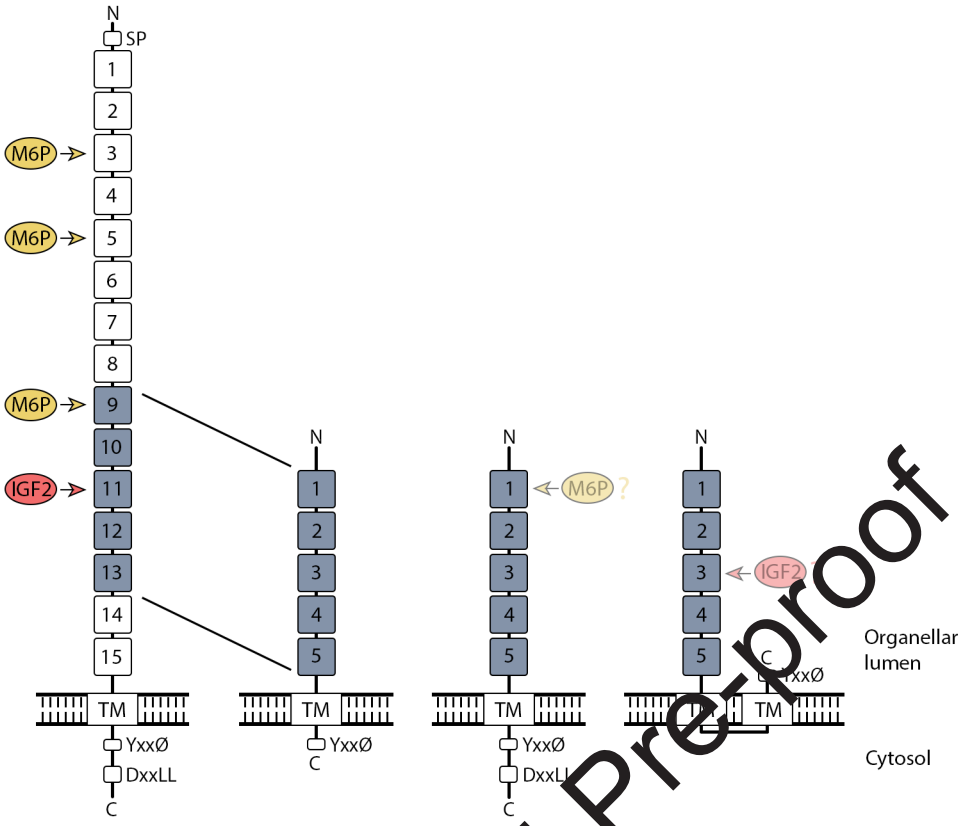

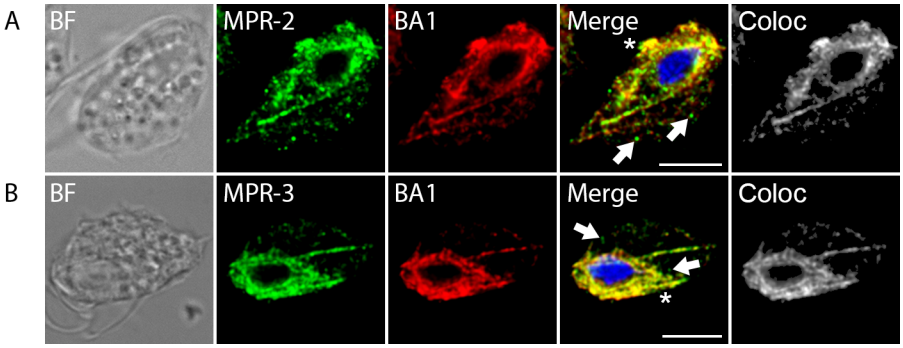

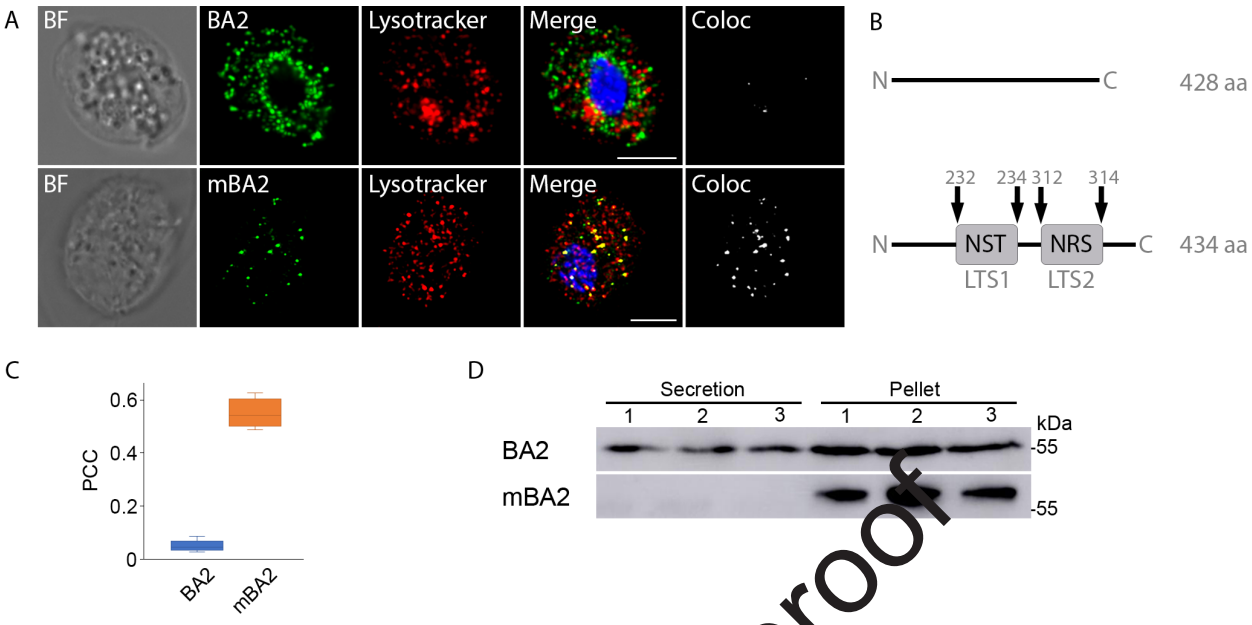

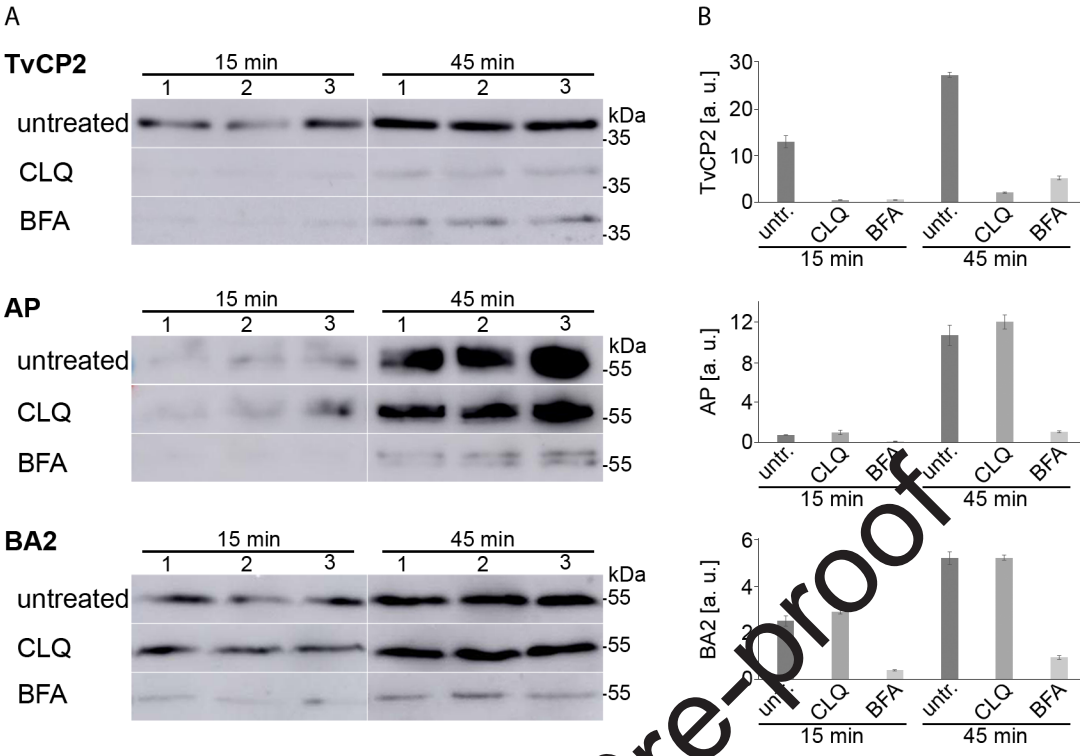

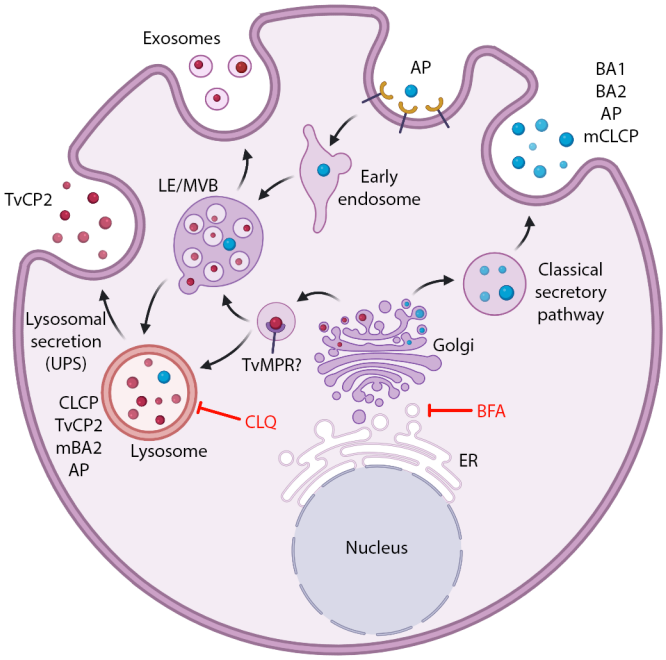

Highlights

- *Trichomonas vaginalis* phagolysosome consist of over 460 proteins
- Lysosomes are involved in secretion of virulence factors such as TvCP2
- N-glycosylation is required for lysosomal protein targeting
- *T. vaginalis* possess homologs of mannose 6-phosphate receptor

Author contributions

NZ, TS, and KH designed and conducted experiments. NZ, performed microscopy. IH, and PR designed experiments. VŽ, KZ, JD and JT, performed data analyses. NZ, and JT, conceived study, wrote the manuscript, acquired funding.

In Brief

Lysosomes represent a central degradative compartment of eukaryotes, yet little is known about biogenesis and function of this organelle in the parasitic protist *Trichomonas vaginalis*. We analysed the phagolysosomal proteome that consists of over 460 proteins including important virulence factors. We demonstrated that glycosylation is involved in lysosomal protein targeting in *T. vaginalis*, which is unprecedented in parasitic protists. In addition to the classical secretory pathway, lysosomes are involved in unconventional protein secretion.

Dynamic secretome of *Trichomonas vaginalis*: Case study of β-amylases*[S]

Jitka Štáfková‡, Petr Rada‡, Dionigia Meloni‡, Vojtěch Žárský‡, Tamara Smutná‡, Nadine Zimmann‡, Karel Harant‡, Petr Pompach§¶, Ivan Hrdý‡, and Jan Tachezy‡‖

The secretion of virulence factors by parasitic protists into the host environment plays a fundamental role in multifactorial host–parasite interactions. Several effector proteins are known to be secreted by *Trichomonas vaginalis*, a human parasite of the urogenital tract. However, a comprehensive profiling of the *T. vaginalis* secretome remains elusive, as do the mechanisms of protein secretion. In this study, we used high-resolution label-free quantitative MS to analyze the *T. vaginalis* secretome, considering that secretion is a time- and temperature-dependent process, to define the cutoff for secreted proteins. In total, we identified 2 072 extracellular proteins, 89 of which displayed significant quantitative increases over time at 37 °C. These 89 *bona fide* secreted proteins were sorted into 13 functional categories. Approximately half of the secreted proteins were predicted to possess transmembrane helixes. These proteins mainly include putative adhesins and leishmaniolysin-like metallopeptidases. The other half of the soluble proteins include several novel potential virulence factors, such as DNaseII, pore-forming proteins, and β-amylases. Interestingly, current bioinformatic tools predicted the secretory signal in only 18% of the identified *T. vaginalis*-secreted proteins. Therefore, we used β-amylases as a model to investigate the *T. vaginalis* secretory pathway. We demonstrated that two β-amylases (BA1 and BA2) are transported via the classical endoplasmic reticulum-to-Golgi pathways, and in the case of BA1, we showed that the protein is glycosylated with multiple *N*-linked glycans of $Hex_5HexNAc_2$ structure. The secretion was inhibited by brefeldin A but not by FLI-06. Another two β-amylases (BA3 and BA4), which are encoded in the *T. vaginalis* genome but absent from the secretome, were targeted to the lysosomal compartment. Collectively, under defined *in vitro* conditions, our analysis provides a comprehensive set of constitutively secreted proteins that can serve as a reference for future comparative studies, and it provides the first information about the classical secretory pathway in this parasite. *Molecular & Cellular Proteomics 17: 10.1074/mcp.RA117.000434, 304–320, 2018.*

From the ‡Department of Parasitology, ¶Department of Biochemistry, Charles University, Faculty of Science, BIOCEV, Vestec, Czech Republic; §Institute of Biotechnology CAS, v. v. i., BIOCEV, Vestec, Czech Republic

Received October 28, 2017
Published, MCP Papers in Press, December 12, 2017, DOI 10.1074/mcp.RA117.000434
Author contributions: J.x., P.R., D.M., V.x., T.S., N.Z., K.H., P.P., I.H., and J.T. performed the research; J.x., P.R., V.x., and J.T. analyzed data; I.H. and J.T. designed the research; and J.T. wrote the paper.

Trichomonas vaginalis is an anaerobic, aerotolerant pathogen that causes trichomoniasis, the most widespread nonviral sexually transmitted disease in humans. Although the majority of infections are asymptomatic, approximately one-third of infected women develop symptoms such as vaginitis and urethritis (1). In addition, trichomonad infection has been associated with poor birth outcomes and increased risk of Human Immunodeficiency Virus (HIV) acquisition (2). In men, the infection is rarely symptomatic; however, the parasite can damage sperm cells (3, 4), and chronic infection has been associated with prostate cancer (5, 6).

In the female urogenital tract, *T. vaginalis* is challenged by factors such as nutrient limitation, the host immune response, physiological changes during the menstrual cycle, the continual flow of vaginal fluid, and coexistence with other members of the vaginal microbiota (7). Upon transmission to men, the parasite must adapt to the different environmental conditions within the male urogenital tract, including increased concentrations of zinc in the prostatic fluid that may kill the parasite (8, 9). Thus, the establishment of trichomonad infection within such hostile environments is dependent on multifactorial host–parasite interactions that involve both contact-dependent and contact-independent mechanisms (10). The former include the adherence of the parasite to vaginal epithelial cells, the contact-dependent extracellular killing of host cells (11–14), and active phagocytosis of host cells and bacteria (15, 16). The contact-independent mechanisms include the secretion of soluble biologically active molecules, particularly proteases with diverse effects (10, 17, 18). Finally, *T. vaginalis* has been shown to pack specific sets of macromolecules into microvesicles (exosomes) that are secreted and that influence the parasite's binding to the host cell (19).

With regard to nutrients, the energy metabolism of *T. vaginalis* is dependent on glucose to generate ATP via anaerobic fermentation in the cytosol and via the extended glycolytic pathway in hydrogenosomes, an anaerobic form of mitochondria (20, 21). The main source of glucose in the vaginal fluid is likely free glycogen derived from vaginal epithelial cells (VECs)

(22–26). To be utilized by *T. vaginalis*, glycogen and glucose-containing polymers must be extracellularly digested to monomeric glucose, which is then transported into the cells. Glycogen-hydrolyzing enzymes include endo-acting α-amylases (EC 3.2.1.1) that randomly hydrolyze α-1,4-linkages of glycogen, exo-acting β-amylases (EC 3.2.1.2) that hydrolyze α-1,4-linkages of glycogen at the nonreducing end to liberate β-maltose, and α-glucosidases (EC 3.2.1.20) that act on α-1,4-linkages of oligosaccharides to liberate D-glucose. Early studies suggested that *T. vaginalis* secretes α-glucosidase to hydrolyze maltose to glucose (27). More recently, enzymes with α-amylase and β-amylase activities that utilize glycogen as a substrate were found to be released by *T. vaginalis* (28, 29).

High-resolution mass-spectrometry-based proteomic studies have been used to analyze the *T. vaginalis* surface proteome (30) and the exosome proteome (19), which have revealed a number of new candidate proteins with potential roles in *T. vaginalis*–host interactions and in the parasite's pathogenicity. More recent quantitative proteomic analyses have identified surface membrane proteins that are released to the *T. vaginalis* environment upon cleavage by rhomboid protease (31). The best-studied group of secreted proteins is the proteases, including cysteine proteases and metalloproteases (17, 32, 33). Kucknoor *et al.* (34) identified 32 various secreted proteins, including a putative adhesin, AP65, via 2-D SDS-PAGE followed by MALDI-TOF (34). In addition, Twu *et al.* showed that the parasite secretes a macrophage migration inhibitory factor (5). However, information about the *T. vaginalis* secretome remains rather incomplete.

The major challenge for studies of the secretome using high-resolution MS is to identify *bona fide* secreted proteins and avoid artifacts caused by protein contamination. Here, we used quantitative MS and considered the fact that secretion is a time- and temperature-dependent process in defining the cutoff for *T. vaginalis*-secreted proteins. After bioinformatic sorting of the secreted proteins, we focused on β-amylases as model secreted proteins to investigate the *T. vaginalis* secretory pathway. Moreover, β-amylases are absent from humans and animals and may provide a suitable target for the development of novel antiparasitic strategies.

EXPERIMENTAL PROCEDURES

Cell Cultivation—*T. vaginalis* strain Tv17–48 was isolated from a symptomatic patient, and the axenic culture was immediately stored in liquid nitrogen (35). The strain was cultivated in tryptone-yeast extract-maltose medium (TYM) supplemented with 10% inactivated horse serum (36).

Cell Incubation and Sample Preparation—*T. vaginalis* cells in the logarithmic phase of growth were harvested by centrifugation and washed twice in isotonic Doran's medium (37) with 15 mM maltose (Doran's medium with maltose). The cells were then resuspended at a concentration of 1×10^6 cells/ml, and 15 ml of suspension was incubated in 15 ml tubes for 10, 30, 60, and 120 min at 37 °C. Control cells were incubated for 60 and 120 min on ice. After incubation, the cells were removed by centrifugation at 1,000 × *g* for 5 min at 4 °C, and then the supernatant was centrifuged at 10,000 × *g* for 10 min to remove cell debris, filtered through a 0.22 μm filter, and centrifuged at 100,000 × *g* for 75 min to remove microvesicles (5). The proteins in the final supernatant were precipitated with TCA for 10 min at 4 °C (one volume of TCA to four volumes of supernatant). The precipitated proteins were pelleted at 12,000 × *g* for 20 min at 4 °C, washed with cold acetone, dried, and stored at −80 °C.

Cell Integrity Assays—During the incubation described above, the cell integrity was monitored under a light microscope using the trypan blue exclusion test (38). In parallel, at each time point, we determined the free activity of the cytosolic enzyme NADH oxidase in the cell suspension (39). In addition, aliquots of trichomonad suspensions taken at each time point were processed for transmission electron microscopy. The cell samples were centrifuged at 3 000 × *g* for 10 min and fixed in 2.5% glutaraldehyde and 5 mM $CaCl_2$ in 0.1 M cacodylate buffer, pH 7.2, overnight at 4 °C. The cells were then postfixed in 0.1 M cacodylate buffer containing 1.6% ferricyanide, 10 mM $CaCl_2$, and 2% OsO_4 at 4 °C for 15 min, dehydrated in acetone, and embedded in the epoxy resin EMBed 812 (Electron Microscopy Sciences, Hatfield, PA, USA). Ultrathin sections were stained with uranyl acetate and observed using a JEOL JEM-1011.

Protein Preparation—The cell-free samples of TCA-precipitated proteins were dissolved in 100 mM triethylammonium bicarbonate buffer with 2% sodium deoxycholate, reduced with 5 mM tris(2-carboxyethyl)phosphine for 30 min at 60 °C, and alkylated with 10 mM S-methyl methanethiosulfonate for 10 min at room temperature. Total protein concentrations were measured via the bicinchoninic acid assay (Sigma-Aldrich, St. Louis, MO, USA). Next, 100 μg of proteins were digested with trypsin (trypsin:protein ratio 1:50) overnight at 37 °C. After digestion, 1% trifluoroacetic acid (TFA) was added. Sodium deoxycholate was removed by extraction to ethyl acetate as previously described (40). The remaining ethyl acetate was removed using vacuum centrifugation at 45 °C for 10 min, and then 1% TFA was added. The samples were desalted using C18 sorbent (Supelco 66883-U, supplied by Sigma-Aldrich). The eluents were dried and resuspended in 20 μl of 1% TFA.

Mass Spectrometry Data Acquisition—A nano reversed-phase column (EASY-Spray column, 50 cm × 75 μm inner diameter, PepMap C18, 2 μm particles, 100 Å pore size) was used for nanoLC-MS analysis. Mobile phase buffer A consisted of water, 2% acetonitrile, and 0.1% formic acid. Mobile phase B consisted of 80% acetonitrile and 0.1% formic acid. Two micrograms of each sample were loaded onto the trap column (Acclaim PepMap300, C18, 5 μm, 300 Å Wide Pore, 300 μm × 5 mm) at a flow rate of 15 μl/min. The loading buffer consisted of water, 2% acetonitrile, and 0.1% TFA. Peptides were eluted with a gradient from 2% to 40% B over 60 min at a flow rate of 300 nl/min. The peptide cations eluted were converted to gas-phase ions via electrospray ionization and analyzed on a Thermo Orbitrap Fusion (Q-OT- qIT, Thermo Fisher Scientific, Waltham, MA, USA). Spectra were acquired with a 2 s duty cycle. Full MS spectra were acquired in the Orbitrap within a mass range of 350–1,400 *m/z*, at a resolution of 120,000 at 200 *m/z* and with a maximum injection time of 50 ms. The most intense precursors were isolated by quadrupole ion trapping with a 1.6 *m/z* isolation window and fragmented via higher-energy collisional dissociation with the collision energy set to 30%. Fragment ions were detected in the ion trap with the scan range mode set to normal and the scan rate set to rapid with a maximum injection time of 35 ms. The fragmented precursors were excluded from fragmentation for 60 s.

Analysis of Mass Spectrometry Data—For label-free quantification (LFQ), the data were processed in MaxQuant LFQ version 1.5.8.3 (41). Searches were performed using the latest version of the *T. vaginalis* database from UniProt (release 2017_4, 60,330 entries) and a common contaminant database. Trypsin was used to generate the pep-

tides, and two missed cleavages were allowed. The protein modifications were set as follows: cysteine (unimod nr: 39) as static and methionine oxidation (unimod: 1384) and protein N terminus acetylation (unimod: 1) as variable. The precursor ion mass tolerance in the initial search was 20 ppm, the tolerance in the main search was 4.5 ppm, and the fragment ion mass tolerance was 0.5 Da. The false discovery rates for peptides and for proteins were set to 1%.

For each identified protein, the cell localization and secretory pathway signal were predicted using the SignalP 4.1 server (http://www.cbs.dtu.dk/services/TMHMM/), TargetP 1.1 server (http://www.cbs.dtu.dk/services/TargetP/), and SecretomeP 2.0 server (http://www.cbs.dtu.dk/services/SecretomeP/). Transmembrane helixes and topology were predicted using the TMHMM server v. 2.0 (http://www.cbs.dtu.dk/services/TMHMM/). Conserved domains were predicted using Pfam 31.0 (http://pfam.xfam.org/), and distant homologies were detected using the HHpred search against the CD database https://toolkit.tuebingen.mpg.de and Evolutionary Classification of Protein Domains (42) Molecular function gene ontology (http://geneontology.org/page/molecular-function-ontology-guidelines) and manual curation were used to sort the identified proteins.

Experimental Design and Statistical Rationale—Three independent biological experiments were performed, and each biological sample was analyzed in three technical replicates using LFQ mass spectrometry. Proteins with LFQ values determined in at least two biological replicates with two valid values within the technical replicates were used for further processing. Changes in the LFQ values between two consecutive time points were calculated for each biological replicate as the difference in the LFQ binary logarithm between the means of technical replicates. The significance of each change was estimated using Student's *t* test. To distinguish actively released proteins from contaminants, we used two criteria: (i) the secreted protein displayed more significant increases than decreases in LFQ values over time, and (ii) the difference between the LFQ values for a given protein at 37 °C and 4 °C was greater than 1 LFQ unit. The secretion score (SecS) was then calculated as the sum of all decreases and significant increases (p value < 0.05). Hierarchical clustering was performed using the standard UPGMA hierarchical clustering method with the Scipy package (https://www.scipy.org/). Secreted proteins were ordered according to the means of LFQ values of technical replicates at 37 °C. Boxplot analysis of dominant clusters was performed based on the ratio [sum LFQ values (10 min, 30 min)+1]/[sum LFQ values (60 min, 120 min)+1]. The median, 25th, and 75th percentiles were computed for each cluster using the Scipy package (https://www.scipy.org/).

Glycopeptide MS Analysis—The BA1 coding gene was subcloned into the modified TagVag vector (43) to allow for the expression of BA1 in *T. vaginalis* with a streptavidin tag at the C terminus. The logarithmic cell culture (2.5 liter) was harvested, the cells were broken by sonication, and the cell lysate was spun down by ultracentrifugation (100,000 × *g* for 25 min at 4 °C). Tagged BA1 was isolated from the supernatant using the Strep-Tactin system (IBA GmbH, Göttingen, Germany). The purity of the isolated protein was checked by SDS-PAGE.

Recombinant BA1 protein was transferred to 50 mM ammonium bicarbonate buffer, pH 7.8, with Amicon Ultra 0.5 ml centrifugal filters MWCO 3 kDa (Merck, Darmstadt, Germany). Twenty micrograms of BA1 protein were reduced by dithiothreitol (Sigma-Aldrich) and alkylated by iodoacetamide (Sigma-Aldrich). The protein was digested by trypsin (Promega, Madison, WI, USA) overnight at 37 °C. To reduce the size of certain tryptic peptides, the endoproteinase Glu-C (Roche, Basel, Switzerland) was added to the sample and incubated overnight at 25 °C. The peptide mixture was separated by a reversed-phase HPLC connected to a 15 T solariX XR mass spectrometer (Bruker Daltonics, Billerica, MA USA) operating in data-dependent mode. Data were processed by the DataAnalysis 4.2 software (Bruker Daltonics), and glycopeptides were identified by manual data curation based upon measured mass values. Annotated, mass-labeled spectra for all glycopeptides identified are presented in Fig. S1*A*–S1*G*.

β-Amylase Phylogeny—The *T. vaginalis* BA1 protein sequence was used as a query for a BLAST search in the NCBI RefSeq protein database (GenBank release 220.0), and 1,312 homologues were used to build a preliminary phylogeny using Fast Tree (44). Then, 166 representative sequences were manually selected and aligned using MAFFT (45), and the alignment was trimmed with BMGE (354 sites) (46). The phylogenetic tree was inferred using PhyloBayes (47) v. 4.1 under the CAT + GTR model with a burn-in of 1,000 generations and a postburn-in sampling of ~30,000 generations. The maximum likelihood bootstrap support was calculated using PHYML (48) with the best-fit model (LG+I+G4) and 200 bootstrap replicates.

Quantitative Real-Time PCR—Trichomonads were grown in TYM medium lacking maltose with 5% inactivated dialyzed fetal bovine serum (Sigma-Aldrich) and supplemented with either maltose or oyster glycogen at a final concentration of 5%. The cells were subcultured twice under these conditions (48 h) prior to RNA isolation. The iron-depleted cells were subcultured daily in TYM medium supplemented with 5% inactivated dialyzed fetal bovine serum, 5% maltose, and 60 μM 2,2-dipyridyl (Sigma-Aldrich) for 5 days prior to RNA isolation.

An RNA Isolation Kit (Pharmacia, Whitehouse Station, NJ, USA) was used to extract the total RNA from the cells, and the complementary DNA was synthesized using a SuperScript VILO™ cDNA Synthesis Kit (Thermo Fisher Scientific). The RNA was isolated in quadruplicate. The DNATopII, α-tubulin, and actin genes were selected as reference genes for quantitative RT-PCR (qRT-PCR) analysis (49). The specific primers for the amplification of β-amylases are listed in Table S1. Gene expression levels were evaluated using a LightCycler 480 instrument (Roche). Each amplification reaction (10 μl) contained specific primers (400 nM final concentration), 20 ng of cDNA template, iQ SYBR Green Supermix (Bio-Rad, Hercules, CA, USA) and RNase-free water. PCR thermal cycling conditions: 95 °C for 3 min followed by 50 cycles of 95 °C for 10 s, 63 °C for 20 s, and 72 °C for 30 s. The specificity of the amplified PCR product was assessed by performing a melting curve analysis. The PCR data were analyzed using the GenEx software (MultiD Analyses). Relative gene expression levels were normalized to the expression levels of reference genes selected by the Normfinder software (https://moma.dk/normfinder-software).

Cellular Localization of Biotinylated β-Amylases—A partial sequence of *T. vaginalis* protein disulfide isomerase (TVAG_267400) encoding the first 75 amino acids (AAs) was amplified by PCR from genomic DNA and fused at the C terminus with *Escherichia coli* gene for biotin ligase (BirA, WP_023308552) amplified from pET21a-BirA (50). Protein disulfide isomerase-BirA was subcloned to modified pTagVag (43), in which the C-terminal hemagglutinin tag was replaced with the 2xV5 epitope tag and the KQEL sequence, and the neomycin phosphotransferase cassette was replaced with the puromycin-N-acetyltransferase gene (pTagVag-V5-Pur). The vector was introduced into *T. vaginalis* by electroporation as previously described (43), and transformants were selected in the presence of 40 μg/ml puromycin (strain Tv17–48-BirA).

The β-amylase-coding genes BA1–4 were amplified by PCR and subcloned into the modified pTagVag, into which we introduced a sequence encoding the biotin acceptor peptide (AP, GLNDIFEAQKIEWHE), which allowed for the production of recombinant proteins with a C-terminal AP tag. The BA1–4 genes were expressed under the control of the native promotor (ca. 500 bp of upstream noncoding sequences). The constructs were electroporated into the Tv17–48-BirA strain, and the double transformants were selected in the pres-

ence of 200 μg/ml geneticin and 40 μg/ml puromycin. All primers used for gene amplification and cloning are listed in Supplemental Table S1.

Immunofluorescence Microscopy—For biotin labeling, the double transformants were incubated in TYM medium with 1 mM biotin for 30 min at 37 °C. Cells were then fixed in 1% formaldehyde for 30 min, washed in PEM (100 mM PIPES, 1 mM EGTA, 0.1 mM MgSO4) buffer (51) and placed on high-performance cover glasses (Carl Zeiss, Oberkochen, Germany). The attached cells were treated in 1% Triton X-100 for 20 min in PEM and stained using rabbit polyclonal α-V5 Ab[1] (Sigma-Aldrich) and the secondary antibody Alexa Fluor 594 donkey α-rabbit Ab (Life Technologies, Carlsbad, CA, USA). Biotinylated proteins were detected using streptavidin Alexa Fluor 488 conjugate (Life Technologies). Structured illumination microscopy (SIM) was performed on a 3D N-SIM microscope (Nikon Eclipse Ti-E, Nikon, Japan) equipped with a Nikon CFI SR Apo TIRF objective (100x oil, NA 1.49). The structured illumination pattern projected into the sample plane was created on a diffraction grating block (100 EX V-R 3D-SIM) at laser wavelengths of 488 and 561 nm. The excitation and emission light were separated by filter sets SIM488 (excitation 470–490, emission 500–545) and SIM561 (excitation 556–566 nm, emission 570–640 nm). The emission light was projected through a 2.5x relay lens onto the chip of an EM CCD camera (AndoriXon Ultra DU897, 10 MHz at 14-bit, 512 × 512 pixels, Andor Technology, Belfast, U.K.). Three-color *z*-stacks (*z*-step: 125 nm) were acquired in the NIS-Elements AR software (Laboratory Imaging, Prague, Czech Republic). The laser intensity, EM gain, and camera exposure time were set independently for each excitation wavelength. The intensity of the fluorescence signal was maintained within the linear range of the camera. Fifteen images (three rotations and five phase shifts) were recorded for every plane and color. The SIM data were processed in the NIS-Elements AR software. Before sample measurement, the symmetry of the point spread function was checked with 100 nm red fluorescent beads (580/605, Carboxylate-Modified Microspheres, Life Technologies) mounted in Prolong Diamond Antifade Mountant (Life Technologies) and optimized by adjusting the objective correction collar. The signal for 4,6-diamidine-2-phenylindole dihydrochloride (DAPI) was observed in wide-field mode.

Effect of Inhibitors on β-Amylase Glycosylation and Secretion—Trichomonads episomally expressing HA-tagged BA1–4 were inoculated into TYM medium (1×10^5 cells/ml) supplemented with 5 μg/ml tunicamycin (Sigma-Aldrich) and grown for 24 h. The control cells were grown without tunicamycin. After 24 h, the cells were harvested by centrifugation, and the cell lysate was examined by Western blot analysis with mouse monoclonal α-HA Ab (Sigma-Aldrich). Brefeldin A (Sigma-Aldrich) and FLI-06 (Sigma-Aldrich) were tested using *T. vaginalis* episomally expressing HA-tagged BA1–3. The cells (1×10^6 cells/ml of TYM without serum) were preincubated for 30 min at 24 °C with brefeldin A (50 μg/ml) or FLI-06 (50 μM), and then the cells were washed with the medium and incubated with the inhibitors for 5 and 60 min at 37 °C. The cells were then removed by centrifugation, and the proteins in the supernatant were precipitated by TCA as described above and examined by Western blot analysis with mouse monoclonal α-HA Ab. Western blots were quantified using ImageJ v1.47 (National Institute of Health, Bethesda, MD, USA), and statistical analysis was performed using the Mann-Whitney nonparametric test (GraphPad Software, Inc., La Jolla, CA, USA).

Treatment of β-Amylases with N-glycosidase F (PNGase F)—*T. vaginalis* strains expressing HA-tagged BA1–4 were harvested by centrifugation (~2×10^6 cells), washed twice with 50 mM sodium phosphate buffer, pH 7.5, resuspended in 100 μl of the same buffer with 0.2% SDS and 100 mM β-mercaptoethanol, and denatured at 100 °C for 10 min. Then, Triton X-100 was added to a final concentration of 1%, and a 50 μl aliquot was treated with 1 U PNGase F (Sigma-Aldrich) at 37 °C for 120 min. After incubation, the sample was incubated at 100 °C for 5 min and examined by Western blot analysis with mouse monoclonal α-HA Ab.

Localization of BA4 in Lactoferrin-Labeled Vesicles—After preliminary experiments to optimize the conditions, trichomonads episomally expressing HA-tagged BA1–4 were incubated at 20 °C for 10 min in TYM with 450 μg/ml lactoferrin (Sigma-Aldrich) labeled with FITC as previously described (http://www.ridgeviewinstruments.com). The cells were then washed twice in TYM and processed for immunofluorescence microscopy as described above. BA1–4 were labeled using mouse monoclonal α-HA Ab (Sigma-Aldrich) and the secondary Alexa Fluor 594 donkey α-mouse Ab (Life Technologies).

RESULTS

Analysis of Secreted Proteins Using Quantitative Mass Spectrometry—To study the secretome of *T. vaginalis,* we developed a protocol for analyzing the time-dependent accumulation of extracellular proteins via high-resolution nano LC coupled with ESI-linear-ion trap and MS/MS LFQ. The cells were incubated in Doran's medium with maltose for 10, 30, 60, and 120 min at 37 °C, and the amounts of secreted proteins were analyzed at each time point. The control cells were incubated for 60 and 120 min on ice. The viability of the cells during incubation was monitored via a trypan blue exclusion test that revealed >99% ($n = 12$) viable cells during all experiments. The intactness of the cells was further monitored via an enzyme assay using NADH oxidase as a cytosolic marker enzyme (Table S2). In addition, the integrity of most cells was confirmed by transmission electron microscopy, which revealed that >95% ($n = 6$) of cells were intact. In some cells, we observed budding of extracellular microvesicles (ectosomes), and occasionally we found destroyed cells with hydrogenosomes (Fig. S2).

LFQ values were calculated for individual proteins at each time point. Altogether, we identified 2,072 proteins (Table S3). To distinguish *bona fide* secreted proteins from contaminants, we applied two main criteria. First, the amount of the secreted protein significantly increased over time (Fig. 1), and second, the LFQ values for a given protein at 37 °C were greater than LFQ values at 4 °C for more than 1 LFQ unit. Then, for each protein, we calculated SecS as the sum of the differences in LFQ values determined for each time point. The application of these criteria resulted in a list of 89 actively released proteins (Table I) that were manually sorted into 13 functional categories considering TrichoDB annotations, HHpred searches, Pfam motif identifications, Evolutionary Classification of Protein Domains classification, and molecular function gene

[1] The abbreviations used are: Ab, antibody; AP, acceptor peptide; DAPI, 4′,6-eiamidino-2-phenylindole; FITC, fluorescein isothiocyanate; HA, hemagglutinin; qRT-PCR, quantitative RT-PCR; PEM, 100 mM PIPES, 1 mM EGTA, 0.1 mM $MgSO_4$; PNGase F, N-glycosidase F; SecS, secretion score; SIM, structured illumination microscopy; TMD, transmembrane domain; TBSR, trichomonas beta-sandwich repeat protein; TYM, tryptone-yeast extract-maltose medium.

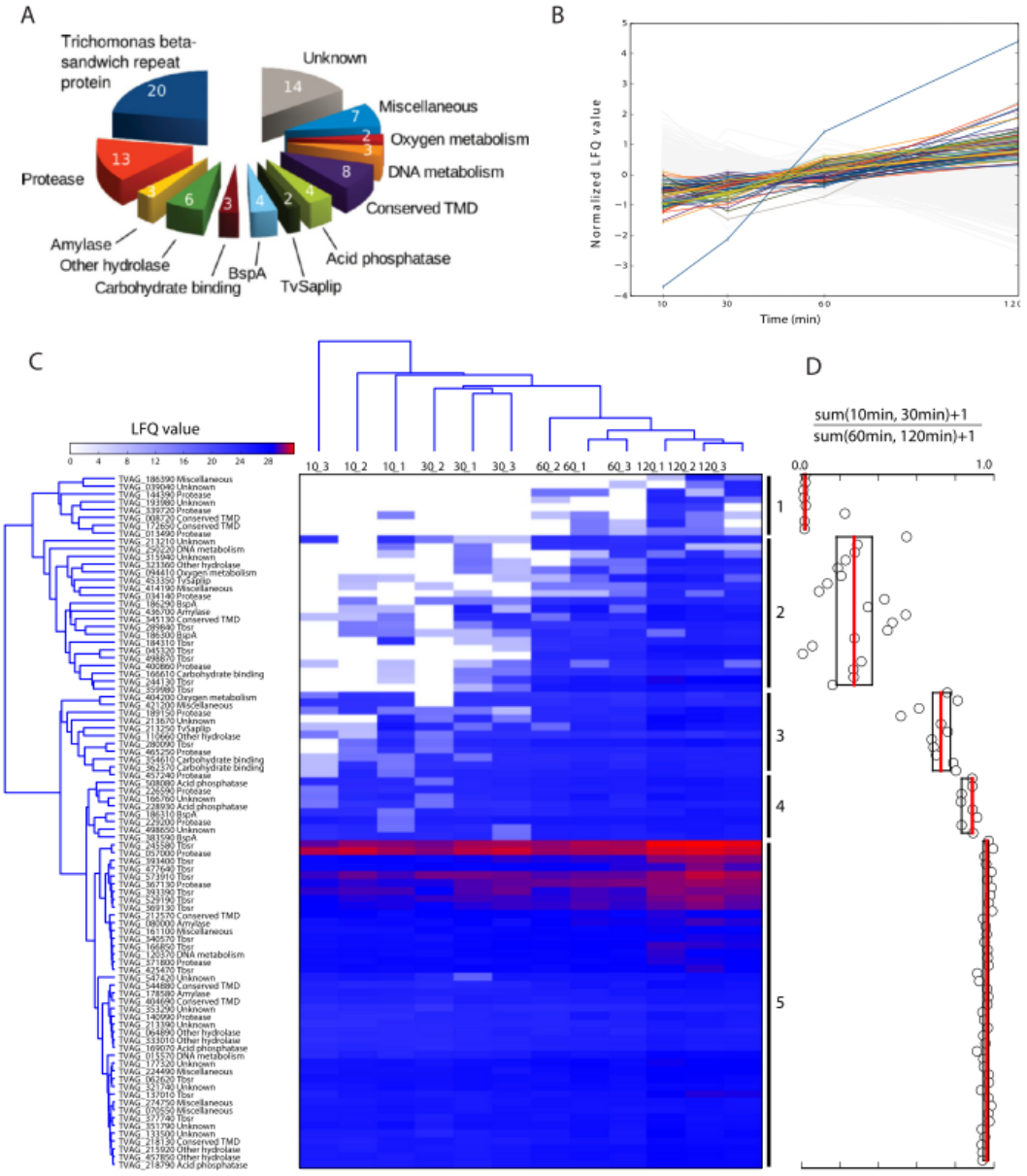

FIG. 1. **Proteins secreted by *T. vaginalis*.** (*A*) Functional categories. (*B*) Normalized LFQ values (binary logarithm) determined for proteins released between 10 and 120 min of incubation of *T. vaginalis* in Doran's medium with maltose at 37 °C. Secreted proteins are color-coded as in (*A*), and proteins in gray are under the defined cutoff. Accession numbers of color-coded proteins are given in Fig. S3. (*C*) Hierarchical clustering. The means of LFQ values of three technical replicates for three biological replicates were clustered over 10–120 min cell incubation at 37 °C. X_Y; X, time point in min; Y, code of biological experiment according to Table S3. (*D*) Five dominant clusters were tested by boxplot analysis as the ratio [sum LFQ values (10 min, 30 min)+1]/[sum LFQ values (60 min, 120 min)+1]. The median (red line) and 25th and 75th percentiles were computed for each cluster and are shown as boxplots. Circles indicate [sum LFQ values (10 min, 30 min)+1]/[sum LFQ values (60 min, 120 min)+1] calculated for each protein.

ontology (GOMF) names (Fig. 1, Table I, and Table S3). Most categories contain both soluble proteins and proteins with predicted transmembrane domains (TMD) (Table I, Table S3).

The actively released proteins were then ordered by hierarchical clustering according to LFQ values over 10–120 min at 37 °C (Fig. 1*C*). This analysis revealed five main clusters with different dynamics of protein release. The most striking difference appeared between 10 to 30 min *versus* 60 to 120 min, which is supported by boxplot analysis (Fig. 1*D*). As indicated by the heat map, proteins in cluster 1 (eight proteins) were

TABLE I
The list of T. vaginalis secreted proteins

Category	Accession No.	Annotation	Length	TMD	TMD-C	SignalP	SecretomeP	SecS
Acid phosphatase	TVAG_218790	acid phosphatase, putative	379	0		0.401	0.433	6.34
	TVAG_508080	acid phosphatase, putative	391	0		0.304	0.470	4.99
	TVAG_169070	acid phosphatase, putative	394	0		0.356	0.406	3.45
	TVAG_228930	acid phosphatase, putative	390	0		0.272	0.486	3.42
Amylase	TVAG_178580	alpha-amylase, putative	494	0		0.374	0.724	1.86
	TVAG_080000	beta-amylase, putative	377	0		0.106	0.568	3.97
	TVAG_436700	beta-amylase, putative	428	0		0.335	0.654	0.67
BspA	TVAG_186310	leucine-rich repeat protein, BspA family	1,363	0		0.109	0.644	5.85
	TVAG_383590	leucine-rich repeat protein, BspA family	927	1	23	0.182	0.260	3.91
	TVAG_186290	leucine-rich repeat protein, BspA family	1,474	0		0.133	0.697	1.43
	TVAG_186300	leucine-rich repeat protein, BspA family	1,434	0		0.554	0.710	1.37
Carbohydrate binding	TVAG_362370	carbohydrate-binding domain, FA58C	224	0		0.416	0.813	4.76
	TVAG_354610	carbohydrate-binding domain, FA58C	218	0		0.178	0.487	2.25
	TVAG_166610	carbohydrate-binding module, cd14489	354	0		0.325	0.755	2.57
Conserved TMD	TVAG_544880	conserved protein	290	1	23	0.109	0.256	7.33
	TVAG_345130	conserved protein	383	1	26	0.373	0.257	5.60
	TVAG_218130	conserved protein	1,085	1	24	0.570	0.572	5.51
	TVAG_404690	conserved protein	593	1	79	0.100	0.19	2.53
	TVAG_212570	conserved protein	624	1	71	0.443	0.345	0.90
	TVAG_172650	conserved protein	356	1	71	0.106	0.121	0.90
	TVAG_008720	conserved protein	1,300	1	24	0.190	0.457	0.47
	TVAG_140990	conserved protein	276	1	12	0.540	0.427	6.86
DNA metabolism	TVAG_015570	deoxyribonuclease II precursor, putative	337	0		0.272	0.658	10.30
	TVAG_250220	DNA replication licensing factor MCM4, putative	752	0		0.102	0.462	0.70
	TVAG_120370	extracellular ribonuclease precursor, putative	233	0		0.279	0.742	4.29
Miscellaneous	TVAG_421200	APC10 subunit of the anaphase-promoting complex	217	0		0.117	0.239	1.20
	TVAG_224490	cystatin-like domain, cd00042	188	0		0.382	0.475	4.19
	TVAG_274750	GTP-binding protein alpha subunit, gna, putative	363	0		0.107	0.617	0.95
	TVAG_186390	guanylate cyclase, putative	1,540	11	374	0.105	0.745	0.30
	TVAG_161100	heat shock protein 70kD, putative	659	0		0.112	0.272	1.29
	TVAG_414190	pqiA integral membrane protein, TIGR00155	1,074	9	29	0.505	0.656	1.29
	TVAG_070550	syntaxin, putative	298	1	4	0.106	0.395	0.70
Other hydrolase	TVAG_064890	alpha-L-fucosidase, putative	1,021	1	27	0.212	0.448	1.81
	TVAG_110660	beta-hexosaminidase, putative	553	1	521	0.198	0.654	1.68
	TVAG_323360	GH36 glycosyl hydrolase family 36, cd14791	2,104	1	19	0.145	0.366	1.36
	TVAG_215920	phospholipase B	621	1	19	0.183	0.48	5.93
	TVAG_333010	phospholipase B	533	0		0.501	0.676	4.47
	TVAG_457850	N-acetylglucosamine-1-phosphodiester alpha-N-acetylglucosaminidase	1,000	1	35	0.600	0.606	6.53
Oxygen metabolism	TVAG_404200	superoxide dismutase, putative	217	0		0.154	0.474	3.04
	TVAG_094410	thioredoxin-like	197	0		0.296	0.908	1.01
Protease	TVAG_339720	M60 peptidase	1,148	1	11	0.483	0.456	0.20
	TVAG_229200	cathepsin C-like protein	433	0		0.215	0.751	2.15
	TVAG_057000	clan CA, family C1, papain-like cysteine peptidase	314	0		0.181	0.399	0.51
	TVAG_034140	clan CA, family C1, papain-like cysteine peptidase	317	0		0.257	0.525	0.24
	TVAG_457240	clan CA, family C40, NlpC/P60 superfamily cysteine peptidase	275	0		0.208	0.57	2.13
	TVAG_400860	clan MA, family M8, protease GP63	589	0		0.101	0.337	1.79
	TVAG_226590	clan MA, family M8, surface protease GP63	637	1	22	0.105	0.111	4.66
	TVAG_367130	clan MA, family M8, surface protease GP63	630	1	21	0.519	0.248	3.40
	TVAG_371800	clan MA, family M8, surface protease GP63	704	1	14	0.252	0.047	3.02
	TVAG_013490	clan MG, family M24, aminopeptidase P-like metallopeptidase	383	0		0.100	0.443	0.30
	TVAG_465250	clan SB, family S8, subtilisin-like serine peptidase	768	1	2	0.311	0.500	2.93
	TVAG_144390	peptidase C1A subfamily	573	1	53	0.118	0.616	0.30
	TVAG_189150	peptidase M60 domain	1,247	1	21	0.304	0.437	8.44
TBSR protein	TVAG_244130	conserved protein	751	1	53	0.323	0.405	12.31
	TVAG_045320	conserved protein	581	1	7	0.244	0.194	9.80
	TVAG_137010	conserved protein	1,080	1	62	0.475	0.417	7.22
	TVAG_289840	conserved protein	972	1	69	0.656	0.364	6.88
	TVAG_280090	conserved protein	763	1	62	0.122	0.369	6.60
	TVAG_498870	conserved protein	734	1	6	0.175	0.210	6.35
	TVAG_393400	conserved protein	563	1	2	0.377	0.500	5.75

TABLE I—*continued*

Category	Accession No.	Annotation	Length	TMD	TMD-C	SignalP	SecretomeP	SecS
	TVAG_245580	conserved protein	2,365	1	66	0.184	0.388	4.58
	TVAG_166850	conserved protein	748	1	61	0.132	0.444	4.35
	TVAG_062620	conserved protein	1,365	1	8	0.533	0.561	3.61
	TVAG_184310	conserved protein	1,239	1	7	0.173	0.423	3.47
	TVAG_377740	conserved protein	391	0		0.101	0.408	3.37
	TVAG_573910	conserved protein	1,225	1	63	0.113	0.330	3.33
	TVAG_477640	conserved protein	621	0		0.280	0.520	3.24
	TVAG_425470	conserved protein	2,061	1	66	0.172	0.407	2.92
	TVAG_529190	conserved protein	1,088	0		0.524	0.507	2.82
	TVAG_340570	conserved protein	752	1	6	0.243	0.250	2.61
	TVAG_393390	conserved protein	563	1	2	0.238	0.437	2.29
	TVAG_369130	conserved protein	523	1	3	0.097	0.318	1.86
	TVAG_359980	conserved protein	1,592	1	43	0.171	0.383	1.63
TvSaplip	TVAG_213250	TvSaplip8	126	0		0.653	0.944	3.53
	TVAG_453350	TvSaplip6	131	0		0.382	0.673	1.03
Unknown	TVAG_213670	conserved protein	733	1	29	0.149	0.314	8.74
	TVAG_133500	conserved protein	255	0		0.133	0.636	6.80
	TVAG_213390	conserved protein	285	0		0.227	0.125	5.34
	TVAG_177320	conserved protein	963	1	44	0.154	0.610	4.93
	TVAG_498650	conserved protein	988	2	14	0.217	0.509	4.10
	TVAG_351790	conserved protein	991	2	15	0.115	0.594	2.50
	TVAG_353290	conserved protein	252	0		0.276	0.455	2.24
	TVAG_547420	conserved protein	158	0		0.430	0.663	1.66
	TVAG_321740	conserved protein	803	1	19	0.202	0.617	1.52
	TVAG_213210	conserved protein	1,023	1	55	0.269	0.421	0.76
	TVAG_193980	conserved protein	511	0		0.122	0.409	0.30
	TVAG_315940	conserved protein	296	1	11	0.327	0.309	0.20
	TVAG_039040	conserved protein	554	1	49	0.109	0.253	0.20
	TVAG_166760	unknown protein	927	1	44	0.179	0.485	5.26

Length, number of amino acids; TMD, number of predicted transmembrane helixes; TMD-C, number of amino acids from the last TMD to the C-terminus; SignalP prediction of signal peptide (default cutoff value 0.450); SecretomeP, prediction of nonclassical protein secretion (default cutoff value 0.600); SecS, secretion score indicating time-dependent protein secretion.

entirely absent (seven proteins) or present in a low quantity (one protein) during 10–30 min incubation (late secreted proteins). Two of the proteins were detected only after 120 min of incubation (TVAG_186390, and TVAG_193980). On the other side of the spectrum, proteins of Group 5 (52 proteins) were present in relatively high quantity beginning 10 min after incubation (early secreted proteins) and included a subcluster of the most abundant proteins, such as TVAG_057000. We suspected that differences in the dynamics of protein secretion may reflect the presence or absence TMD; however, we did not find such a correlation.

Transmembrane Proteins—Predictions of TMD using the TMHMM software detected 51 secreted proteins with putative TMDs, among which 46 proteins possess a single-spanning TMD and 5 proteins possess 2–11 TMDs (Table I). The peptides determined in the secretome corresponded exclusively to the soluble protein domains, whereas the TMD domains were predicted based on the corresponding AA sequences in TrichDB. The largest group of single spanning proteins (17 entries) is a heterogeneous group of unknown proteins that we named Trichomonas beta-sandwich repeat (TBSR) protein for the presence of a glycosyl hydrolase domain-like of a beta-sandwich structure at the N terminus followed by 2–5 immunoglobulin-like beta-sandwich domains and a conserved transmembrane domain close to the C terminus. Most of the TBSR proteins are grouped into two clusters. Cluster 2 contains seven TBSR proteins, including TVAG_244130, TVAG_045320, and TVAG_289840, that are among the 10 top proteins with the highest SecS (Table I, Table S3). Nine TBSR proteins with TMD and three TBRS proteins without TMD are grouped in cluster 5 (Fig. 1*C*). These TBSR proteins are among the most abundant proteins in the secretome with the top TBSR protein TVAG_245580. A single TBSR protein is present in cluster 3 (Fig. 1*C*). The topology of TMD at the C terminus of TBSR proteins and the high score for secretory signal prediction at the N terminus (Table I, and Table S3) correspond to type I membrane proteins with the N-terminal part outside the cell and the C-terminal part facing the cytosol (52). Analysis of the C termini revealed that 11 TBSR proteins possess an NPXY-type signal for endocytic internalization, which further supports their type I topology. We also found the NPXY motif at the C termini of two proteins in the conserved TMD category (Fig. S4). Interestingly, most of the C-terminal domains of TBSR proteins and two conserved TMD proteins possess the DDPFA motif that was previously noted at the C terminus of 21 surface TvBspA proteins (53). Four TBSR proteins scattered among cluster 2, 3, and 5 possess the motif for parasite rhomboid protease

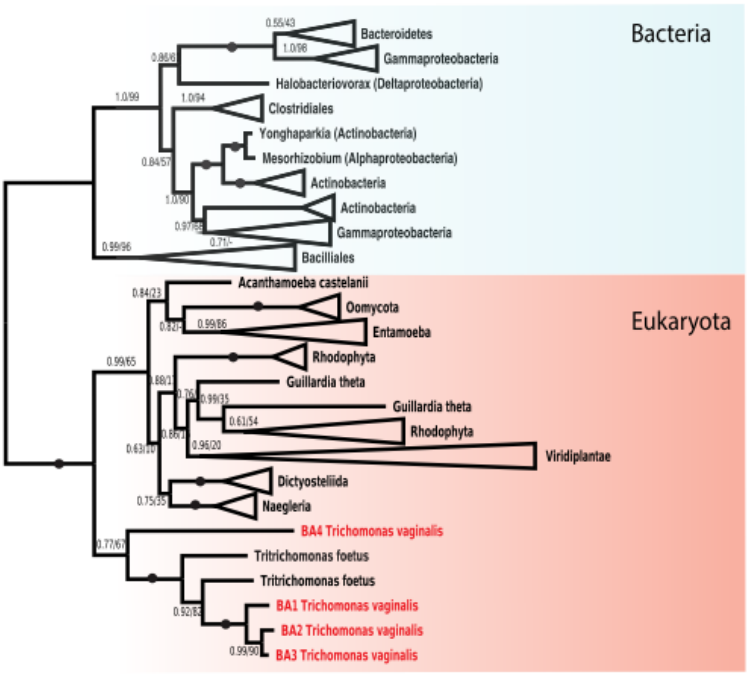

FIG. 2. **Phylogeny of β-amylases.** The phylogeny of beta-amylase homologues inferred by PhyloBayes (CAT+GTR model) and PhyML (LG+I+G model). For each branch, the posterior probability and ML bootstrap support are given. Branches with maximum support (1.0/100) are indicated by black circles. Supports with posterior probability below 0.5 are omitted.

within TMD (Fig. S4) (31). The other transmembrane proteins consist of seven proteases, including three GP63-like membrane proteases, a single TvBspA protein, four putative hydrolases, 10 unknown proteins, and three proteins of miscellaneous category.

Soluble Proteins—The second half of the *T. vaginalis* secretome consisted of soluble proteins of various categories. The highest SecS of the soluble proteins belonged to a putative deoxyribonuclease II family protein (TVAG_015570, TvDNaseII). The other soluble proteins include four acid phosphatases of the histidine phosphatase family; three soluble TvBspA proteins; three putative carbohydrate-binding proteins; two other proteins involved in DNA metabolism; two oxygen-metabolizing enzymes; six proteases, including papain-like cysteine peptidase TvCP2 of cluster 5 (TVAG_057000), which appeared to be the most abundant soluble protein; three TBSR proteins; two proteins with saposin-like domains; and seven hydrolases (Table I). The largest number of soluble proteins (12 proteins) was in the miscellaneous category of proteins with known functional domains but with currently unclear functions in the *T. vaginalis* secretome. Finally, eight soluble proteins belong to the category of unknown proteins.

Glycoside Hydrolases—For further investigation, we selected soluble glycoside hydrolases as model secreted proteins. These enzymes have the potential to metabolize external glycogen, a key substrate for the energy metabolism of the parasite. Searches in our dataset revealed the presence of a single α-amylase (TVAG_178580, glycoside hydrolases family 13) and two β-amylases (glycoside hydrolases family 14) (http://www.cazy.org/). In the *T. vaginalis* genome, proteins with α-amylase domains are encoded by at least 19 genes that form three distinct clades (Fig. S5). The secreted α-amylase TVAG_178580 belongs to clade I together with two other paralogues in the genome. Another α-amylase of clade II (TVAG_112500) was identified among the proteins under the SecS cutoff.

Four β-amylase paralogues are encoded in the *T. vaginalis* genome, among which we identified TVAG_436700 (BA1) grouped in cluster 2 and TVAG_080000 (BA2) grouped in cluster 5 (Fig. 1*C*). Two other paralogues were named BA3 (TVAG_175670) and BA4 (TVAG_236600). Comparing the AA sequences of BA1–4 revealed that BA1–3 are highly similar, with a high AA sequence identity of 72.9–88.6%, whereas BA4 displayed only 35.2–36.5% sequence similarity to the other paralogues. In addition, BA4 possesses a 19 AA N-terminal extension and a predicted N-terminal transmembrane helix (17–33 AA). BA3 and BA4 were not identified in the secretome and were not present among the proteins below the SecS cutoff.

Peculiar Distribution of β-Amylases in Eukaryotes—The secretion of β-amylase by *T. vaginalis* is noteworthy, as the production of this enzyme has been observed in only a few eukaryotic lineages, including land plants and *Entamoeba histolytica* (54). Thus, to gain further insight into β-amylase distribution, we searched for β-amylase coding genes across eukaryotic supergroups (Fig. 2 and Fig. S6). In addition to *T. vaginalis,* we identified β-amylase genes in the related bovine pathogen *Tritrichomonas fetus. Naegleria gruberi,* and *N.*

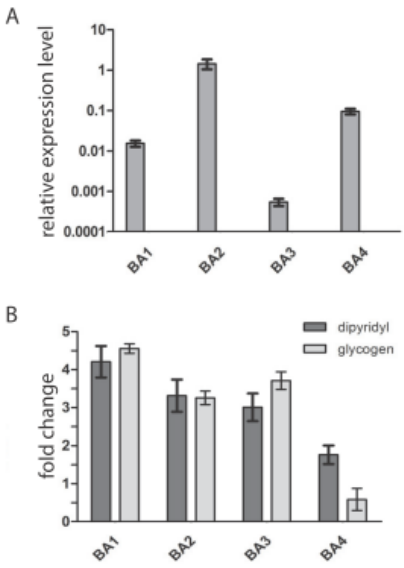

FIG. 3. **Effect of environmental factors on expression of β-amylases analyzed by qRT-PCR.** (*A*) Relative mRNA expression levels of BA1–4 in *T. vaginalis* cultivated in standard TYM medium. Expression levels of β-amylases were normalized using the DNATopII reference gene. (*B*) Relative mRNA expression level of BA1–4 in *T. vaginalis* cultivated in TYM when maltose is replaced with glycogen or in standard TYM medium with a restricted level of iron. Data are expressed as -fold increases relative to the expression of the corresponding gene in standard TYM medium. Error bars represent the standard deviation of the mean.

fowleri appeared to be the only other members of the Excavata supergroup with putative β-amylase-coding genes. As expected, we found β-amylases in land plants, but we also found orthologues in members of the Chlorophyta and Rhodophyta groups. Moreover, we identified β-amylase genes in several members of Oomycota and Cryptophyta. Whereas patchy distribution is apparent in the other eukaryotic groups, β-amylases appear to be common in Amoebozoa. However, animals and fungi appear to be devoid of β-amylases.

Expression of β-Amylases and Influence of Environmental Conditions—The presence of only two of four β-amylase paralogues in the *T. vaginalis* secretome may reflect differences in gene expression among BA1–4 under certain environmental conditions. First, using qRT-PCR, we compared BA1–4 expression in trichomonads cultivated in standard medium with maltose and detected transcripts for all four paralogues (Fig. 3*A*). The gene for BA2 showed the highest expression level, which corresponded to the highest LFQ values determined for BA2 in the secretome. The expression of *ba1* was lower by two orders of magnitude, and *ba3* displayed the lowest expression. Interestingly, the expression of *ba4* was higher than that of *ba1*. When maltose was replaced by glycogen, the expression level significantly increased for *ba1–3*, whereas *ba4* expression showed no significant effect (Fig. 3*B*). We observed a similar trend when trichomonads were cultivated under iron-limited conditions, which resulted in increased transcription of *ba1–3* with no effect on *ba4* (Fig. 3*B*). Next, we expressed recombinant BA3 and BA4 under the control of a strong promotor of succinyl CoA synthase with a C-terminal HA tag in *T. vaginalis* (55). BA1 and BA2 were expressed as a positive control. The transformed cells were incubated for 60 min in TYM. BA1, BA2, and a low level of BA3 were detected in cell-free TYM, but BA4 was not (Fig. 4). All four proteins were detected in the cell lysates. These experiments confirmed our suspicion that BA4 is not secreted, whereas the secretion of BA1–3 depends on the expression level.

Secretion of β-Amylases via Classical Secretory Pathway—The secretory pathway in *T. vaginalis* has not yet been studied. Thus, we were interested in whether *T. vaginalis* β-amylases are secreted via the classical endoplasmic reticulum (ER)-to-Golgi secretory pathway or a nonclassical secretory pathway that is independent of the ER (56). The predictions of classical and nonclassical secretion using the SignalP/TargetP and SecretomeP servers, respectively, were not conclusive (Table I, Table S3). Thus, we prepared *T. vaginalis* strain Tv17–48-BirA expressing biotin ligase (BirA) fused at the N terminus with the first 75 AA of protein disulfide isomerase to target BirA to the ER and with the V5 tag at the C terminus for BirA visualization. This cell line allows for the specific biotinylation of proteins containing the AP tag within the ER and their subsequent visualization using fluorochrome-conjugated avidin. When we co-expressed BA1, BA2, and BA4 in this cell line, all β-amylases were biotinylated and detected in the ER (Fig. 5). We observed a strongly labeled ring of ER around the nucleus and a rich ER network within the *T. vaginalis* cell. Moreover, BA1 and BA2 appeared in rod-like structures close to the nucleus whose appearance corresponds to that of the Golgi apparatus, whereas no Golgi labeling was observed in the cells expressing BA4. Multiple attempts to express BA3 in the Tv17–48-BirA strain under the control of a native promotor were not successful. Therefore, we expressed BA3 in Tv17–48 strain without BirA (Fig. S7). The BA3 was observed in ER structures, whereas its presence in the Golgi apparatus was not conclusive. These data indicate that recombinant BA1 and BA2 are biotinylated within the ER and transported to the Golgi apparatus.

To gain further insight into the secretion mechanisms, we tested the effect of two secretion inhibitors, brefeldin A and FLI-6, with different modes of action. Brefeldin A causes a collapse of the Golgi apparatus via stimulation of retrograde transport from the Golgi to the ER (57), whereas FLI-06 inhibits the recruitment of cargo to the ER and trans-Golgi network exit sites (58). The treatment of *T. vaginalis* with brefeldin A clearly inhibited BA1, BA2, and BA3 secretion, as expected for the ER–Golgi secretory pathway. Interestingly, we observed no effect of FLI-06 on BA1–3 secretion despite the use of a range of concentrations up to 50 μM (Fig. 6).

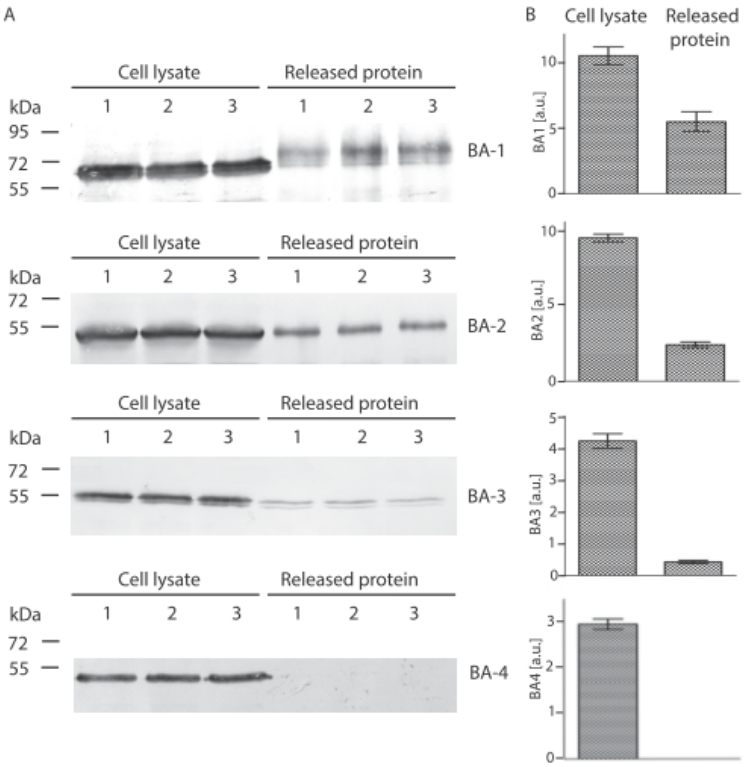

FIG. 4. **Test of BA-3 and BA4 secretion in Tv17–48 strain.** (*A*) HA-tagged versions of BA1, BA2, BA3, and BA4 were expressed under a strong promotor using the TagVag vector. BA1 and BA2, which were detected in the *T. vaginalis* secretome, were used as a positive control. Cells were incubated for 60 min at 37 °C in TYM, and BA proteins were then detected using an antitag antibody by immunoblotting of the cell lysate (L) and of the cell-free TYM (S). Each experiment was performed in three biological replicates. (*B*) Bar graph shows the relative amount of BA proteins associated with cell and released to the media that were quantified from three independent experiments. Error bar indicates standard deviation. a.u., arbitrary unit.

N-Linked Glycosylation of T. vaginalis β-Amylases—N-linked glycosylation is a major modification of secretory proteins upon their translocation to the ER. Searches for the conserved sequon NX[ST], which serves as a glycan acceptor, predicted seven glycosylation sites in BA1, none in BA2, one in BA3, and two in BA4 (Table S4). To investigate the predicted N-glycosylation, we expressed HA-tagged BA1–4 in *T. vaginalis* and treated the cell lysate from each strain with N-glycosidase F (PNGase F), which cleaves *N*-linked oligosaccharides. Western blot analysis of the treated and untreated lysates showed the most prominent shift in molecular weight in BA1 (~11 kDa), which is consistent with the prediction of the largest number of glycosylation sites in this protein (Fig. 7*A*). Untreated BA3 appeared as a double band that was shifted by ~1.5 kDa by PNGase treatment. Although two glycosylation sites were predicted for BA4, we did not observe any shift in this case.

Next, we treated the *T. vaginalis* strains expressing HA-tagged BA1–4 with tunicamycin, a nucleoside antibiotic that inhibits *N*-linked glycan biosynthesis. The immunoblot analysis of *T. vaginalis* incubated for 24 h with tunicamycin revealed a series of BA1 forms of 51–63 kDa that differ by ~1 kDa (Fig. 7*B*), indicating impaired N-glycosylation. However, BA3 formed a double band under both conditions. Next, we expressed streptavidin-tagged BA1 in the Tv17–48 strain, purified the protein by affinity chromatography, and subjected the purified protein to MS analysis. The analysis confirmed that all seven predicted sites in BA1 were glycosylated. Moreover, all seven glycosylated peptides contained glycans with the same composition of Hex_5HexAc_2 (Table S5).

BA3 and BA4 Are Present in Lactoferrin-Labeled Vesicles—BA4 protein is apparently not secreted into the *T. vaginalis* environment, and only small amount of BA3 is released when it is expressed under a control of a strong promotor. Thus, we were interested in whether these proteins are recruited to the lysosomal compartment. To label the endosomal/lysosomal compartment, we incubated trichomonads in medium containing FITC-labeled lactoferrin, which is known to be internalized via receptor-mediated endocytosis and to release lactoferrin-associated iron upon reaching the acidified compartment (59, 60). After incubation, the cells were processed for immunofluorescence microscopy by labeling the HA-tagged β-amylases. For comparison, we performed the same experiment with BA1–2. As described above, BA4 appeared in the ER structure surrounding the nucleus and in numerous vesicles scattered within the cell. FITC-labeled lactoferrin appeared in tiny endosomes and in large vesicles corresponding to lysosomes, in which it was co-localized with BA4 (Fig. 8). Lactoferrin-labeled vesicles were co-stained also with BA3. In contrast, labeling of BA2 did not co-localize with lactoferrin. BA1-labeled structures were mostly distinct from lysosomes, although 18% ($n = 3$) of lactoferrin-labeled vesicles also displayed a BA1 signal. These results indicate that BA4 and BA3 are targeted to the *T. vaginalis* lysosomal compartment,

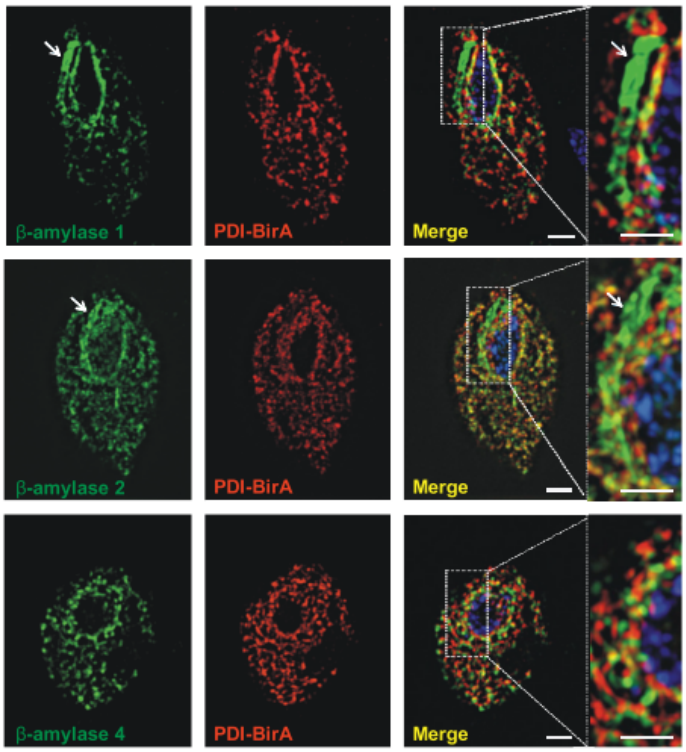

FIG. 5. **Visualization of β-amylases in the secretory pathway using super-resolution fluorescence microscopy (SFM).** BA1, BA2, and BA4 with AP tag were biotinylated by BirA in ER and visualized using Alexa Fluor 488 avidin conjugate (green). BirA targeted to ER was visualized using rabbit polyclonal α-V5 Ab and the secondary Alexa Fluor 594 donkey α-rabbit Ab (red). The nucleus is labeled with 4′,6-diamidino-2-phenylindole (DAPI). Arrows indicate Golgi apparatus. Bar = 2.5 μm.

whereas secretion of BA2 and that of most of BA1 are independent of lysosomes.

DISCUSSION

Products secreted by parasitic protists play a fundamental role in the host–parasite relationship. Here, we analyzed the *T. vaginalis* secretome using high-resolution LFQ MS. Altogether, we identified 2,072 extracellular proteins, which is the largest protein set of *T. vaginalis* origin identified to date. However, our filter for distinguishing *bona fide* secreted proteins from contaminants resulted in only 89 proteins that fulfilled our strict criteria. Most experimental designs for studying the secretome of parasitic protists are based on a single time period of incubation under optimal conditions to minimize cell lysis, followed by MS analysis of the proteins released to the medium (conditioned medium) (31, 34, 61–64). Although this approach has identified important secreted proteins, eliminating contaminant proteins is problematic. More precise identification could be achieved by quantitative MS analysis of metabolically labeled cells, which makes it possible to define a cutoff based on the ratio of protein levels in the conditioned medium to the corresponding protein levels associated with the cells (65). Our approach was based on the LFQ MS analysis of time- and temperature-dependent secretion. This strategy makes it possible to define a simple cutoff based on the increasing concentration of a given protein over time. We also removed all proteins with similar levels at 37 °C and 4 °C, as exocytosis is a temperature-dependent process.

Analysis of the *T. vaginalis* secretome revealed surprisingly high participation of proteins (over 50%) that contain TMD. Most of these proteins possess a single C-terminal transmembrane helix (47 proteins), and of this majority, 40 proteins were previously found in the *T. vaginalis* surface proteome (30). Most likely, these proteins are embedded in the cellular membrane via the C-terminal TMD, and their N-terminal domains are subsequently released to the environment upon proteolytic cleavage. Indeed, Riestra *et al.* (31) found that *T. vaginalis* possesses an active rhomboid secretory protease, TvROM1, that is localized in the plasma membrane. This enzyme has been shown to catalyze the cleavage within the TMD of two proteins, TVAG_166850 and TVAG_280090. Moreover, the treatment of TvROM1-transfected cells with the serine protease inhibitor 3,4-dichloroisocoumarin caused a statistically significant decrease in the secretion of four additional proteins with predicted TMDs (31). These proteins were not cleaved by TvROM1, but they all contain a bacterial-like rhomboid substrate motif. All these proteins belong to the family of 17 TBSR proteins that we identified in the secretome. Interestingly, all TBSR proteins with C-terminal TMDs and two conserved TMD proteins possess the endosomal signal

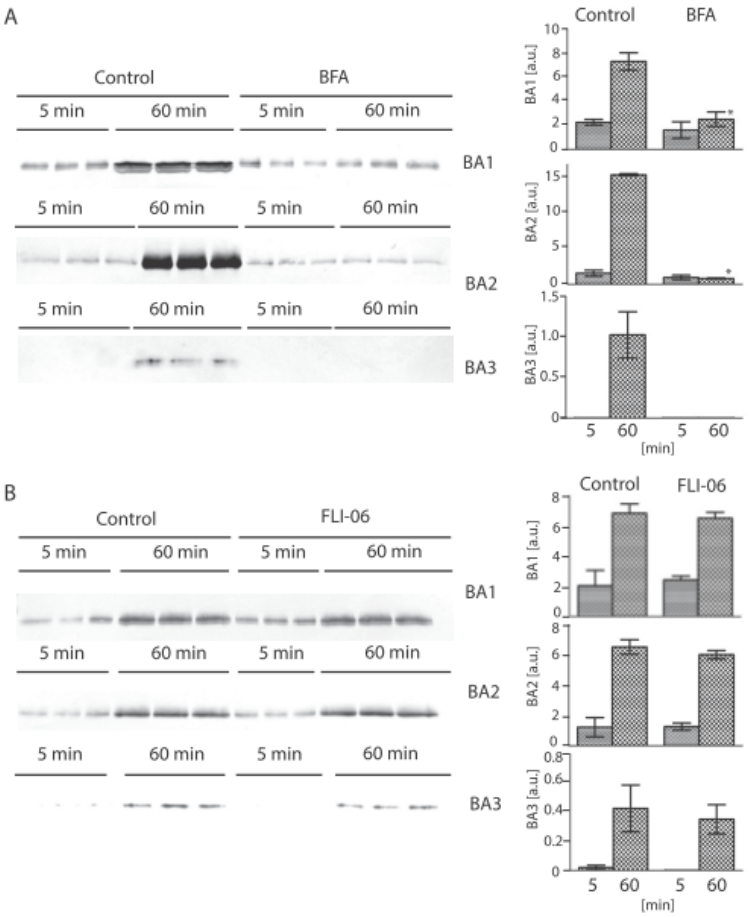

FIG. 6. **Effect of brefeldin A and FLI-06 on BA1–3 secretion.** *T. vaginalis* strains producing HA-tagged BA1–3 were incubated for 5 and 60 min in TYM supplemented with brefeldin A or FLI-06, and secreted BA proteins were detected in conditioned cell-free TYM medium via Western blot analysis with mouse monoclonal α-HA Ab. Control cells were incubated without inhibitors. Bar graph shows the relative amount of secreted BA proteins quantified from three independent experiments. Error bar indicates standard deviation. Star (*) indicates significant difference between relative quantity of protein secreted after 60 min incubation of control cells and cells treated with inhibitor ($p < 0.05$).

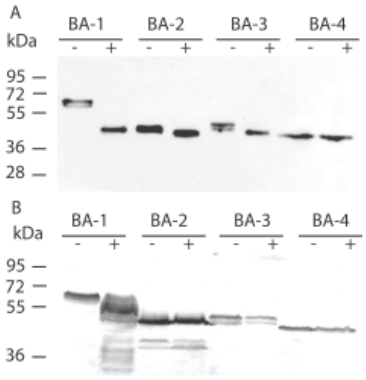

FIG. 7. **Effect of PNGase and tunicamycin on β-amylase glycosylation.** (*A*) Representative Western blot analysis ($n = 3$) of HA-tagged BA1–4 produced by *T. vaginalis* cells that were treated with PNGase F (+) or untreated (-). (*B*) Representative Western blot analysis ($n = 3$) of *T. vaginalis* cell lysate producing HA-tagged BA1–4 in the presence (+) or absence (-) of tunicamycin.

NPX[YFW] at the C terminus facing the cytosol. The same signal was previously observed at the C termini of 15 putative surface TvBspA proteins (53). The NPXY sorting signal is known to mediate the rapid internalization of membrane proteins such as receptors in humans. It would be interesting to test the role of this sorting signal in *T. vaginalis*. The signal may facilitate the internalization of complete proteins, such as receptors with cargo, or it may clear the C-terminal domains after the release of the N-terminal part. Altogether, our results indicate that the proteolytic cleavage of membrane proteins greatly contributes to the protein spectrum in the *T. vaginalis* secretome and that, in addition to TvROM1, other proteases are likely involved in the membrane protein secretion. In contrast to the membrane proteome, there is very low overlap (eight proteins) between our dataset of secreted proteins and the set obtained in a previous proteomic analysis of *T. vaginalis* exosomes (19). This finding is consistent with the concept that secretory proteins and exosomal proteins represent two distinct sets of extracellular proteins released by two different mechanisms.

The function of most of these secreted membrane proteins is unknown; however, members of at least two protein groups, TBSR and TvBspA proteins, are likely involved in the adhesion of the parasite to the host cell. Exogenous expression of the TBSR protein TVAG_166850 leads to increased

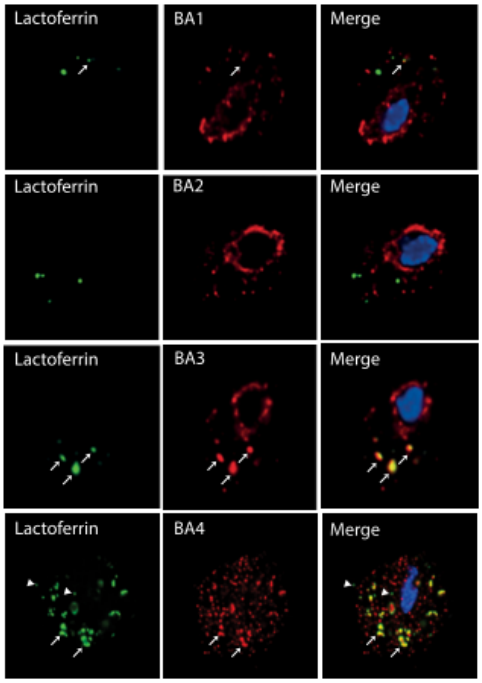

FIG. 8. **Visualization of BA1–4 and lactoferrin-labeled endosomal/lysosomal compartment.** *T. vaginalis* strains expressing HA-tagged BA1–4 were incubated for 10 min with FITC-labeled lactoferrin (green) and then processed for SIM microscopy. BA proteins were visualized using mouse monoclonal α-HA Ab and the secondary Alexa Fluor 594 donkey α-mouse Ab (red). Arrow indicates co-localization of lactoferrin and BA proteins in lysosomes; arrow head indicates small endosomes with lactoferrin that do not contain BA.

attachment of trichomonads to the host ectocervical cells (31). In the secretome, we found six TBSR protein paralogous to TVAG_166850 that may have similar properties. TvBspA proteins are known as membrane adhesins, originally described in *Bacteroides forsythus,* that mediate the co-aggregation of bacteria as well as their adhesion to host cells (53, 66). In the secretome, we identified a single TvBspA protein with C-terminal TMD, TVAG_383590, and three soluble TvBspA proteins, TVAG_186300, TVAG_186290, and TVAG_186310. The latter three proteins have also been found in the surface proteome of two different *T. vaginalis* strains (30). Notably, the *T. vaginalis* genome encodes an extraordinarily large set of TvBspA-like proteins, numbering 911 genes, and there is evidence of the transcription of more than 30% of these genes (53). Thus, the identification of a rather limited number of identical TvBspA proteins exposed to the cell environment in different *T. vaginalis* strains suggests that they have a specific function that should be elucidated in future studies. Interestingly, six hydrogenosomal enzymes involved in energy metabolism have been previously reported to serve as adhesins in addition to their metabolic functions. These enzymes include three paralogues of malic enzyme (AP65 1–3), the α- and β-subunits of succinyl CoA synthetase (AP51, AP33), and pyruvate:ferredoxin oxidoreductase (AP120) (67, 68). We found over 30 hydrogenosomal proteins, including all putative adhesins, in our dataset under the SecS cutoff. These proteins most likely represent hydrogenosomal contaminants resulting from the presence of hydrogenosomes released from some broken cells, which we observed in our samples by electron microscopy. β-Amylases are part of the second half of the *T. vaginalis* secretome, which consists of soluble proteins. These enzymes have been found in several pathogenic protists but are absent in human and animal proteomes. For example, *E. histolytica* expresses eight β-amylases that are proposed to be involved in the utilization of host mucus glycans as a carbon source for energy metabolism and to contribute to the mucosa invasion (69). Our genome searches and phylogenetic analysis revealed that β-amylases are also present in other amoebozoans, in the bovine pathogen *T. fetus*, and in *N. fowleri*, the causative agent of human primary meningoencephalitis. However, nothing is currently known about the role of β-amylase in these pathogens. In *T. vaginalis*, β-amylase likely contributes to the utilization of free glycogen and oligosaccharides in the vaginal fluids by breaking down the substrate into maltose. Indeed, Smith *et al.* 2016 (29) showed that recombinant TVAG_080000 produces a detectable amount of maltose from glycogen. Maltose is then extracellularly hydrolyzed by α-glucosidase, and glucose is taken up via a putative glucose transporter into the cell (27). The proposed production of maltose from glycogen is supported by our finding of two β-amylases (BA1 and BA2) that are actively released to the secretome in a time-dependent manner, although with different dynamics. Whereas BA2 clusters with the most abundant proteins after 10 min of incubation and increases markedly over time (high SecS value), BA1 clusters with proteins of low abundance between 10 and 30 min after incubation and slowly increases (low SecS value). The involvement of BA1 and BA2 in the glycogen metabolism is further supported by the observed up-regulation of corresponding gene transcription when glycogen was added to the cultivation media instead of maltose, as determined by qRT-PCR. Moreover, Smith *et al.* (29) purified proteins with glucosidase activity from culture medium in which *T. vaginalis* strain G3 was grown. In contrast, the conversion of maltose to glucose remains unclear. It has been shown that α-glucosidase (maltase) activity is associated with the *T. vaginalis* outer membrane (27); however, no candidate for α-glucosidase activity has been found either among the list of *T. vaginalis* membrane proteins (30) or in the secretome (this study).

T. vaginalis is currently the only eukaryote that has been shown to actively secrete β-amylases into its environment. In *E. histolytica*, β-amylases have been identified only in the proteome of the lysosomes (54) or associated with the cellular surface (69); however, none of the multiple β-amylase paralogues have been found in the *E. histolytica* secretome (64). Although the secretory pathway in *T. vaginalis* has not been studied, trichomonads possess an ER and a well-developed

Golgi apparatus with a specific structure. The Golgi apparatus is organized along two striated filaments forming a "V"-shaped body. To trace protein transport through the ER–Golgi pathway in *T. vaginalis*, we established a system using specific *in vivo* biotinylation of the target protein by BirA (70). This tool allowed us to demonstrate that both BA1 and BA2 proceed through the ER, where they are labeled by ER-targeted BirA and are subsequently transported to the Golgi apparatus and exported from the cell. As expected, the export was inhibited by brefeldin A, which prevents ER-Golgi transport; however, the export was resistant to FLI-06, which interferes with the function of ER and trans-Golgi network exit sites. These results indicate that BA1 and BA2 are secreted by the classical secretory pathway, but the resistance to FLI-06 suggests that there are likely subtleties in the mechanisms of *T. vaginalis* secretion, in which this parasite may differ from classical models.

Interestingly, BA1 appeared to be remarkably N-glycosylated. According to MS analysis of the purified protein, BA1 possesses seven glycosylation sites that are all glycosylated. In the majority of eukaryotes, N-glycans consist of two N-acetyl glucosamines, nine mannose residues, and three glucose residues that are linked to the sequon NX[ST] in the nascent protein in the ER and then modified in the Golgi apparatus. Based on the reduced set of glycosyltransferases responsible for sequential glycan synthesis, Samuelson *et al.* (71) predicted a simplified glycan structure consisting of GlcNAc2Man5 in *T. vaginalis* and *E. histolytica*. This finding is consistent with the $Hex_5HexNAc_2$ type of glycosylation that we detected in BA1.

Two other β-amylase paralogues encoded in the genome (BA3 and BA4) were not identified either in the secretome or in the membrane proteome. The absence of BA3 in the secretome is consistent with the very low transcription level of the corresponding gene. When BA3 was episomally expressed under the control of a strong promotor, still only low secretion of BA3 was observed, while a majority was associated with the cell. BA4 was not secreted under any conditions, although native *ba4* transcription is comparable with that of *ba1* and *ba2*. This protein appeared to be exclusively associated with the cell. The partial co-localization of BA3 and BA4 with lactoferrin in the endosomal/lysosomal compartment suggests that these amylases are targeted preferentially to lysosomes, similarly to β-amylase EAL51020 in *E. histolytica*. Surprisingly, the transcription of *ba4* was downregulated in the presence of glycogen, which argues against glycogen as a preferential substrate. *T. vaginalis* is a mucin-dwelling parasite that binds and degrades mucin with mucinases (72) and various glycosidases (73). In the *T. vaginalis* secretome, we identified β-hexosaminidase (TVAG_110660), which is also present in *E. histolytica* lysosomes. Thus, oligosaccharides released from sources other than glycogen might serve as an alternative substrate for BA4.

In addition to β-amylases, we identified several other families of soluble proteins in the *T. vaginalis* secretome that may play an important role in the parasite's virulence. As expected, the most prominent family appeared to be proteases. Currently, five proteases (CP2, TVAG_057000; CP3, TVAG_090100; CP4, TVAG_467970; CPT, TVAG_298080; and CP65, TVAG_096740) have been shown to be secreted by *T. vaginalis* (17, 32). Altogether, we identified seven proteases, including soluble GP63-like protease (TVAG_400860), two papain-like cysteine proteases (TVAG_057000; TVAG_034140), NlpC/P60 superfamily cysteine protease (TVAG_457240), cathepsin C protease (TVAG_229200), and two metalloproteases of the M24 (TVAG_013490) and M60 (TVAG_339720) superfamilies. Thus, in our dataset, only CP2, which appeared to be the most abundant soluble protein in the secretome, was previously identified. CP3, CP4, and CPT were found together with 58 other proteases under the SecS cutoff, whereas we did not detect CP65 (Table S3). The observed differences in the secretion of soluble CPs are not surprising. The *T. vaginalis* genome encodes 220 genes for CPs, and the differential expression of CPs between various strains (74) as well as in response to various external conditions has been reported (75).

TvDNaseII displayed the second highest SecS and in hierarchical clustering appeared among abundant early secreted proteins. It has been shown that neutrophils form an extracellular DNA trap (NET) as a form of innate response that degrades virulence factors and kills microorganisms (76, 77). To defend against NET, various pathogens secrete NET-degrading DNases (78, 79). Moreover, in the roundworm *Trichinella spiralis*, members of the secreted DNase II subfamily have been found to counteract host innate immune responses (80). In this context, the high secretion of TvDNaseII by *T. vaginalis* is a noteworthy and attractive topic for further studies.

The TvSaplip category of secreted proteins includes two putative pore-forming proteins, TvSaplip-6 (TVAG_453350) and TvSaplip-8 (TVAG 213250). These proteins belong to the saponin-like protein family, which includes the amoebapore and naegleriapore pore-forming proteins, which are secreted by *E. histolytica* (81) and *N. fowleri*, (82), respectively. TvSaplip-6 and -8 possess a single SAPLIP domain, and the latter contains a predicted signal peptide for the classical secretory pathway. In the *T. vaginalis* genome, there are 12 predicted genes for TvSaplips encoding proteins with 1–7 SAPLIP domains, 11 of which have been found to be transcribed (83). However, TvSaplip-6 and -8 are the first SAPLIP proteins observed to be actively secreted by *T. vaginalis*. In addition, four other SAPLIP proteins (TvSaplip1–4) were found under the SecS cutoff. Further studies are necessary to investigate whether *T. vaginalis* utilizes this potential weapon against host cells or bacteria via the formation of destructive pores within the target membrane.

Our broad analysis of the secretome using high-resolution proteomics and rigorous analyses of the obtained data provides valuable information about new trichomonad virulence factors. Our set of 89 secreted proteins highlights several new protein targets that are highly attractive for future investigations. However, this set of proteins is likely not complete, as we used strict criteria for the data evaluation based on proteins that were constitutively secreted in a time- and temperature-dependent manner. Previous transcriptomic studies have revealed dramatic changes in *T. vaginalis* gene expression in response to various environmental stimuli such as iron level (84), glucose availability (85), interaction with fibronectin (86), and contact with vaginal epithelial cells (87), which may affect various cellular functions, including protein secretion. Therefore, the presented *T. vaginalis* secretome provides a solid set of proteins that are constitutively secreted under defined *in vitro* conditions that can serve as a reference for future comparative studies.

Acknowledgments—We would like to thank Michaela Marcincikova for the excellent technical support and the proteomic core facility BIOCEV.

DATA AVAILABILITY

MaxQuant results were uploaded to the PRIDE partner repository (https://www.ebi.ac.uk/pride/archive/login) with the data set identifier PXD007034 (88) and to MS-Viewer with the search key ajo748srzk (http://msviewer.ucsf.edu/prospector/cgi-bin/msform.cgi?form=msviewer) (89). MaxQuant LFQ version 1.5.8.3 software was deposited at https://drive.google.com/file/d/0B_13YRpRFPM5c0pwVDAzZEVLc2s/view.

* This work was supported by the programs KONTAKT II (LH15254), NPU II (LQ1604), and the Biotechnology and Biomedicine Center of the Academy of Sciences and Charles University CZ.1.05/1.1.00/02.0109 provided by the Ministry of Education, Youth and Sport of the Czech Republic. We acknowledge the Imaging Methods Core Facility at BIOCEV supported by the Ministry of Education, Youth (the Czech-BioImaging RI project LM2015062 and CZ.02.1.01/0.0/0.0/16_013/0001775) and the project Operational Program Prague Competitiveness CZ.2.16/3.1.00/21515 funded by the European Regional Development Fund, and the Center of Molecular Structure (supported by the CIISB research infrastructure (LM2015043 funded by the Ministry of Education, Youth and Sport of the Czech Republic).

S This article contains supplemental material.

‖To whom correspondence should be addressed: Charles University, Faculty of Science, Department of Parasitology, BIOCEV Prùmyslová 595, 252 42 Vestec, Czech Republic. E-mail: tachezy@natur.cuni.cz; Tel.: +420 325 874 144, Fax: +420 224 919 704.

REFERENCES

1. Petrin, D., Delgaty, K., Bhatt, R., and Garber, G. (1998) Clinical and microbiological aspects of *Trichomonas vaginalis*. *Clin. Microbiol. Rev.* **11,** 300–317
2. Kissinger, P., and Adamski, A. (2013) Trichomoniasis and HIV interactions: A review. *Sex Transm. Infect.* **89,** 426–433
3. Tuttle, J. P., Jr, Holbrook, T. W., and Derrick, F. C. (1977) Interference of human spermatozoal motility by *Trichomonas vaginalis*. *J. Urol.* **118,** 1024–1025
4. Benchimol, M., d Andrade R. I, da Silva, F. R., and Burla Dias, A. J. (2008) *Trichomonas* adhere and phagocytose sperm cells: Adhesion seems to be a prominent stage during interaction. *Parasitol. Res.* **102,** 597–604
5. Twu, O., Dessí, D., Vu, A., Mercer, F., Stevens, G. C., de, M. N., Rappelli, P., Cocco, A. R., Clubb, R. T., Fiori, P. L., and Johnson, P. J. (2014) *Trichomonas vaginalis* homolog of macrophage migration inhibitory factor induces prostate cell growth, invasiveness, and inflammatory responses. *Proc. Natl. Acad. Sci. U.S.A.* **111,** 8179–8184
6. Stark, J. R., Judson, G., Alderete, J. F., Mundodi, V., Kucknoor, A. S., Giovannucci, E. L., Platz, E. A., Sutcliffe, S., Fall, K., Kurth, T., Ma, J., Stampfer, M. J., and Mucci, L. A. (2009) Prospective study of *Trichomonas vaginalis* infection and prostate cancer incidence and mortality: Physicians' Health Study. *J. Natl. Cancer Inst.* **101,** 1406–1411
7. Farage, M. A., and Maibach, H. I. (2011) Morphology and physiological changes of genital skin and mucosa. *Curr. Probl. Dermatol.* **40,** 9–19
8. Langley, J. G., Goldsmid, J. M., and Davies, N. (1987) Venereal trichomoniasis: Role of men. *Genitourin. Med.* **63,** 264–267
9. Gardner, W. A., Jr, O'Hara, C., Bailey, J., and Bennett, B. D. (1981) In vitro susceptibility of *Trichomonas vaginalis* to zinc. *Prostate* **2,** 323–325
10. Ryan, C. M., de Miguel, N., Johnson, P. J. (2011) Trichomonas vaginalis: Current understanding of host-parasite interactions. *Essays Biochem.* **51,** 161–175
11. Krieger, J. N., Ravdin, J. I., and Rein, M. F. (1985) Contact-dependent cytopathogenic mechanisms of *Trichomonas vaginalis*. *Infect. Immun.* **50,** 778–786
12. Lin, W. C., Chang, W. T., Chang, T. Y., and Shin, J. W. (2015) The pathogenesis of human cervical epithelium cells induced by interacting with *Trichomonas vaginalis*. *PLoS One.* **10,** e0124087
13. Fiori, P. L., Rappelli, P., Addis, M. F., Mannu, F., and Cappuccinelli, P. (1997) Contact-dependent disruption of the host cell membrane skeleton induced by *Trichomonas vaginalis*. *Infect. Immun.* **65,** 5142–5148
14. Lustig, G., Ryan, C. M., Secor, W. E., and Johnson, P. J. (2013) *Trichomonas vaginalis* contact-dependent cytolysis of epithelial cells. *Infect. Immun.* **81,** 1411–1419
15. Midlej, V., and Benchimol, M. (2010) *Trichomonas vaginalis* kills and eats—Evidence for phagocytic activity as a cytopathic effect. *Parasitol.* **137,** 65–76
16. Juliano, C., Cappuccinelli, P., and Mattana, A. (1991) In vitro phagocytic interaction between *Trichomonas vaginalis* isolates and bacteria. *Eur. J. Clin. Microbiol. Infect. Dis.* **10,** 497–502
17. Sommer, U., Costello, C. E., Hayes, G. R., Beach, D. H., Gilbert, R. O., Lucas, J. J., and Singh, B. N. (2005) Identification of *Trichomonas vaginalis* cysteine proteases that induce apoptosis in human vaginal epithelial cells. *J. Biol. Chem.* **280,** 23853–23860
18. Kusdian, G., Woehle, C., Martin, W. F., and Gould, S. B. (2013) The actin-based machinery of *Trichomonas vaginalis* mediates flagellate-amoeboid transition and migration across host tissue. *Cell Microbiol.* **15,** 1707–1721
19. Twu, O., de Miguel, N., Lustig, G., Stevens, G. C., Vashisht, A. A., Wohlschlegel, J. A., and Johnson, P. J. (2013) *Trichomonas vaginalis* exosomes deliver cargo to host cells and mediate hostratioparasite interactions. *PLoS Pathog.* **9,** e1003482
20. Müller, M., Mentel, M., van Hellemond, J. J., Henze, K., Woehle, C., Gould, S. B., Yu, R. Y., van der Giezen, M., Tielens, A. G., and Martin, W. F. (2012) Biochemistry and evolution of anaerobic energy metabolism in eukaryotes. *Microbiol. Mol. Biol. Rev.* **76,** 444–495
21. Hrdý, I., Tachezy, J., and Müller, M. (2008) Metabolism of trichomonad hydrogenosomes, In: Tachezy, J. (ed), *Hydrogenosomes and Mitosomes: Mitochondria of Anaerobic Euakryotes*, pp. 114–145, Springer-Verlag, Berlin, Heidelberg
22. Mirmonsef, P., Hotton, A. L., Gilbert, D., Gioia, C. J., Maric, D., Hope, T. J., Landay, A. L., and Spear, G. T. (2016) Glycogen levels in undiluted genital fluid and their relationship to vaginal pH, estrogen, and progesterone. *PLoS One.* **11,** e0153553
23. Mirmonsef, P., Hotton, A. L., Gilbert, D., Burgad, D., Landay, A., Weber, K. M., Cohen, M., Ravel, J., and Spear, G. T. (2014) Free glycogen in vaginal fluids is associated with *Lactobacillus* colonization and low vaginal pH. *PLoS One.* **9,** e102467
24. Rajan, N., Cao, Q., Anderson, B. E., Pruden, D. L., Sensibar, J., Duncan, J. L., and Schaeffer, A. J. (1999) Roles of glycoproteins and oligosaccharides found in human vaginal fluid in bacterial adherence. *Infect. Immun.* **67,** 5027–5032

25. Gregoire, A. T. (1963) Carbohydrates of human vaginal tissue. *Nature* **198,** 996
26. Sumawong, V., Gregoire, A. T., Johnson, W. D., and Rakoff, A. E. (1962) Identification of carbohydrates in the vaginal fluid of normal females. *Fertil. Steril.* **13,** 270–280
27. ter Kuile, B. H., and Müller, M. (1995) Maltose utilization by extracellular hydrolysis followed by glucose transport in *Trichomonas vaginalis*. *Parasitol.* **110,** 37–44
28. Huffman, R. D., Nawrocki, L. D., Wilson, W. A., and Brittingham, A. (2015) Digestion of glycogen by a glucosidase released by *Trichomonas vaginalis*. *Exp. Parasitol.* **159,** 151–159
29. Smith, R. W., Brittingham, A., and Wilson, W. A. (2016) Purification and identification of amylases released by the human pathogen *Trichomonas vaginalis* that are active towards glycogen. *Mol. Biochem. Parasitol.* **210,** 22–31
30. de Miguel, N., Lustig, G., Twu, O., Chattopadhyay, A., Wohlschlegel, J. A., and Johnson, P. J. (2010) Proteome analysis of the surface of *Trichomonas vaginalis* reveals novel proteins and strain-dependent differential expression. *Mol. Cell. Proteomics* **9,** 1554–1566
31. Riestra, A. M., Gandhi, S., Sweredoski, M. J., Moradian, A., Hess, S., Urban, S., and Johnson, P. J. (2015) A *Trichomonas vaginalis* rhomboid protease and its substrate modulate parasite attachment and cytolysis of host cells. *PLoS Pathog.* **11,** e1005294
32. Hernández, H. M., Sariego, I., Alvarez, A. B., Marcet, R., Vancol, E., Alvarez, A., Figueredo, M., and Sarracent, J. (2011) *Trichomonas vaginalis* 62 kDa proteinase as a possible virulence factor. *Parasitol. Res.* **108,** 241–245
33. Arroyo, R., Cárdenas-Guerra, R. E., Figueroa-Angulo, E. E., Puente-Rivera, J., Zamudio-Prieto, O., and Ortega-López, J. (2015) *Trichomonas vaginalis* cysteine proteinases: Iron response in gene expression and proteolytic activity. *Biomed. Res. Int.* **2015,** 946787
34. Kucknoor, A. S., Mundodi, V., and Alderete, J. F. (2007) The proteins secreted by *Trichomonas vaginalis* and vaginal epithelial cell response to secreted and episomally expressed AP65. *Cell Microbiol.* **9,** 2586–2597
35. Kulda, J., Vojtěchovská, M., Tachezy, J., Demes, P., and Kunzová, E. (1982) Metronidazole resistance of *Trichomonas vaginalis* as a cause of treatment failure in trichomoniasis—A case report. *Br. J. Vener. Dis.* **58,** 394–399
36. Diamond, L. S. (1957) The establishment of various trichomonads of animals and man in axenic cultures. *J. Parasitol.* **43,** 488–490
37. Doran, D. J. (1959) Studies on trichomonads: III. Inhibitors, acid production, and substrate utilization by 4 strains of *Tritrichomonas foetus*. *J. Protozool.* **6,** 177–182
38. Strober, W. (2001) Trypan blue exclusion test of cell viability. *Curr. Protoc. Immunol.* Appendix 3
39. Linstead, D. J., and Bradley, S. (1988) The purification and properties of two soluble reduced nicotinamide: Acceptor oxidoreductases from *Trichomonas vaginalis*. *Mol. Biochem. Parasitol.* **27,** 125–133
40. Masuda, T., Tomita, M., and Ishihama, Y. (2008) Phase transfer surfactant-aided trypsin digestion for membrane proteome analysis. *J. Proteome. Res.* **7,** 731–740
41. Cox, J., Hein, M. Y., Luber, C. A., Paron, I., Nagaraj, N., and Mann, M. (2014) Accurate proteome-wide label-free quantification by delayed normalization and maximal peptide ratio extraction, termed MaxLFQ. *Mol. Cell. Proteomics* **13,** 2513–2526
42. Vizcaíno, J. A., Csordas, A., Del-Toro, N., Dianes, J. A., Griss, J., Lavidas, I., Mayer, G., Perez-Riverol, Y., Reisinger, F., Ternent, T., Xu, Q. W., Wang, R., and Hermjakob, H. (2016) 2016 update of the PRIDE database and its related tools. *Nucleic Acids Res.* **44,** 11033
43. Hrdy, I., Hirt, R. P., Dolezal, P., Bardonová, L., Foster, P. G., Tachezy, J., and Embley, T. M. (2004) Trichomonas hydrogenosomes contain the NADH dehydrogenase module of mitochondrial complex I. *Nature* **432,** 618–622
44. Price, M. N., Dehal, P. S., and Arkin, A. P. (2010) FastTree 2—Approximately maximum-likelihood trees for large alignments. *PLoS One.* **5,** e9490
45. Katoh, K., and Standley, D. M. (2013) MAFFT multiple sequence alignment software version 7: Improvements in performance and usability. *Mol. Biol Evol.* **30,** 772–780
46. Criscuolo, A., and Gribaldo, S. (2010) BMGE (block mapping and gathering with entropy): A new software for selection of phylogenetic informative regions from multiple sequence alignments. *BMC Evol. Biol* **10,** 210
47. Lartillot, N., Lepage, T., and Blanquart, S. (2009) PhyloBayes 3: A Bayesian software package for phylogenetic reconstruction and molecular dating. *Bioinformatics.* **25,** 2286–2288
48. Guindon, S., Delsuc, F., Dufayard, J. F., and Gascuel, O. (2009) Estimating maximum likelihood phylogenies with PhyML. *Methods Mol. Biol* **537,** 113–137
49. Dos, S. O., de Vargas, R. G., Frasson, A. P., Macedo, A. J., and Tasca, T. (2015) Optimal reference genes for gene expression normalization in *Trichomonas vaginalis*. *PLoS One.* **10,** e0138331
50. Howarth, M., and Ting, A. Y. (2008) Imaging proteins in live mammalian cells with biotin ligase and monovalent streptavidin. *Nat. Protoc.* **3,** 534–545
51. Dawson, S. C., Sagolla, M. S., Mancuso, J. J., Woessner, D. J., House, S. A., Fritz-Laylin, L., and Cande, W. Z. (2007) Kinesin-13 regulates flagellar, interphase, and mitotic microtubule dynamics in *Giardia intestinalis*. *Eukaryot. Cell* **6,** 2354–2364
52. Goder, V., and Spiess, M. (2001) Topogenesis of membrane proteins: Determinants and dynamics. *FEBS Lett.* **504,** 87–93
53. Noël, C. J., Diaz, N., Sicheritz-Ponten, T., Safarikova, L., Tachezy, J., Tang, P., Fiori, P. L., and Hirt, R. P. (2010) *Trichomonas vaginalis* vast BspA-like gene family: Evidence for functional diversity from structural organisation and transcriptomics. *BMC Genomics* **11,** 99
54. Okada, M., Huston, C. D., Oue, M., Mann, B. J., Petri, W. A., Jr, Kita, K., and Nozaki, T. (2006) Kinetics and strain variation of phagosome proteins of *Entamoeba histolytica* by proteomic analysis. *Mol. Biochem. Parasitol.* **145,** 171–183
55. Rada, P., Makki, A. R., Zimorski, V., Garg, S., Hampl, V., Hrdý, I., Gould, S. B., and Tachezy, J. (2015) N-Terminal presequence-independent import of phosphofructokinase into hydrogenosomes of *Trichomonas vaginalis*. *Eukaryot. Cell* **14,** 1264–1275
56. Nickel, W. (2003) The mystery of nonclassical protein secretion. A current view on cargo proteins and potential export routes. *Eur. J. Biochem.* **270,** 2109–2119
57. Fujiwara, T., Oda, K., Yokota, S., Takatsuki, A., and Ikehara, Y. (1988) Brefeldin A causes disassembly of the Golgi complex and accumulation of secretory proteins in the endoplasmic reticulum. *J. Biol. Chem.* **263,** 18545–18552
58. Yonemura, Y., Li, X., Müller, K., Krämer, A., Atigbire, P., Mentrup, T., Feuerhake, T., Kroll, T., Shomron, O., Nohl, R., Arndt, H. D., Hoischen, C., Hemmerich, P., Hirschberg, K., and Kaether, C. (2016) Inhibition of cargo export at ER exit sites and the trans-Golgi network by the secretion inhibitor FLI-06. *J. Cell Sci.* **129,** 3868–3877
59. Peterson, K. M., and Alderete, J. F. (1984) Iron uptake and increased intracellular enzyme activity follow host lactoferrin binding by *Trichomonas vaginalis* receptors. *J. Exp. Med.* **160,** 398–410
60. Tachezy, J., Kulda, J., Bahníkova, I., Suchan, P., Rázga, J., and Schrével, J. (1996) *Tritrichomonas foetus*: Iron acquisition from lactoferrin and transferrin. *Exp. Parasitol.* **83,** 216–228
61. Pollo-Oliveira, L., Post, H., Acencio, M. L., Lemke, N., van den Toorn, H., Tragante, V., Heck, A. J., Altelaar, A. F., and Yatsuda, A. P. (2013) Unravelling the *Neospora caninum* secretome through the secreted fraction (ESA) and quantification of the discharged tachyzoite using high-resolution mass spectrometry-based proteomics. *Parasit. Vectors* **6,** 335
62. Geiger, A., Hirtz, C., Bécue, T., Bellard, E., Centeno, D., Gargani, D., Rossignol, M., Cuny, G., and Peltier, J. B. (2010) Exocytosis and protein secretion in *Trypanosoma*. *BMC Microbiol.* **10,** 20
63. Queiroz, R. M., Ricart, C. A., Machado, M. O., Bastos, I. M., de Santana, J. M., de Sousa, M. V., Roepstorff, P., and Charneau, S. (2016) Insight into the exoproteome of the tissue-derived trypomastigote form of *Trypanosoma cruzi*. *Front. Chem.* **4,** 42
64. Ujang, J. A., Kwan, S. H., Ismail, M. N., Lim, B. H., Noordin, R., and Othman, N. (2016) Proteome analysis of excretory-secretory proteins of *Entamoeba histolytica* HM1:IMSS via LC-ESI-MS/MS and LC-MALDI-TOF/TOF. *Clin. Proteomics* **13,** 33
65. Silverman, J. M., Chan, S. K., Robinson, D. P., Dwyer, D. M., Nandan, D., Foster, L. J., and Reiner, N. E. (2008) Proteomic analysis of the secretome of *Leishmania donovani*. *Genome Biol.* **9,** R35
66. Sharma, A., Sojar, H. T., Glurich, I., Honma, K., Kuramitsu, H. K., and Genco, R. J. (1998) Cloning, expression, and sequencing of a cell surface antigen containing a leucine-rich repeat motif from *Bacteroides forsythus* ATCC 43037. *Infect. Immun.* **66,** 5703–5710

67. Engbring, J., O'Brien, J. L., and Alderete, J. F. (1996) *Trichomonas vaginalis* adhesin proteins display molecular mimicry to metabolic enzymes, In: Kahane, and Ofek (eds), *Toward Anti-Adhesion Therapy for Microbial Diseases*, pp. 207–223, Plenum Press, New York
68. Meza-Cervantez, P., González-Robles, A., Cárdenas-Guerra, R. E., Ortega-López, J., Saavedra, E., Pineda, E., and Arroyo, R. (2011) Pyruvate: ferredoxin oxidoreductase (PFO) is a surface-associated cell-binding protein in *Trichomonas vaginalis* and is involved in trichomonal adherence to host cells. *Microbiology* **157,** 3469–3482
69. Thibeaux, R., Weber, C., Hon, C. C., Dillies, M. A., Avé, P., Coppée, J. Y., Labruyère, E., and Guillén, N. (2013) Identification of the virulence landscape essential for *Entamoeba histolytica* invasion of the human colon. *PLoS Pathog.* **9,** e1003824
70. Martincová, E., Voleman, L., Pyrih, J.,Žárský, V., Vondráčková, P., Kolísko, M., Tachezy, J., and Doležal, P. (2015) Probing the biology of *Giardia intestinalis* mitosomes using *in vivo* enzymatic tagging. *Mol. Cell. Biol.* **35,** 2864–2874
71. Samuelson, J., Banerjee, S., Magnelli, P., Cui, J., Kelleher, D. J., Gilmore, R., and Robbins, P. W. (2005) The diversity of dolichol-linked precursors to Asn-linked glycans likely results from secondary loss of sets of glycosyltransferases. *Proc. Natl. Acad. Sci. U.S.A.* **102,** 1548–1553
72. Lehker, M. W., and Sweeney, D. (1999) Trichomonad invasion of the mucous layer requires adhesins, mucinases, and motility. *Sex Transm. Infect.* **75,** 231–238
73. Connaris, S., and Greenwell, P. (1997) Glycosidases in mucin-dwelling protozoans. *Glycoconj. J.* **14,** 879–882
74. Cuervo, P., Cupolillo, E., Britto, C., González, L. J., FC, E. S.-F., Lopes, L. C., Domont, G. B., and De Jesus, J. B. (2008) Differential soluble protein expression between *Trichomonas vaginalis* isolates exhibiting low and high virulence phenotypes. *J. Proteomics* **71,** 109–122
75. Figueroa-Angulo, E. E., Rendón-Gandarilla, F. J., Puente-Rivera, J., Calla-Choque, J. S., Cárdenas-Guerra, R. E., Ortega-López, J., Quintas-Granados, L. I., Alvarez-Sánchez, M. E., and Arroyo, R. (2012) The effects of environmental factors on the virulence of *Trichomonas vaginalis*. *Microbes. Infect.* **14,** 1411–1427
76. Brinkmann, V., Reichard, U., Goosmann, C., Fauler, B., Uhlemann, Y., Weiss, D. S., Weinrauch, Y., and Zychlinsky, A. (2004) Neutrophil extracellular traps kill bacteria. *Science* **303,** 1532–1535
77. Urban, C. F., Reichard, U., Brinkmann, V., and Zychlinsky, A. (2006) Neutrophil extracellular traps capture and kill *Candida albicans* yeast and hyphal forms. *Cell Microbiol.* **8,** 668–676
78. Buchanan, J. T., Simpson, A. J., Aziz, R. K., Liu, G. Y., Kristian, S. A., Kotb, M., Feramisco, J., and Nizet, V. (2006) DNase expression allows the pathogen group A *Streptococcus* to escape killing in neutrophil extracellular traps. *Curr. Biol.* **16,** 396–400
79. Zhang, X., Zhao, S., Sun, L., Li, W., Wei, Q., Ashman, R. B., and Hu, Y. (2017) Different virulence of *Candida albicans* is attributed to the ability of escape from neutrophil extracellular traps by secretion of DNase. *Am. J. Transl. Res.* **9,** 50–62
80. Liu, M. F., Wu, X. P., Wang, X. L., Yu, Y. L., Wang, W. F., Chen, Q. J., Boireau, P., and Liu, M. Y. (2008) The functions of deoxyribonuclease II in immunity and development. *DNA Cell Biol.* **27,** 223–228
81. Leippe, M., Andrä, J., Nickel, R., Tannich, E., and Müller-Eberhard, H. J. (1994) Amoebapores, a family of membranolytic peptides from cytoplasmic granules of *Entamoeba histolytica*: Isolation, primary structure, and pore formation in bacterial cytoplasmic membranes. *Mol. Microbiol.* **14,** 895–904
82. Herbst, R., Marciano-Cabral, F., and Leippe, M. (2004) Antimicrobial and pore-forming peptides of free-living and potentially highly pathogenic *Naegleria fowleri* are released from the same precursor molecule. *J. Biol. Chem.* **279,** 25955–25958
83. Hirt, R. P., de Miguel, N., Nakjang, S., Dessi, D., Liu, Y. C., Diaz, N., Rapelli, P., Acosta-Serano, A., Fiori, P. L., and Mottram, J. C. (2011) *Trichomonas vaginalis Pathobiology: New insights from the Genome Sequence*, 1st Ed., pp. 87–130, Elsevier, Amsterdam
84. Horváthová, L., Šafariková, L., Basler, M., Hrdy, I., Campo, N. B., Shin, J. W., Huang, K. Y., Huang, P. J., Lin, R., Tang, P., and Tachezy, J. (2012) Transcriptomic identification of iron-regulated and iron-independent gene copies within the heavily duplicated *Trichomonas vaginalis* genome. *Genome Biol. Evol.* **4,** 1017–1029
85. Huang, K. Y., Chen, Y. Y., Fang, Y. K., Cheng, W. H., Cheng, C. C., Chen, Y. C., Wu, T. E., Ku, F. M., Chen, S. C., Lin, R., and Tang, P. (2014) Adaptive responses to glucose restriction enhance cell survival, antioxidant capability, and autophagy of the protozoan parasite *Trichomonas vaginalis*. *Biochim. Biophys. Acta* **1840,** 53–64
86. Huang, K. Y., Huang, P. J., Ku, F. M., Lin, R., Alderete, J. F., and Tang, P. (2012) Comparative transcriptomic and proteomic analyses of *Trichomonas vaginalis* following adherence to fibronectin. *Infect. Immun.* **80,** 3900–3911
87. Gould, S. B., Woehle, C., Kusdian, G., Landan, G., Tachezy, J., Zimorski, V., and Martin, W. F. (2013) Deep sequencing of *Trichomonas vaginalis* during the early infection of vaginal epithelial cells and amoeboid transition. *Int. J. Parasitol.* **43,** 707–719
88. Vizcaíno, J. A., Csordas, A., Del-Toro, N., Dianes, J. A., Griss, J., Lavidas, I., Mayer, G., Perez-Riverol, Y., Reisinger, F., Ternent, T., Xu, Q. W., Wang, R., and Hermjakob, H. (2016) 2016 update of the PRIDE database and its related tools. *Nucleic Acids Res.* **44,** 11033
89. Baker, P. R., and Chalkley, R. J. (2014) MS-viewer: A web-based spectral viewer for proteomics results. *Mol. Cell. Proteomics* **13,** 1392–1396